

**MICROMECHANICAL TESTING OF
SINGLE COLLAGEN TYPE I FIBRILS**

J.A.J. van der Rijt

Members of the committee:

Chairman/ Secretary:	prof. dr. ir. A.A. Blik	University of Twente Faculty Dean
Promotor:	prof. dr. J. Feijen	University of Twente
Assistant Promotor:	dr. ir. M.L. Bennink	University of Twente
Members:	prof. dr. J. Greve	University of Twente
	prof. dr. G.J. Vancso	University of Twente
	prof. dr. F.P.T. Baaijens	Eindhoven, University of Technology
	dr. P.J. Dijkstra	University of Twente
	dr. R.A. Bank	TNO / Gaubius Laboratory Leiden
	dr. ir. M. Hendriks	Medtronic / Bakken Research Center

The research described in this thesis was financially supported by Medtronic Bakken Research Center B.V., Maastricht, The Netherlands.

This publication was sponsored by Medtronic Bakken Research Center B.V., Maastricht, the Netherlands and the Dutch Society for Biomaterials and Tissue Engineering (NBTE).



Micromechanical testing of single collagen type I fibrils - by J.A.J. van der Rijt
PhD thesis, University of Twente, Enschede, The Netherlands, 2004.

With references - With summary in English and Dutch.

ISBN 90-365-2082-7

Copyright © 2004 by J.A.J. van der Rijt. All rights reserved.

Cover design by J.A.J. van der Rijt, E.A. Helfrich and Y.J.T. van der Zijpp.

Cover: Muscles and ligaments of the leg. Reprinted and adapted from Th. O. McCracken, "Nieuwe atlas van de menselijke anatomie.", Uniepers Abcoude, ©2000, by permission of Visible productions, Fort Collins, CO, USA.

Cover: Hierarchical organisation of collagen substructures in a tendon. Reprinted and adapted from Connective Tissue Research, J. Kastelic, A. Galeski and E. Baer, "The multicomposite structure of tendon", vol. 6, p. 11-23, 1978, by permission of Taylor & Francis, Inc, <http://www.taylorandfrancis.com>.

Back: Table IX of muscles. Reprinted and adapted from W.F. Richardson and J.B. Carman, "A. Vesalius - On the fabric of the human body - II - The ligaments and muscles.", ©2000, by permission of Norman Publishing, San Francisco, USA.

Printed by PrintPartners Ipskamp, Enschede, The Netherlands, 2004.

MICROMECHANICAL TESTING OF SINGLE COLLAGEN TYPE I FIBRILS

PROEFSCHRIFT

ter verkrijging van
de graad van doctor aan de Universiteit Twente,
op gezag van de rector magnificus,
prof. dr. F.A. van Vught,
volgens besluit van het College van Promoties
in het openbaar te verdedigen
op woensdag 13 oktober 2004 om 16.00 uur

door

Joost Adrianus Johannes van der Rijt

geboren op 23 augustus 1975
te Zeeland (NBr)

Dit proefschrift is goedgekeurd door:

Promotor: prof. dr. J. Feijen

Assistent-promotor: dr. ir. M.L. Bennink

"In omnibus requiem quaesivi, et nusquam inveni nisi in angulo cum libro."
Thomas a Kempis

Aan mijn ouders

Voor Meike en David

Table of contents

Chapter 1	General Introduction	1
Chapter 2	The Structure and Mechanical Properties of Collagen	5
Chapter 3	Tensile Testing of Single Collagen Fibrils, an Atomic Force Microscopy Approach	39
Chapter 4	Mechanical Properties of Single Collagen Type I Fibrils	65
Appendix	Effect of Bending of a Collagen Fibril During Tensile Testing	93
Chapter 5	Chemical Modification (Cross-linking) of Collagen Fibrils - Influence on Mechanical Properties	103
Chapter 6	The Structural Organisation of Collagen Fibrils in Relation to Their Mechanical Properties	123
Chapter 7	Conclusions and Outlook	141
Appendix A	Diameter Change of Tensile Tested Collagen Fibrils - Theory and Experiment	147
Appendix B	Calculations on the Influence of the Relative Error in the Dimensions of the Cantilevers on Their Stiffness and Resonance Frequency	151
Appendix C	Overview of Mechanically Tested Collagen Fibrils	153
Appendix D	Change in D-period of Collagen Fibrils Upon Tensile Testing	157
Summary		159
Samenvatting		165
Dankwoord		171
Curriculum Vitae		175

CHAPTER 1

General introduction

"Die Natur ist eine unerschöpfliche Quelle der Forschung." - A. v. Humboldt

1.1 Collagen

Collagen is the most abundant protein in the human body. The word collagen is derived from the Greek word kollagene, meaning glue forming.¹ Its main function is providing structural stability to tissue. The mechanical behaviour and function of bone, tendon, skin, cartilage, intestine, blood vessels, heart valves and eyes for example are enabled by the presence of different types of collagen. Collagen not only has an important function in its native form in tissue, but its derivatives are frequently used in daily life applications. Denaturation of collagen leads to the formation of gelatine, a process which has been known since ancient times. Pliny wrote in 50 AD: 'Glue is cooked from the hides of bulls'. Collagen is the basic constituent of leather, gelatine in food and personal care products.² The biopolymer is a common constituent of soaps, shampoos, facial creams and body lotions.³ These applications also represent the current major industrial use of collagen. Purified collagen has also been extensively applied as a biomaterial in tissue replacement, suture material and as a matrix for drug delivery.^{3, 4}

1.2 Collagen structure

Currently, around 25 types of collagen have been described, of which type I is the most abundant. Type I collagen belongs to the class of fibre forming collagens, which makes it an important constituent of ligaments, bone and skin. The structure of an Achilles tendon for example is highly complex with a number of hierarchical organisation states between the smallest building block, the polypeptide chain, and the tendon (Fig 1.1).

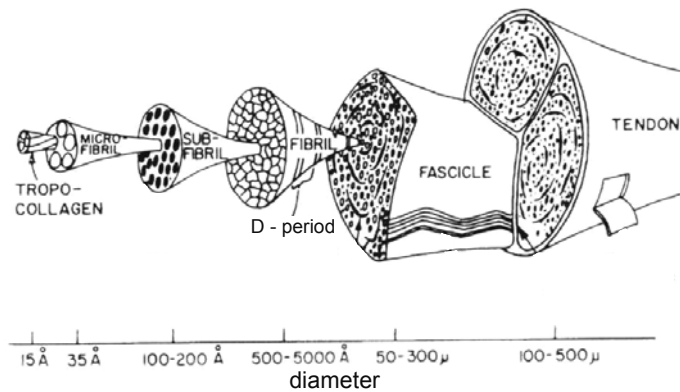


Figure 1.1 Hierarchical organisation of collagen substructures in a tendon. The figure is taken from Kastelic *et al.*, 1980.⁵ Reprinted and adapted from *Symposium of Society for Experimental Biology - Mechanical Properties of Biological Materials, Symposium XXXIV*, author: J. Kastelic and E. Baer, *Deformation in tendon collagen*, 1980, with permission from Cambridge University Press. The image was published earlier in *Connective Tissue Research*, J. Kastelic, A. Galeski and E. Baer, "The multicomposite structure of tendon", vol. 6, p. 11-23, 1978, reproduced by permission of Taylor & Francis, Inc, <http://www.taylorandfrancis.com>.

The characteristic building block of collagen is the triple helix. The structure of the triple helix was unraveled in the 1950s soon after the structure of DNA was unveiled.⁶ The triple helix is formed by three polypeptide chains, in which the triplet Gly-X-Y repeats, where X and Y are generally proline or hydroxyproline residues. The spontaneous aggregation of triple helices towards fibrous structures takes place *in vivo* and can also be induced *in vitro*. In tissue containing collagen type I, the collagen fibril is an important structural entity (Fig. 1.1). It is part of the extracellular matrix, which surrounds cells to provide structural stability.

Collagen fibrils can be distinguished by their specific periodic banding pattern of 67 nm, which can be visualized by electron microscopy (EM) and atomic force microscopy (AFM). With a length up to millimetres and a diameter between 50 and 500 nm, fibrils can be visualized with an optical microscope.

1.3 Collagen cross-linking

Collagen is not very sensitive to enzymatic degradation, a property that is related to its structural function in the body. Collagenase is the only enzyme known able to degrade fully assembled collagenous structures.² For implantation of collagen-based biomaterials, its structural stability needs to be enhanced by cross-linking. Cross-linking of collagen also takes place *in vivo* and is one of the reasons for the ageing of collagen-based tissues such as skin and ligaments. Cross-linking of collagen alters its mechanical properties and leads to a higher stiffness and strength.

The relation between the mechanical properties of collagen and its structure has not been completely unraveled. Cross-linking occurs at specific locations in the collagen structure and leads to covalent bonds between structural elements. It is not fully clear to what extent the substructures in a collagenous structure are linked together by cross-linking. Therefore, the effect of different cross-linking agents on the mechanical properties of collagen cannot yet be predicted or designed.

1.4 Structural analysis via force spectroscopy

The current understanding of the relation between the collagen structure and its mechanical properties is limited. In the last decade the use of micropipettes⁷, Atomic Force Microscopy⁸ and Optical Trapping⁹ has enabled force spectroscopy of single molecules, proteins, biomembranes and molecular aggregates. Force spectroscopy of single collagen triple helices using an Optical Trap has been described in literature.¹⁰ The mechanical properties of all other substructures that constitute a collagenous material (see Fig. 1.1) remain indistinct. To obtain more insight into the mechanical properties of these structures, micromanipulation techniques seem most suitable because of the large range in forces (between piconewtons and micronewtons) and extensions (from nanometres to millimetres) possible.

1.5 Current challenges

Up to date, the structure of the collagen triple helix has not been unraveled at atomic resolution, because the internal structure of collagen is semi-crystalline. To obtain more insight in the mechanical behaviour of collagen related to its structure, it is essential to determine the properties of the substructures. Furthermore, the effect of cross-linking on the mechanical properties of substructures may give insight into its effect in fully assembled collagen. Lack of detailed information on the assembly of collagen structures and limited results on the mechanical properties of collagen materials lead to a poor understanding of the structure-property relationship of collagen. It is essential to obtain more insight into this relationship because of the important function of collagen in the human body and its widespread use in biomedical applications.

1.6 Objectives

The objective of this study is to determine the mechanical properties of single collagen fibrils either at ambient conditions, or immersed in an aqueous environment. Information on the mechanical properties of collagen fibrils will provide a better insight on its micromechanical behaviour, which in principle opens a pathway for describing the macroscopic mechanical behaviour via extrapolation and modelling.

The aim of this work was directed to three main topics.

- The development of a micromanipulation methodology for the fixation of a single collagen fibril between a substrate and a force transducing element.
- Tensile testing of single collagen fibrils either at ambient conditions or immersed in an aqueous environment, and evaluation of the influence of cross-linking of fibrils on their mechanical properties.
- Relating the mechanical behaviour of single collagen fibrils to the structure and properties of the constituting triple helices and microfibrils.

1.7 Outline of the thesis

In this thesis the following subjects will be covered. In chapter 2 the current understanding of the structure and corresponding mechanical properties of collagen and its substructures will be reviewed. In chapter 3 the methodology to enable fixation and subsequent tensile testing of collagen fibrils is described. The mechanical behaviour of native collagen fibrils at ambient conditions and in aqueous media using the method described in chapter 3, is discussed in chapter 4. In chapter 5 the influence of cross-linking reagents, such as glutaraldehyde and a carbodiimide-based reagent, on the mechanical properties of collagen fibrils is evaluated. The obtained information on the structure and mechanical properties of collagen fibrils is further discussed in chapter 6, and an attempt is made to explain the differences in mechanical behaviour of non-treated and cross-linked fibrils at the molecular level. In chapter 7 the most important conclusions of this study are summarized and an outlook is given on new research projects based on the developed methodology.

1.8 References

- 1 K. E. Kadler, *Protein Profile - Extracellular matrix I*, 1994, **1**, 519.
- 2 J. B. Weiss and S. Ayed, in 'An introduction to collagen', ed. J. B. Weiss and M. I. V. Jayson, Churchill Livingstone, Edinburgh, 1982.
- 3 C. Meena, S. A. Mengi, and S. G. Deshpande, *Proc. Indian Acad. Sci.*, 1999, **111**, 319.
- 4 E. Gentleman, A. N. Lay, D. A. Dickerson, E. A. Nauman, G. A. Livesay, and K. C. Dec, *Biomaterials*, 2003, **24**, 3805.
- 5 J. Kastelic and E. Baer, Symposium of Society for Experimental Biology - Mechanical Properties of Biological Materials, Cambridge University Press, Cambridge, 1980.
- 6 G. N. Ramachandran, in 'Structure of collagen at a molecular level', ed. G. N. Ramachandran, Academic Press, London, 1967.
- 7 M. G. Poirier and J. F. Marko, *J. Muscle Res. Cell. Motility*, 2002, **23**, 409.
- 8 G. Binnig, C.F. Quate, C. Gerber, *Phys. Rev. Lett.*, 1986, **56**, 930.
- 9 J. T. Finer, R. M. Simmons, and J. A. Spudich, *Nature*, 1994, **368**, 113.
- 10 Y. L. Sun, Z. P. Luo, A. Fertala, and K. N. An, *Biochem. Biophys. Res. Comm.*, 2002, **295**, 382.

CHAPTER 2

The Structure and Mechanical Properties of Collagen

"Amino-acids in chains
Are the cause, so the X-ray explains,
Of the stretching of wool
And the strength when you pull,
And show why it shrinks when it rains."

A.L. Patterson

2.1 Introduction

The most abundant protein in vertebrates, accounting for 25% of the total amount of protein in the body, is collagen. In humans, 2/3 of all proteins are collagen type proteins.¹ At this time 25 distinct collagen types have been characterized, of which type I is the most abundant.^{2, 3} Collagen type I is found throughout the human body, except in cartilaginous tissues.³ The location of collagen types I-XI in the human body is presented in table 2.1.⁴⁻⁶

*Table 2.1 Collagen type I-XI and their occurrence in the human body.*⁴⁻⁶

Collagen type	Main location
I - heterotrimer	Skin, bone, tendon, cornea, lung, liver, muscle, teeth, arterial wall, placenta
I - homotrimer	Skin, tumour, tendon, liver, dentine, fibroblasts
II	Cartilage, intervertebral disc
III	Skin, aorta, uterus, placental tissues, heart, liver, lung, nerve, arterial wall, connective tissue of organs
IV	Basement membranes, lens capsule, placenta, tumour, aorta
V	Placental tissue, skin, bone, tendon, cornea, aorta, nerve, lung, liver, muscle, uterus
VI	Blood vessels, uterus, ligament, skin, lung, kidney
VII	Skin
VIII	Culture medium from endothelial and astrocytoma cells
IX	Cartilage, intervertebral disc
X	Cartilage, calcified cartilage
XI	Cartilage, intervertebral disc

Collagen type I is synthesized intracellularly by transcription from the DNA sequences of the collagen $\alpha 1(I)$ gene and the collagen $\alpha 2(I)$ gene into procollagen pre-mRNA. Processing of the mRNA forms the pro- $\alpha 1(I)$ mRNA and pro- $\alpha 2(I)$ mRNA. Translation and cleavage of the signal peptides leads to the formation of type I collagen precursor molecules, which are the single stranded pro α -chains with a molecular mass of ~ 150000 . Enzymatic hydroxylation of some proline residues and glycosylation initiates helix formation. The triple helical procollagen molecule with a molecular mass of ~ 450000 is formed, which is secreted to the extracellular matrix.⁴⁻⁶

The procollagen triple helix contains a globular C- and a trimeric N-propeptide.⁴ The function of the C- and N-propeptide is to regulate the aggregation of collagen triple helices *in vivo*.⁷ In the extracellular matrix of the cell the propeptides are enzymatically removed by procollagen N- and C-proteinases to give the triple helix with a molecular mass of ~ 300000 .⁴ The collagen triple helix generated (Fig. 2.1), is generally called tropocollagen and has a length of approximately 300 nm and a diameter of 1.4 nm.¹

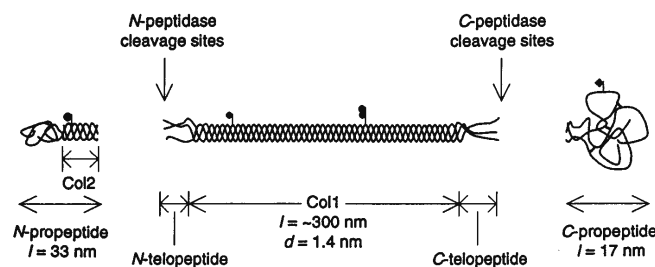


Figure 2.1 Schematic representation of the procollagen triple helix and the C- and N-terminal propeptides, which are enzymatically cleaved. Reprinted from *Protein Profile - Extracellular Matrix I*, K.E. Kadler, "General overview of collagens", vol. 1, p. 519-524, ©1994, with permission from Elsevier.

The removal of the non-helical propeptides initiates self-assembly of the triple helices, which ultimately leads to the formation of collagen fibrils. Finally, enzymatic oxidative deamination of lysine and hydroxylysine residues with the formation of aldehyde groups will take place. These aldehyde groups undergo reactions with amine functionalized amino acid residues to provide covalent cross-links at the intra- and interhelical level, which stabilize the collagen fibrils. These cross-linking reactions consist of a complex cascade of condensation reactions and rearrangements.

For collagen I, it is hypothesized that the cell regulates the processes of synthesis, post-translational processing, packaging, secretion of the polypeptides and assembly into microfibrils, fibrils, fibres and ultimately into fibre bundles. By studying these processes, it was found that the topography of the cell surface and intracellular spaces determine the orientation of the matrix. Cells (e.g. collagen producing fibroblasts) are thought to exert forces on the fibrillar matrix through their cell membrane and thus to shape the structure of the extracellular

matrix.^{8, 9} The binding between the cell surface and collagen has recently been discovered to proceed via interaction between GER (Gly-Glu-Arg) and GER-like motifs and the $\alpha 1\beta 1$ and $\alpha 2\beta 1$ integrins on eukaryotic cells. The GER domains are located in the flexible domains of fibril-forming collagens, suggesting a mechanical coupling between the cell and the extracellular matrix.¹⁰

Abnormalities in the molecular structure of native collagen have been associated with various disorders such as excessive joint laxity, poor ligament healing, abnormal fracture healing, enthesitis (infection of the attachment between the tendon/ligament and the bone), soft tissue degeneration, collagen-related skin diseases, or abnormal wound healing. Genetic disorders of the gene encoding for collagen lead to severe disfunctionalities of collagen in bone (osteogenesis imperfecta), skin and joints (Ehlers Danlos syndrome), arteries (Marfan syndrome) and cartilage development (chondrodystrophies).^{4, 11} Many of these diseases result from insufficient cross-linking between collagen triple helices in the fibrils.¹²

Its biocompatibility, biodegradability and weak antigenicity makes collagen a highly suitable material for biomedical applications.³ The nonhelical telopeptides constituting the C- and N-terminal residues of the triple helix are the only fragments of the triple helix that can be degraded by proteinases other than the collagen-specific collagenase.¹³

Historically, the major application of collagen in medicine has been as suture material (catgut).¹⁴ In later years, collagen-based biomaterials have been used in cardiovascular surgery, plastic surgery, orthopaedics, urology, neurology and ophthalmology. The use of collagen as a biomaterial has several advantages.³

- readily available and easy isolation and purification from tissues
- non-antigenic, biodegradable and bioresorbable
- non-toxic and biocompatible
- possesses high tensile strength and low deformability
- haemostatic
- simple formulation
- functional groups allow chemical modification
- biodegradability can be tuned by cross-linking
- collagen can be combined with synthetic polymers.

However, there are also some disadvantages:³

- high cost of pure type I collagen
- batch to batch variation in quality of isolated collagen
- hydrophilicity leading to swelling
- variability in enzymatic degradation rate
- handling is difficult compared to synthetic polymers
- side effects such as bovine spongiform encephalopathy (BSF) and mineralization.

Because of the growing concern for bioburdens associated with bovine and other animal sources of collagen, alternative pathways and sources for the production and isolation of collagen are under investigation. Expression of collagen in yeast and via a transgene methodology has been accomplished and via genetic engineering, recombinant human collagen can be produced. These developments in genetic modification of collagen might provide new information on the structure and properties of collagen.¹⁵

2.2 Collagen structure

2.2.1 Primary and secondary structure - polypeptide

The primary structure of collagen is the polypeptide chain, a linear array of α -amino acids. In collagen the triplet Gly - X - Y repeats, where X and Y are generally proline or hydroxyproline residues (Fig. 2.2). These two amino acids direct the chain conformation locally by the rigidity of their ring structures.¹⁶ The polypeptide chains, which contain ~1000 α -amino acid residues, form left-handed helices.¹⁷ Model polypeptides have been synthesized, containing this triplet sequence, showing helix formation similar to native collagen.¹⁸

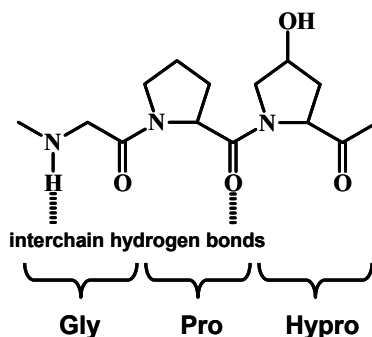


Figure 2.2 Chemical structure of the triplet sequence (Gly-Pro-HyPro), a major sequence found in collagen.

2.2.2 Tertiary structure - Triple helix

2.2.2.1 Triple helix structure

The triple helix contains three polypeptide chains, in which the C- and N-terminal residues of the chains are aligned.¹⁶ Collagen type I triple helices are composed of two $\alpha 1(I)$ -chains and a $\alpha 2(I)$ -chain.³ The triple helix is stabilized by the formation of hydrogen bonds between the N-H of the glycine residues of one chain and C=O of the proline residues of another chain, resulting in ~1 hydrogen bond per triplet.

The single polypeptide chains having a left-handed helical conformation assemble into triple helices (length: ~300 nm and diameter: ~1.5 nm), which have a right-handed helical conformation.¹⁶ The assembly takes place by association of the procollagen chains forming

the C- to the N-terminal residues. After removal of the propeptides by C- and N-proteinases, the collagen triple helices will self-assemble into fibrils. The high stability of the triple helix has been a subject of several studies and is ascribed to:

- Intra- and inter-helical hydrogen bonds, including water-mediated hydrogen bonds.
- The inductive effect of the hydroxyl group of hydroxyproline residues.
- The asymmetry of the collagen triple helix, since it is composed of two $\alpha 1$ -chains and one $\alpha 2$ -chain.

The amino acid sequence of the polypeptide chains in the collagen type I triple helix is known for over two decades.¹⁹ The molecular structure of the triple helix though, has not been completely unraveled. X-ray crystallography, the standard method for structural analysis on the atomic level has been frequently used, but because collagen is a semi-crystalline material, the resolution at which the structure can be unravelled is limited.⁶ Up to date, the maximal resolution of the molecular structure of the collagen triple helix has been determined via X-ray diffraction using synchrotron radiation at an anisotropic resolution of 0.54 nm in axial, and 0.10 nm in lateral direction.²⁰

The N- and C-terminal telopeptides for example have a non-triple helical conformation. Their conformation has recently been reported, based on X-ray diffraction studies, showing a hairpin conformation of the C-terminal telopeptide, which folds back on to the triple-helix.¹² This hairpin conformation has also been proposed for the N-terminal telopeptide of the collagen $\alpha 1(I)$ chain.²¹

Although the crystal structure of native collagen triple helices is not known, X-ray diffraction of single crystals of the synthesized model polypeptide $(\text{Gly-Pro-Hypro})_n$ revealed an unique structural packing.¹ The specific hydrogen bonding pattern in these triple helices is visualized in Fig. 2.3.²²

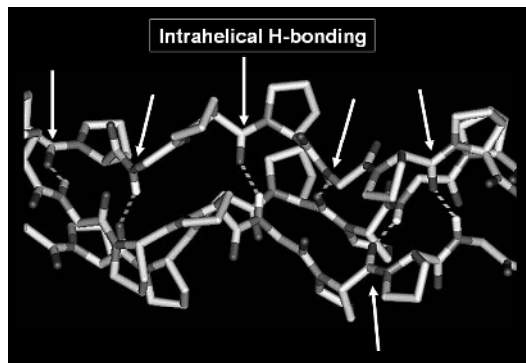


Figure 2.3 Hydrogen bonding interaction between polypeptide chains in a triple helix based on $(\text{Gly-Pro-Hypro})_n$, reprinted from the course "Principles of Protein Structure" Birckbeck College, University of London, 2003, with permission of dr. J. Walsbaw.²²

2.2.2.2 Triple helix - stabilization of the structure

Intra-chain hydrogen bonding and water-mediated hydrogen bonding stabilizes the collagen triple helix. Hydroxyproline plays an essential role for it facilitates the formation of intra- and inter-chain hydrogen bonds through H₂O bridges.^{23 24} Per Gly-X-Y triplet, with Y generally hydroxyproline, maximally six water molecules are involved.²⁵ This ultimately leads to an extensive hydrogen bonding network at the outside of the collagen triple helix.²⁶

The existence of this network has been validated by thermodynamic analysis²⁷, studies on hydrogen exchange with D₂O²⁸, and X-ray data obtained from model peptides.^{28 - 30} Raman spectroscopy revealed a continuous rearrangement of the network of bound water molecules when the distance between the triple helices was changed by applying an osmotic stress on collagen films.^{31 32}

A. Hydrogen bonding models and experimental evidence

Indirect evidence for the water-mediated hydrogen bond stability was found from changes in O-H and N-H vibrational bands of collagen samples using Raman spectroscopy, while changing the separation between triple helices by an osmotic stress. The observed spectral changes were attributed to continuous rearrangements in the network of bound water molecules, instead of removal of bulk water.³¹ Moreover, the presence of water-mediated hydrogen bonds via hydroxyproline residues was suggested from thermal denaturation experiments of triple helices.²⁷

B. Inductive effect of Hydroxyproline residues

The stabilization of collagen triple helices by hydrogen bonds is limited, because the (hydroxy)proline residues of the three polypeptide chains cannot act as hydrogen bond donors. The presence of secondary hydrogen bonds, which are mediated by water bridges, is still under debate. The denaturation temperature of collagenous proteins appears to depend on the amount of hydroxyproline present in the protein.³³

The water-mediated hydrogen bond model was doubted because of the high entropic cost of building and maintaining the estimated 500 water molecules in the organised water layer surrounding a triple helix.^{33, 34} A major contribution to the stabilization of the triple helix is thought to arise from the 3D structure of the triple helix and from non-bonded interactions of the imino rings.²⁴

More recently, evidence for an inductive effect of the OH group of the hydroxyproline residues was obtained from the denaturation temperatures of model peptides (Pro-Pro-Gly)₁₀, (Pro-Hyp-Gly)₁₀ and (Pro-Flp-Gly)₁₀ in which Flp = 4-fluoroproline. The fluorine atom exerts a stronger inductive effect than the hydroxyl group and thereby favours the trans-conformation of the 4-Flp residue in the collagen triple helix. The denaturation temperature of triple helices with the sequence (Pro-Flp-Gly)₁₀ was found to be 50°C higher than that of the oligopeptide with the sequence (Pro-Pro-Gly)₁₀.

For the oligopeptide with the sequence (Pro-Hyp-Gly)₁₀ a denaturation temperature 28°C higher than that of (Pro-Pro-Gly)₁₀ was observed.³⁴

C. Asymmetry of the triple helix

The inductive effect of the hydroxyl group of hydroxyproline stabilizing the triple helix structure was questioned in a recent paper by C.A. Miles *et al.*²⁷ They argued that the structural asymmetry of the collagen type I triple helix contributes substantially to its stability. One argument used in the inductive effect model, the high energetic cost of the water-mediated hydrogen bonding network, was overruled by pointing to the extremely high enthalpy of denaturation of collagen compared to other proteins by a factor 3-4.²⁷

By mixing the oligopeptides (Pro-Pro-Gly)₁₀ and (Pro-Hyp-Gly)₁₀, a mixture of triple helices was obtained that could partly be separated by HPLC. Increasing the portion of (Pro-Hyp-Gly)₁₀ in the samples revealed an almost linear increase in the melting temperature from [(Pro-Pro-Gly)₁₀]₃ at 45°C to [(Pro-Hyp-Gly)₁₀]₃ at 65°C. The melting enthalpy increased non-linearly and was maximal at a (Pro-Pro-Gly)₁₀ to (Pro-Hyp-Gly)₁₀ ratio of 1:2.

NMR studies on these mixtures revealed that the triple helices are asymmetrically packed. The (Pro-Hyp-Gly)₁₀ chain is shifted towards the C-terminal residues of the triple helix, resulting in a more favourable hydrogen bonding between the chains.¹⁸

Another factor contributing to the stability of the helices is the formation of internal hydrogen bonds in collagen triple helices between Gly-amide (N-H) and (Hyp)Pro-amide (C=O) groups. These interactions were calculated to be too weak to account for the high denaturation enthalpy. It is concluded that extra stabilization of the triple helix is caused by water molecules interacting with the surface of the triple helix. The asymmetry of the heterotrimer is assumed to favour this additional hydrogen bonding.¹⁸

D. Summary

Water-mediated hydrogen bonding via a network of water molecules surrounding the triple helix surface was held responsible for the stability of the triple helix. The stabilizing effect of this hydration network was doubted by pointing to the high entropic cost of such a network. The non-bonded interactions of the imino rings and the inductive effect of the hydroxygroup of hydroxyproline were claimed to account for the stability of the triple helix.

In a recent finding, the asymmetry of the triple helix was found to stabilize the triple helix. The asymmetry was thought to enable a more efficient hydrogen bonding network involving water molecules surrounding the triple helices.

2.2.3 Microfibril

2.2.3.1 Microfibril structure

Collagen triple helices aggregate in an organised fashion, ultimately into fibrils. It is generally accepted that the so called 'five stranded Smith microfibril', an assembly of five triple helices in a filamentous structure with a 4 nm diameter, is an intermediate (Fig. 2.4). The aggregation of these triple helices occurs in a "quarter staggered" fashion.

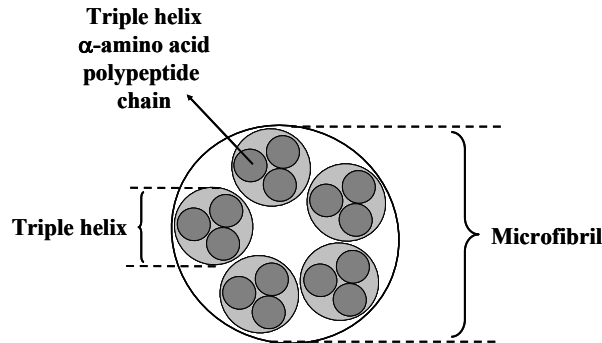


Figure 2.4 Organisation of five triple helices in the cross-section of a microfibril. The triple helices are oriented in a staggered fashion in the lateral direction of the microfibril as shown in Fig. 2.5.

When collagen is stained negatively, a series of dark and light bands are observed in the electron microscope.³⁵ The stain, which is only present in the gap (or hole) region leads to a dark band and the overlap region appears as a light band.¹⁷ The distance of gap and overlap is called the D-period, which is 67 nm wide.

Although the structure of the microfibril is difficult to visualize by microscopy, recent AFM and electron microscopy results on corneal fibrils have shown that these structures exist.³⁶⁻³⁸ In the microfibril the triple helices are separated by intervals of ~ 42 nm (0.6 D) from its neighbouring triple helix in the longitudinal direction of the microfibril (Fig. 2.5).³⁹

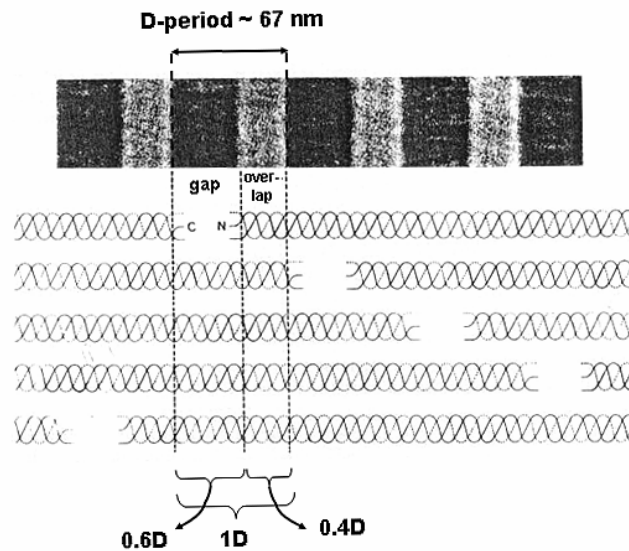


Figure 2.5 Two-dimensional impression of the aggregation of triple helices in a microfibril. The D-period, a 67 nm repeat banding pattern visible by electron microscopy and AFM, originates from staggered aggregation of the triple helices in microfibrils. In the light band the triple helices overlap and in the gap region only four triple helices are present. Reprinted and adapted from *Cell Biology of Extracellular Matrix*, ed. E.D. Hay, author: T.F. Linsenmayer, Chapter 1 - collagen, 2nd ed., 1991, with permission from Plenum Press, NY.³⁵

The triple helices in the microfibril are arranged in a left-handed spiral (Fig. 2.6).^{40, 41} The orientation of the telopeptides in the microfibril was studied by X-ray diffraction. It was found that the telopeptides were oriented such that covalent and non-covalent interactions between the microfibrils are possible. This explains why individual microfibrils have not been isolated up to date.⁴²



Figure 2.6 Left-handed spiral aggregation of triple helices in the microfibril. Sketched based on the figure by J. Woodhead-Galloway, *Connective tissue matrix*, vol. 5, "Two theories of the structure of the collagen fibril", ed. D. W. L. Hukins, Verlag, Weinheim, 1984.⁴³

An alternative structural model of the microfibril has been proposed, in which the five triple helices are compressed into an overall pseudo-hexagonal lattice. This alternative packing is needed to account for the observations in NMR studies of fibrils immersed in solution, showing that triple helices can undergo rapid axial motion. This suggests that the triple helix backbone can undergo reorientation in the fibril.⁴⁴

2.2.3.2 Water-mediated hydrogen bonding between triple helices

In section 2.2.2.2 it was shown that hydrogen bonds are important in the assembly and stability of the three α -amino acid polypeptide chains in a triple helix and that water-mediated hydrogen bonds between triple helices lead to stabilization of the structure. In this section the interactions between triple helices, which are involved in the spontaneous aggregation of triple helices into microfibrils, will be discussed.

In many biological materials strong forces based on water-mediated hydrogen bonding between the macromolecules, have been observed at a 0.1-0.2 nm distance. These forces have been related to a hydrogen-bonding network of water molecules at the macromolecular surface. Similar forces have been observed between collagen type I triple helices in water.⁴⁵ It has been calculated that the energy needed for collagen triple helices to aggregate into a microfibril is only $2.5 k_B \cdot T$.⁴⁶

Exerting an osmotic stress on triple helices in collagen films and determining the net force between the helices, while changing the temperature, pH and concentration of added hydrogen bond competing molecules (alcohols), revealed that these factors did not influence the hydrophobic interactions between the triple helices. Therefore, the influence of hydrophobic interactions between triple helices was stated to be negligible. The similarity with force curves observed for other macromolecules and the magnitude of the force suggested the presence of water-mediated hydrogen bonding between polar residues at the triple helix surfaces, instead of the occurrence of electro-static, double-layer or static forces between the triple helices.^{47, 48}

2.2.3.3 Other non-covalent interactions between triple helices

Other studies based on model peptides provided a different explanation for the attracting forces between triple helices leading to the formation of microfibrils. A microfibril model polypeptide was prepared via computerized molecular modelling. The model consisted of an aggregate of five triple helices with the sequence $(3(\text{Gly-Pro-Hyp})_{105})$, which was energy minimised. The amino acid residues in the model were subsequently replaced by the amino acid and sequence known present in native collagen. This new model, based on the bovine collagen type I sequence, was energy minimized again to verify the D-staggered organisation of triple helices. Hydrophobic and hydrophilic regions in the microfibril could be designated and the diameter of the microfibril in the hydrophilic segments appeared to be larger compared to that of the hydrophobic segments.

The hydrophobic segments were found to possess a higher amount of triple helical character compared to the hydrophilic segments. This finding suggests a contribution of hydrophobic interactions to the stabilization of the microfibril⁴⁹, which is actually opposite to the results described in section 2.2.3.2.

In a similar study, non-bonded van der Waals interactions and electronic interactions were reported to stabilize the microfibril and regulated the specific interactions between triple helices.⁴¹

2.2.4 Subfibril

2.2.4.1 Subfibril structure and evidence

Longitudinal and lateral aggregation of microfibrils will result in the formation of fibrils. The existence of an intermediate structure is sometimes addressed in literature. In a review by Kastelic and Baer in 1980⁵⁰ it was stated that: "The aggregation of triple helices into a collagen fibril consists of three substructures. They comprise the collagen triple helix, the microfibril consisting of five triple helices in cross section and a tetragonal lattice of microfibrils possibly forming subfibrils."

Like in the previous section the existence of subfibrils has been proposed as early as 1964, but evidence came available more recently from EM and AFM studies. However, AFM imaging of intermediate structures during aggregation of triple helices in solution by change of pH and temperature, did not result in the observation of the subfibril structure as an isolated intermediate between microfibrils and fibrils.^{51, 52}

Still, extensive evidence for the presence of subfibrils has been claimed in a number of studies.

The internal structure of fibrils often is not visible in electron microscopy images. In some occasions, the fibrils were found to be built from fibre-like structures (subfibrils). The observed subfibrils had a range of diameters and all showed a D-period. The thinnest subfibrils were found to have a thickness of ~4.0 nm, similar to that of a microfibril (3.5 nm). It is thought that by aggregation of microfibrils, subfibrils of various thicknesses are formed. The internal organisation can vary, leading to collagen fibrils with spiral or chequered banding patterns. The variation in width of the subfibrils can cause differences in these banding patterns. The origin of these patterns is depicted in Fig. 2.7.⁵³

The mechanism by which the self-assembly of collagen triple helices takes place remains unclear, despite the numerous studies devoted to this subject. Researchers generally use the aggregation of triple helices in solution to study the self-assembly process called fibrillogenesis. At low pH in such solutions collagen triple helices are in equilibrium with aggregates comprising 5 to 17 triple helices, and which can be 2 to 3 triple helices in length.⁹

Other studies like X-ray diffraction or AFM imaging of collagen structures come to similar conclusions. The smallest aggregates are 4-10 nm in diameter, having a 67 nm banding pattern (D-period) and are termed microfibrils or subfibrils.⁵⁴⁻⁵⁷

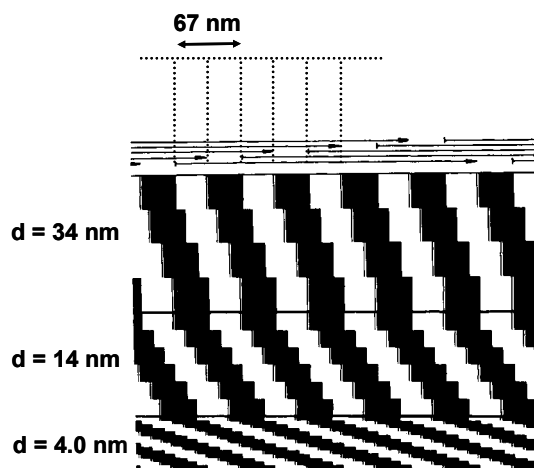


Figure 2.7 Schematic illustration of spiral banded fibrils showing the subfibrils at different width and a constant D-period aggregation. The 4.0 nm width corresponds to the microfibril structure. Adapted and reprinted from *J. Supramol. Struct.*, K.A. Piez and A. Miller, ©1974 by permission of Wiley-Liss, Inc., a subsidiary of John Wiley & Sons, Inc.⁵³

2.2.5 Fibril

2.2.5.1 Fibril structure

Aggregation of collagen microfibrils or subfibrils results in the formation of fibrils. These fibrils are cylindrical in shape with a diameter of 10-500 nm.⁵⁸ The morphology of the fibril *in vivo* is defined by extracellular spaces at the surface of specific cells. Collagen fibrils were reported to possess a right-handed helical twist.⁵⁹

Despite many years of research, the molecular organisation of the collagen fibril is not fully elucidated. The structural models for the collagen fibril are based on attempts to transform the 2D aggregation of triple helices via microfibrils or subfibrils into a 3D model.⁵⁹

One model considers the fibril's lateral packing as non-crystalline and more liquid-like (Fig. 2.8), which is underlined by NMR studies revealing significant mobility in the intermolecular interactions between collagen triple helices.⁶⁰ The other model describes the fibril's internal structure as more crystalline than liquid. The triple helices are pre-organised in microfibrils or subfibrils. The fibrils are built from these intermediate structures (Fig. 2.9).⁵⁹

The structural models of the fibril structure consisting of microfibrils and subfibrils, and the quasi-hexagonal fibril without these substructures, are shown in Fig. 2.9 and 2.8, respectively.

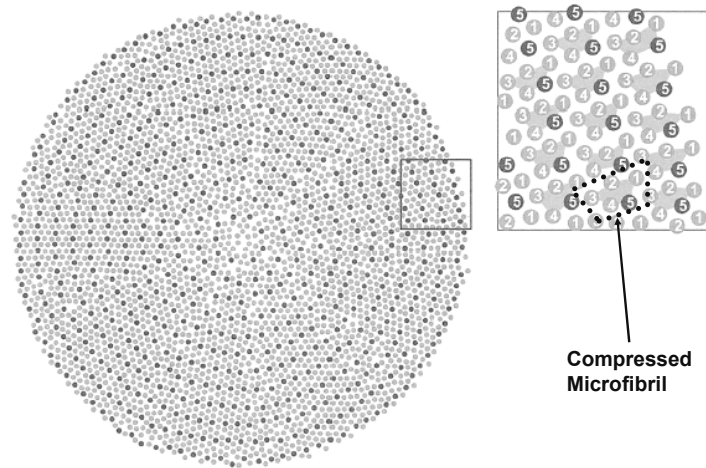


Figure 2.8 On the left the quasi-hexagonal packing of triple helices in a collagen fibril is shown. On the right the internal structure is magnified showing the organisation of five triple helices in a compressed microfibril. Because of the dense packing of the triple helices, the structured organisation of microfibrils in the fibrils is lost in this model. Reprinted and adapted from *Journal of Structural Biology*, D.J.S. Hulmes, "Building collagen molecules, fibrils and suprafibrillar structures", vol. 137, p. 2-10, ©2002, with permission from Elsevier.⁶⁰ The left image showing the quasi-hexagonal packing was published before and was reprinted here from *Biophysical Journal*, D.J.S. Hulmes, T.J. Wess, D.J. Prockop and P. Fratzl, "Radial packing, order, and disorder in collagen fibrils", vol. 68, p. 1661-1670, ©1995, with permission from the Biophysical Society.⁵⁸

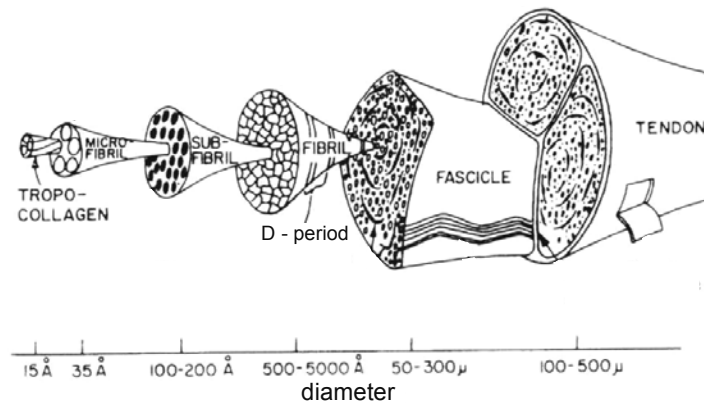


Figure 2.9 Hierarchical organisation of collagen substructures in a tendon. This organisation corresponds to the microfibril type model of the collagen structure. The figure is taken from Kastelic et al., 1980.⁵⁰ Reprinted and adapted from *Symposium of Society for Experimental Biology - Mechanical Properties of Biological Materials, Symposium XXXIV*, author: J. Kastelic and E. Baer, "Deformation in tendon collagen", 1980, with permission from Cambridge University Press. The image was published earlier in *Connective Tissue Research*, J. Kastelic, A. Galeski and E. Baer, "The multicomposite structure of tendon", vol. 6, p. 11-23, 1978, reproduced by permission of Taylor & Francis, Inc, <http://www.taylorandfrancis.com>.

Combination of both models led to an alternative model, in which the 'Smith'-type microfibril model (Figs. 2.4 and 2.5) containing five triple helices in the unit cell, was compressed to obtain a quasi-hexagonal lattice of the microfibrils in cross-section, which correlates with the structure depicted in Fig. 2.8.⁶¹

The packing of the microfibrils in the fibril has been a subject of different modelling studies. Trus and Piez⁶¹ proposed a quasi-hexagonal lattice of microfibrils, whereas Hulmes *et al.*^{58, 60, 62} proposed a concentric organisation with elements of order and disorder in the packing of the microfibrils.

2.2.5.2 Fibril structural models - evidence

A - Microfibril containing models

In the microfibril based model (Fig. 2.9), the five triple helices have orientational freedom in the gap zone due to their staggered organisation, while in the overlap zone they are tightly packed.⁴⁰

Micro-computed tomography has shown that fibrils have either a helical structure (C-type) or a less pronounced spiral shape (T-type). Fibrils in rat tail tendons are of the T-type and have a parallel arrangement of smaller aggregates. Even epitaxial fibrils have been described, which have a hollow inner core.⁵⁹ The organisation of microfibrils in corneal collagen fibrils as studied with electron tomography, revealed the microfibrils to be tilted by $\sim 15^\circ$ to the axial direction of the 36 nm thick fibrils. This microfibril aggregation leads to a right-handed helix.⁶³

The disorder present in polypeptide chain segments of the triple helices constituting collagen fibrils has been related to the difference in the D-period of the collagen fibril.⁶⁴ The overlap region of the fibrils is thought to be composed of highly ordered, tilted triple helices segments, which are linked together by more disordered segments, which are found in the gap region. The higher mobility of chains in the gap region is caused by a higher water content, a lower packing density, and a lower content of hydroxyproline residues and aromatic residues.^{65, 66} In the telopeptide regions the higher mobility leads to higher freedom in orientation. This could lead to a change in direction of the triple helices away from the quasi-hexagonal packing.^{65, 66}

The quasi-hexagonal packing of triple helices into a fibril without intermediate microfibrils has been proposed by Hulmes *et al.*⁶² In the axial direction due to the staggered order of the triple helices the D-period is found. In the lateral direction the packing of the triple helices is less organised. To model the structure of a 100 nm diameter fibril, the stacking of 3800-4000 triple helices (with a diameter of 1.08 nm) per cross section in the overlap region was energy-minimised. Two extremes were calculated: a crystalline quasi-hexagonal packing and a liquid-

like disordered one. An optimal correspondence with the known fibril properties was obtained by a model containing a concentric ring.⁵⁸

The quasi-crystalline models for collagen fibrils do not take into account the appearance of helical arrangements of subfibrils or microfibrils in the fibril. Structural research of collagen from skin, cornea, ligaments and interstitial connective tissue has shown that helical arrangements may be more consistent with X-ray data, related to the anatomical site and have a uniform diameter.⁵⁹

B - Model which allows a higher flexibility of triple helices in a fibril

The flexibility of triple helices in higher order structures has been studied using solid state NMR. A reconstituted collagen fibre, composed of fibrils which were labelled via incorporation of ¹³C-containing glycine residues, were analyzed using ¹³C-NMR relaxation experiments to obtain insight into the dynamics of the collagen triple helix polypeptide backbone. It was found that the polypeptide backbone motion was segmental, while the side chains of the amino acid in the polypeptide had a higher flexibility. The molecular flexibility of the backbone of the triple helices was hypothesized to enable small conformational changes, when placed under stress.⁶⁷ Using ¹³C-labelled collagen fibrils, the mobility of triple helices within the fibril was studied. It was found that rapid axial motion is possible, which allows triple helices to reorient within the fibril. Therefore, the highly organised packing of triple helices in a fibril was doubted. A liquid-crystalline structural model describing the organisation of triple helices in the fibril could account for the rotational freedom of the triple helices.⁴⁴

The rotational freedom of collagen triple helices in a fibril as observed by NMR suggests that the current models of assembly of subfibrils or microfibrils into fibrils lead to a structure with a crystalline content which is too high. The models are generally based on the results of X-ray diffraction studies, which cannot provide structural information on the amorphous content of the fibril.⁵⁹

To account for this discrepancy, a new model was developed, which was based on liquid-crystalline properties. Highly concentrated solutions of helices in concentrated acetic acid displayed liquid-crystalline ordering under polarized light. Upon neutralization using ammonia vapour collagen fibrils were formed, containing the same liquid-crystalline order.⁶⁸ Unfortunately, the relevance of this finding for native fibrils is doubtful, because under physiological conditions the liquid-crystalline behaviour was not observed.

A study by Hulmes *et al.*⁶⁰ suggested that the liquid-crystalline behaviour does not occur in collagen triple helix aggregates, but in aggregates of procollagen. Procollagen is a triple helix whose N- and C-propeptides have not yet been enzymatically cleaved (details Fig. 2.1). The liquid-crystalline order is thought to occur in the vicinity of the cell surface. Transformation of procollagen into collagen by enzymatic cleavage of the N- and C-propeptides triggers fibrillogenesis, which induces the pre-organisation of the triple helices.⁶⁰

Fibrils which cross other fibrils on a surface show flattening. When fibrils turn in orientation, buckling of the fibril occurs instead of loop formation. The buckling of the fibril leads to local disappearance of the D-period. It was found that fibrils can be laterally compressed and when overlapping each other, the structure of the underlying fibril is visible in the top fibril as obtained by AFM imaging. Furthermore, AFM imaging revealed a height to width ratio of 1:4 for fibrils on a surface. The structure of fibrils was suggested to be composed of a hard shell and a weaker core. At the fibril surface the triple helices should be more highly cross-linked compared to the core region. When the fibril undergoes high stresses, the outer shell might rupture, leaving the soft core intact for repair of the outer surface. During bending of a bundle of fibrils over a structure, the indentation property of the tube-like fibril would minimize deformation of the opposite side of the fibril in contact with the structure.⁶⁹

In conclusion, each model is a trade-off without accounting for all structural evidence. In general, X-ray diffraction techniques correlate better with the quasi-crystalline models, while morphological investigations favour the microfibril-based models.⁵⁹

2.2.5.3 Fibrillogenesis

A. Mechanisms

Type I collagen triple helices (tropocollagen) can be extracted at low pH and at low temperatures (around 0°C) from young tissues (tendon, skin). Such an acidic solution of triple helices will spontaneously form fibrils upon an increase in pH or temperature.⁷⁰ This process called fibrillogenesis, was found to occur *in vitro* as well as *in vivo*, and is guided by the structural properties of the triple helices. Fibrils with the characteristic D-period banding pattern are formed.^{71, 72} Fibrils formed by fibrillogenesis *in vitro* have a broader distribution in diameter and length, compared to fibrils formed *in vivo*.⁹ The mechanism of fibrillogenesis has been investigated intensively. From these studies it has been concluded that the self-assembly of triple helices into fibrils is an entropy-driven process⁷¹ and that the information encoded in the triple helices that directs fibrillogenesis is located in the telopeptides and regions low in (hydroxy)-proline residues at around 0.4D distance from the ends of the triple helices.⁷²

The rate of fibrillogenesis and the length and thickness of the fibrils formed depend on the collagen concentration used, and the buffer, pH, temperature, and ionic strength applied. Among these parameters the temperature has the strongest effect and from fibrillogenesis rates an activation energy of 243 kJ·mol⁻¹ has been determined.^{73, 74} When such an experiment is performed, two stages in the process can be distinguished, which can be monitored by turbidimetry measurements. First, a nucleation stage occurs, followed by a growth phase in which the light scattering rapidly increases. The activation energy of the nucleus formation and the size of the nuclei were found to be constant over the temperature range studied.⁷⁵

In the growth phase, the length and diameter of the fibrils are increasing, which implies that axial and lateral growth can take place simultaneously.⁷⁶

AFM imaging has become a powerful tool to study the existence of intermediate structures in the fibrillogenesis process. In combination with other techniques, such as light scattering and X-ray diffraction, valuable information on the process has been obtained. When the temperature of a triple helix solution is increased above 4°C, the initially present monomeric triple helices and small aggregates (dimers and trimers) form short microfibrils of ~2 nm in diameter and ~2 μm in length. These structures grow in length and diameter and finally fibrils were imaged with the 67 nm D-period present. The assembly process based on the AFM images is depicted in Fig. 2.10.⁷⁶ This aggregation mechanism may explain why the fibril's diameter can deviate along its length.^{51, 52, 76}

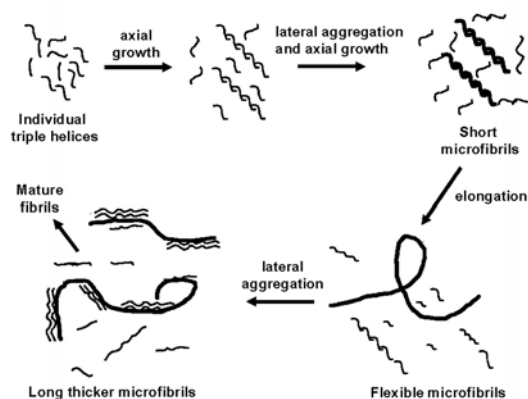


Figure 2.10 Model of collagen fibrillogenesis proposed based on AFM images of intermediate structures during self-assembly of triple helices. Reprinted and adapted from *ACS Symposium Series*, vol. 694, eds. B.D. Ratner, V. Tsukruk, authors: M.C. Goh, M.F. Paige, P. Markiewicz, I. Yadegari, M. Edirisinghe, "The formation of fibrillar structures from biopolymers", p. 94-108, ©1998, with permission from American Chemical Society.⁷⁶

B. Fibrillogenesis - interactions

Fibrillogenesis has been studied by measurement of the interaction between collagen triple helices in fibres by osmotic stress and X-ray diffraction. Collagen fibrillogenesis was found not to be regulated by ionic and hydrophobic interactions. The formation of water-mediated hydrogen bonds between triple helices was argued to be essential in fibrillogenesis. During fibrillogenesis sugar molecules and polyols were added to investigate their ability to inhibit fibrillogenesis, because of their competition with water bridges. It was found that the effect of the addition of the co-solvent was highly dependent on the structure of the solvent, which defines the hydrogen-bonding pattern of the solvent (more details: section 2.2.3.2).⁴⁷

The hydration shell of organised water molecules surrounding isolated triple helices is reduced by 25% upon aggregation during fibrillogenesis. This leads to a decrease in bound water molecules, making fibrillogenesis an entropy-driven process.⁷⁷

The fibrillogenesis process has been modelled using the diffusion-limited aggregation of rod-like particles in 2D. Short overlaps of the rods were found in the aggregates and the structure of the rods had little influence on the final morphology of the aggregate.⁷⁸ In a diffusion/collision model the aggregation of rod-like particles from solution was simulated. Similar to the previous example, the specific interactions between rods had little influence on the final fibril morphology. The packing density was found to be independent of the overall fibril shape. Therefore, it was suggested that the overall fibril morphology is regulated by the aggregation of rod-like particles from solution. The main role of the collagen-specific interactions is thought to align the triple helices as they are growing into the fibril and to maintain the fibril's stability.⁷⁹

C. Fibrillogenesis - telopeptides

When the telopeptides (non-helical ends of triple helices) are removed by treatment with the enzymes pepsin or pronase, the nucleation time in the fibrillogenesis process increased. Fibrils that are formed from pronase pre-treated triple helices showed a less pronounced D-period banding pattern compared to non-treated triple helices.⁷⁵ However, pepsin pre-treated triple helices do form fibrils having a D-period, although the rate of fibrillogenesis was retarded. On the other hand, when the triple helices were treated with pronase over a long time period, the D-banding pattern was no longer observed in the fibrils generated, because cleavages in the triple helical domain had occurred. This led to the conclusion that the rate of fibrillogenesis is regulated by the telopeptides, whereas the assembly itself is regulated by domains located at the helical ends of the triple helix.⁸⁰

D. Fibril growth

Lateral packing of collagen fibrils during fibrillogenesis *in vitro* leads to growth and thickening of the fibrils. Fibrils formed were observed to grow in length only from tapered and symmetrical tips and affinity of binding of triple helices to the tips is much higher than to the shaft of the fibril. It was suggested that an intermediate structure is acting, which regulates the addition of triple helices to the tip, but limits the diameter of the growing fibril (Fig. 2.11).⁸¹

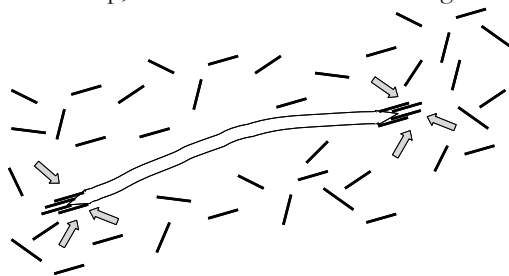


Figure 2.11 Binding of triple helices to a growing collagen fibril (not to the actual scale). The triple helices bind preferentially at the fibril ends, while triple helices have a lower affinity of binding to the shaft of the fibril.

E. Alternative collagen fibril structures

Because of the non-covalent nature of the interactions, the fibrillogenesis process can be influenced by e.g. temperature and ionic strength. Fibril morphologies other than those comprising the D-period have been observed. Two important examples of morphologically different fibrils are termed segment long spacing (SLS) fibrils and fibrous long spacing (FLS) fibrils (Fig. 2.12).^{59, 82}

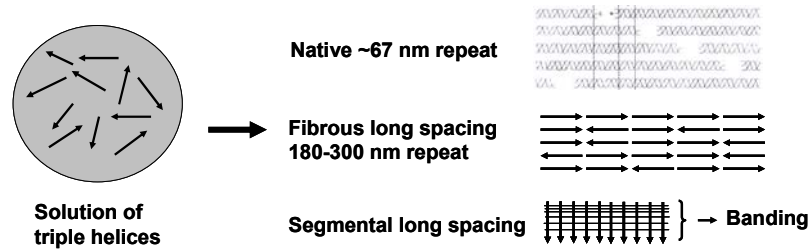


Figure 2.12. Overview of orientations of triple helices in collagen fibrils leading to different morphologies. Native structure reprinted and adapted from *Cell Biology of Extracellular Matrix*, ed. E.D. Hay, author: T.F. Linsenmayer, Chapter 1 - collagen, 2nd ed., 1991, with permission from Plenum Press, NY.³⁵

FLS type fibrils are formed when macromolecules with a high negative charge, such as α_1 -acid glycoprotein, hyaluronic acid or chondroitin sulphate are added prior to fibrillogenesis. The FLS fibrils have lengths of tens of μm and a diameter of ~ 150 nm, in which the triple helices are lined up in blocks with a random orientation of their C- and N-terminal residues.⁸³

The formation of segmental-long-spacing (SLS) collagen structures with a length of ~ 280 nm is observed in the presence of adenosine triphosphate (ATP) during fibrillogenesis. EM and AFM investigation revealed these SLS structures to be composed of triple helices, which are oriented perpendicular to the normal direction in fibrils. This results in a banding pattern corresponding to specific domains of the triple helices. A correlation between the location of positively charged regions in the triple helix and the banding pattern was found.^{84, 85}

2.2.6 Collagen fibre

Fibroblasts excrete collagen fibrils, which orient in the direction of external stresses and aggregate into fibres. The fibrils within the fibre are tilted, leading to a macroscopic crimped structure, which is visible under the optical microscope.^{86, 87} When the fibre is placed under stress, the macroscopic crimp is removed during the first 1% of strain.^{88, 89} The collagen fibres aggregate to become part of the structural skeleton of tissues, such as tendons and ligaments, bones, skin and blood vessels.

2.3 Collagen - Mechanical properties

2.3.1 Introduction

Although the structure of collagen has been studied in detail over several decades, the mechanical properties of collagen have been mainly investigated at the macroscopic level. Unfortunately, current experimental methods are unable to provide mechanical information on individual collagen fibrils.¹¹

2.3.2 Mechanical properties of collagen triple helices

2.3.2.1 Mechanical properties of collagen triple helices

When a bovine Achilles tendon immersed in a saline solution is loaded at a constant force the structural changes can be analyzed by X-ray diffraction. In the wide-angle X-ray diffraction (WAXD) pattern of collagen, the distance between neighboring amino acids in the triple helix can be measured. The changes in the distance are related to the molecular deformation and the macroscopic tensile force applied. Using the Hodge and Petruska model¹⁷ for the assembly of triple helices in the fibrils the stress and strain values of single triple helices could be determined. In Fig. 2.13 the stress-strain data of four different measurements on tendons are presented and from the linear relationship a Young's modulus of ~ 3 GPa was calculated.⁹⁰

Silver *et al.*⁹¹ determined the mechanical properties of turkey tendon and calculated the modulus of triple helices using the volume fraction of collagen in the tendon and the ratio of macroscopic to microscopic strain. The viscous and elastic component of the stress-strain curve were separated and a modulus of 3 to 4.2 GPa was calculated.⁹¹

Similarly, from the stress-strain curves of self-assembled collagen fibres an elastic modulus of 6.4 GPa was obtained for type I collagen triple helices. The results of these studies led to the conclusion that the elastic portion of the viscoelastic behaviour represents the stretching of the collagen triple helices. Cross-linking increases the elastic portion and the authors state that the viscous portion reflects the viscous slipping of fibrils, a process that is hindered by the formation of cross-links.⁷

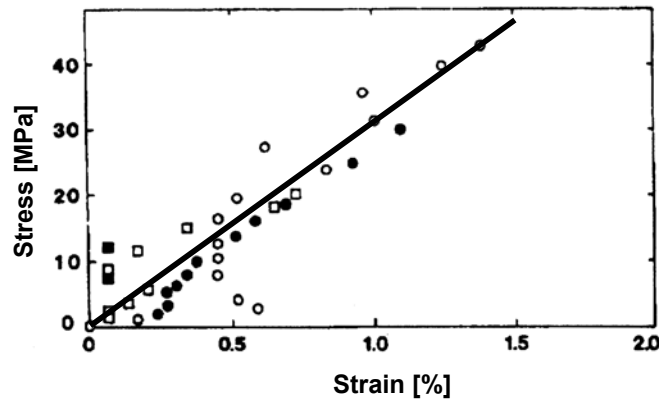


Figure 2.13 Stress-strain curve of a single triple helix, obtained by X-ray diffraction. The results of the analysis of four tendons are shown, a tentative line representing the Young's modulus is shown in the graph. Reprinted and adapted from *J. Biomech.*, N. Sasaki and S. Odajima, "Stress-strain curve and Young's modulus of a collagen molecule as determined by the X-ray diffraction technique", vol. 29(5), p. 655-658, ©1996, with permission from Elsevier.

Type I collagen triple helices are not completely rigid. At characteristic distances from the C-terminal residues, amino acid sequences are present that lack the amino acids proline and hydroxy-proline. From the persistence length, which was determined from electron microscope images of triple helices, the Young's modulus was calculated. Assuming the radius of the triple helix to be 0.5 nm, a modulus of 5.1 GPa was calculated. Including the amino acid side chains of the polypeptides in the triple helix gives a radius of 0.7 nm and a modulus of 3.0 GPa.⁹² Similar studies have been performed to calculate the mechanical properties of the triple helix and typical values for the Young's modulus obtained range between 3 and 5 GPa.^{46 93}

New nanoscale manipulation techniques have become available in recent years. One of these techniques is the use of optical tweezers in which one bead is held in focus of a laser beam and is used as a force sensor, while a second bead is fixed by for example a micropipette. Single biomacromolecules can be fixed and stretched to study their force-extension relationship. For the fixation of the triple helix between the beads, procollagen triple helices were biotinylated at the propeptides. Two streptavidin-coated polystyrene beads were used to bind to the propeptides and the force-extension curve (Fig. 2.14) showed a sharp increase when the procollagen triple helix was stretched close to its contour length. Using the worm-like chain model the persistence length of the procollagen was calculated to be 14.5 ± 7.3 nm and the procollagen had a contour length of 309 ± 41 nm. The finding that the persistence length is much smaller than the contour length, suggests the collagen triple helices to be flexible under physiological conditions.

A Young's modulus of 12.2 GPa was calculated from the obtained persistence length of 14.5 nm and a radius of 0.28 nm. A Young's modulus of 350 MPa was calculated when using a radius of 0.68 nm.²

In conclusion, when comparing the Young's moduli of a single triple helix determined from the elastic fraction of the stress-strain curve (~ 3 or ~ 6 GPa), the contour length (~ 3 or 5 GPa), hydrodynamic studies (3.1 GPa) and viscoelastic measurements (4.1 GPa) with force spectroscopy using optical tweezers (350 MPa or 12.2 GPa, with a radius of 0.68 or 0.28 nm, respectively) reveals a rather large difference.

The authors have attributed this difference to the different media applied during mechanical testing, the used diameter of the triple helix in calculations and possible influence of the applied structural- or mathematical model.

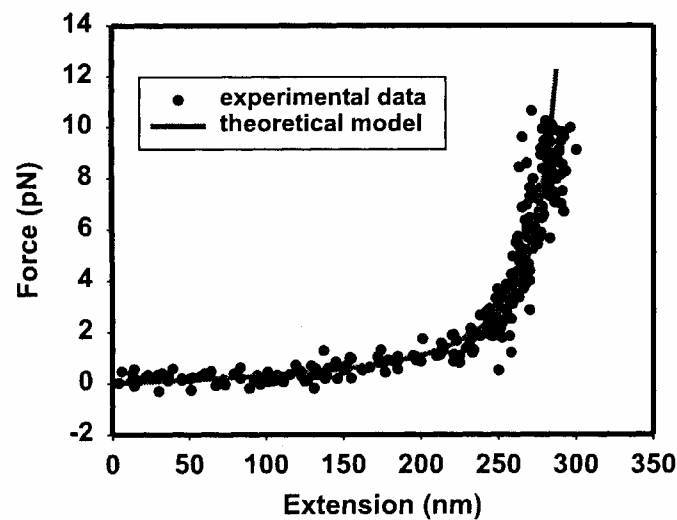


Figure 2.14 Force-extension curve of a single collagen triple helix, obtained by an optical trapping technique. The experimental data were fitted using the worm-like chain (WLC) model. The figure was taken from Sun et al., 2002 Reprinted from *Biochem. Biophys. Res. Commun.*, Y.L. Sun, Z.P. Luo, A. Fertala and K.N. An, "Direct quantification of the flexibility of type I collagen monomer", vol. 295(2), 382-386, ©1996, with permission from Elsevier.

2.3.2.2 Deformation behaviour of collagen triple helices

Deformation of collagen fibrils can occur via two mechanisms. Firstly, elongation of the triple helix which constitute the fibril is possible. The second mechanism consists of sliding of triple helices in the fibril with respect to each other. Both mechanisms can act when collagenous structures are loaded and lead to a change in the D-period of the fibril.

A. Elongation of triple helices

Type I collagen triple helices can be modelled as an array of rigid blocks separated by flexible blocks. These blocks are around 6-12 amino acids in length.¹⁰ The triple helix is stabilized by stiffer regions composed of the Gly-X-Y sequence to prevent stress-induced denaturation of the protein. Because the triple helices are aggregated in a staggered fashion, averaging of the stiffness of the flexible and rigid domains will occur. It is stated that under stress the flexible regions take the initial deformation, thus storing elastic energy.¹⁰

The elasticity of collagen has also been attributed to the removal of thermally activated microkinks in the triple helices during stress. This hypothesis was based on X-ray diffraction studies during stress experiments on rat tail tendon fibres.⁹⁴ Tensile testing of a tendon leads to straightening of small kinks in the collagen structure at small strains. This phenomenon begins at the fibrillar level and continues at the triple helix level. At higher strains triple helices within the fibril slide, leading to permanent deformation of the fibrils as observed by X-ray diffraction.⁹⁵

Force-extension curves of collagen triple helix aggregates were obtained by the following approach. A drop of a suspension containing aggregates of collagen triple helices from bovine Achilles tendon origin was placed on a glass substrate. The non-covalent interactions between an AFM tip while approaching and retracting the glass substrate were recorded and attributed to force-distance curves of the collagen triple helix aggregates. The force-extension experiments were also conducted on a polished piece of rat femur bone. It was hypothesized that sacrificial bonds within or between collagen triple helices form and reform during these experiments. When collagen triple helices are placed in a calcium-containing HEPES buffer more sacrificial bonds reform and more energy dissipation occurs compared to the results obtained in a buffer without calcium ions.⁹⁶ Later studies revealed that on a molecular basis the energy storage in a tendon involves the stretching of flexible domains in the triple helices. The elastic modulus is related to this phenomenon and is reduced when cross-links are absent (as in fibrils prepared by reconstitution of triple helices).

The above described mechanisms, which were postulated to occur upon loading tendon fibres are all likely to take place. Finally, it has been shown that the elastic modulus is directly related to the fibril length, and although fibril diameter plays a certain role, fibril length was found to be far more important.^{7, 97}

B. Sliding of helices

The sliding of triple helices can proceed via two pathways. The triple helices can slide blockwise (Fig. 2.15a) or with respect to each other (Fig. 2.15b). Both modes lead to an increase in the collagen D-period.⁶⁴

In a creep experiment, performed on a bovine Achilles tendon, the deformations at the triple helix level, leading to a change in the D-period, were analyzed by X-ray diffraction.

The deformation results in elongation of triple helices, increase in the gap region of the D-period and slipping of triple helices, and was found to start at a minimal stress of ~ 10 MPa. The first mode was responsible for the largest deformation, while the two others caused changes in the ratio between the width of the overlap and width of the gap region.⁶⁴

In a relaxation experiment on a single RTT fibre, it was shown that the D-period initially increased, but was retained within 12 h. The increase in the D-period was attributed to the sliding of triple helices with respect to each other.⁹⁹

The internal deformation of rat tail tendons during tensile testing was studied using X-ray diffraction. Before rupture of the tendon, the D-period pattern was lost. This process was explained by the slipping of substructures in the tendon with a diameter smaller than 10 nm. The lost D-period can be explained by slipping of triple helices, but the obtained diameter range of the slipping substructures suggests that microfibril slipping might also occur.⁵⁰

By adsorbing collagen fibrils on PET (Mylar) and subsequent deformation of the PET sheets, the collagen fibrils were strained to rupture. The collagen D-period of the fibrils was found to increase with extension of the sheets and to remain increased after rupture of the fibril. It was argued that the largest deformation of the fibril occurs in the polar regions of the triple helices, which are poor in (hydroxy)proline residues.¹⁰⁰

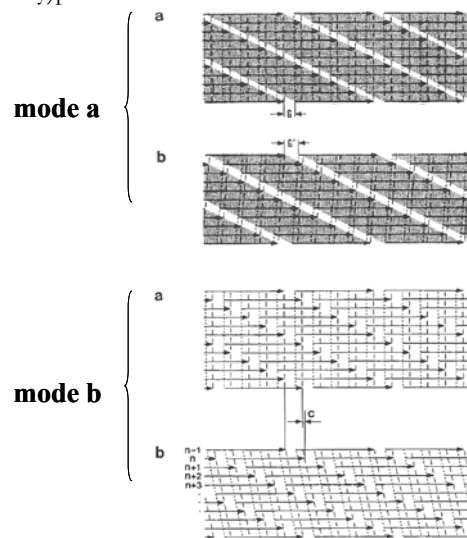


Figure 2.15 Rearrangement of triple helices in a fibril. (a) Increase in the gap region, where the interactions between laterally adjoining triple helices are retained. (b) Relative slipping of laterally adjoining triple helices. Reprinted and adapted from *J. Biomech.*, N. Sasaki and S. Odajima, "Elongation Mechanism of Collagen Fibrils and Force-Strain Relations of Tendon at Each Level of Structural Hierarchy", vol. 29(9), p. 1131-1136, ©1996, with permission from Elsevier.⁹⁸

C. Influence of cross-linking

The cross-link density of collagen fibres (from animals with different ages) appears not to influence the deformation behaviour, which was attributed to a first sliding of the triple helices before stretching of the telopeptide region occurs. At larger extensions also the telopeptides become stretched, which allows more deformation to take place, resulting in irreversible sliding of triple helices (Fig. 2.16).⁹⁹

Rat tail tendons from cross-link deficient animals can resist only weak forces in the fibrillar structure, causing shear within a fibril at higher forces. The absence of cross-links leads to slipping of triple helices with respect to each other, which suggests the triple helices to be organised in line.⁴²

From the stress-strain curve of a RTT fibre immersed in phosphate buffer two different moduli can be distinguished. These moduli were dependent on the age of the animal, going to a constant value after 20 months of age. The D-period was found to increase upon increasing strain with a maximal increase at ~11% strain. With the age of the animal the cross-link density within the fibre increased, leading to reduced permanent damage at high strains.⁵⁰

The cross-link density can be increased further by chemical reagents leading to even better resistance to tearing under static loads, but with lower damping properties and a lower resistance to pulsating loads.¹⁰¹

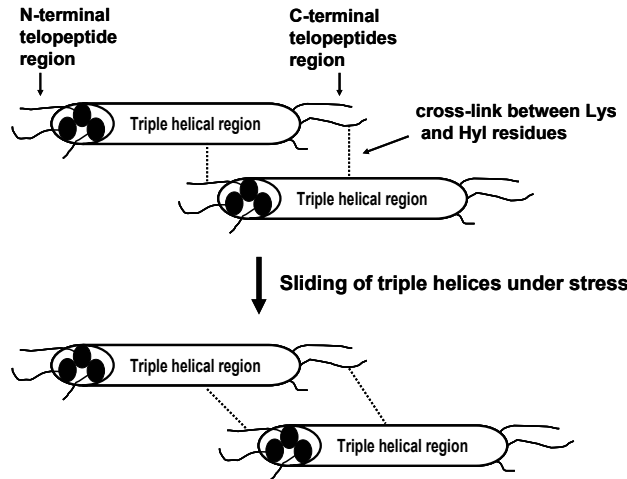


Figure 2.16 Sliding of the triple helices leads to an increase in the D-period and an increase in the number of residues per D-period from 235 to 237. This causes stretching of the cross-links that bind two triple helices between the triple helical domain and the N-terminal and C-terminal $\alpha 1(I)$ telopeptides.⁹⁹

In conclusion, both elongation and sliding of triple helices is reported in X-ray studies of tendons and ligaments under stress. The change in the collagen D-period resulting from both deformation mechanisms was generally observed, but in most cases this change was found to be non-permanent.

2.3.3 Mechanical properties of fibrils

2.3.3.1 Mechanical properties of fibrils

Based on the ultimate tensile strength of fibrous collagen structures, the stress at break of a collagen fibril was estimated to be 1 GPa.¹⁰² In another study an estimate for the stress at break of 147-294 MPa of individual fibrils was reported, based on the calculation of the collagen content in a tendon.¹⁰³

Sasaki *et al.*⁹⁸ calculated the stress-strain curves of a single collagen fibril from changes in the D-period by X-ray analysis of a bovine Achilles tendon immersed in saline under stress. The tendon was loaded at various constant stress values and the change in collagen D-period was recorded. During loading of the tendon, creep occurs. The D-period change is calculated from the remaining D-period value after this creep. The stress-induced change in the 67 nm repeat of the fibrils constituting the tendon was defined as the strain in the fibril structure. By assuming that the tendon cross-sectional area is composed of a bundle of fibrils (Fig. 2.9), the stress on the individual fibrils was calculated. At 4% strain a stress value of approximately 20 MPa was calculated. From the stress-strain curves a Young's modulus of 430 MPa was determined (Fig. 2.17).⁹⁸ The triple helix has a Young's modulus three times higher (data according to Fig. 2.13) than that of the fibril.

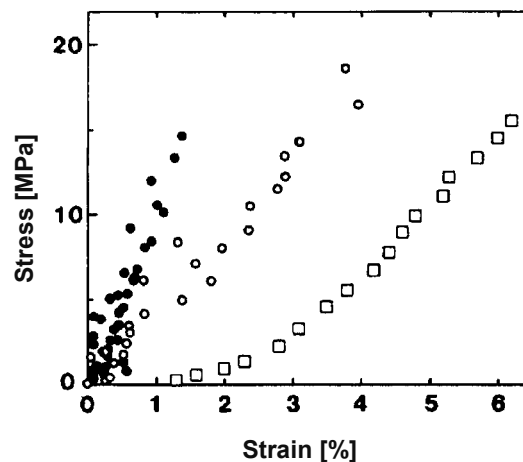


Figure 2.17 Stress-strain curve of a tendon (open squares), a collagen fibril (open dots) and a triple helix (closed dots), obtained by X-ray diffraction during loading of a bovine Achilles tendon. The strain of the fibril was calculated from the change in D-period as determined by X-ray diffraction. The strain of the tendon was determined via a tensile test. Reprinted and adapted from J. Biomech., N. Sasaki and S. Odajima, "Elongation Mechanism of Collagen Fibrils and Force-Strain Relations of Tendon at Each Level of Structural Hierarchy", vol. 29(9), p. 1131-1136, ©1996, with permission from Elsevier.⁹⁸

The deformation mechanism proposed involves: ⁹⁸

- a) Triple helix elongation
- b) Increase in the gap region (Fig. 2.15a)
- c) Slipping of laterally adjoining triple helices (Fig 2.15b)

2.3.4 Mechanical properties of a collagen fibre

Self-assembled collagen fibres were tensile tested, yielding stress-strain curves with a J-shaped curve. The initial or toe region is non-linear with an increasing slope, this results in a maximal slope in the linear region. The curve of rat tail tendon (RTT) fibres has a different shape. The RTT fibres display an S-shaped curve with a modulus that is first increasing and after remaining constant in the linear region, reduces again at elongations exceeding 10% strain.¹⁰⁴

Self-assembled collagen fibres are composed of fibrils with a range in diameter. The fibril diameter could be correlated with the low strain modulus of the fibre, while the high strain modulus and ultimate tensile strength were independent of the average fibril diameter.⁹

In tissue, the fibrils are not aligned in the direction of external forces, because the forces acting on the tissue are rarely uniaxial. Furthermore, perfectly aligned fibrils would cause a low resilience meaning that large deformations will easily lead to fracture. Thus, fibrils possess a crimped morphology in tendons and are organised in a wavy pattern in absence of stress, which allows a certain deformation under small stresses upon removal of this crimp.¹⁰⁵

2.4 Conclusion

Due to its biocompatibility, mechanical performance and feasibility of chemical modification, collagen can be used in a variety of biomedical applications. The complex relationship between the collagen structure and physical and mechanical properties remains an important topic for future studies.

2.4.1 Structure

The collagen polypeptide chain is composed of repeating Gly-X-Y units, in which the amino acids X and Y are mostly proline and hydroxyproline residues. Two equal polypeptide chains and a distinct third one form the most stable triple helices, whose origin has been studied extensively. The majority of reports attribute this stability to hydrogen bonding between the polypeptide chains and water-mediated hydrogen bonding at the intra- and interhelical level. Hydroxyproline is assigned as an essential residue for the stability of collagen for its ability to form hydrogen bonds through the hydroxyl group, but this is not a generally accepted theory. The inductive effect of the hydroxyl group and/or the steric hindrance of the hydroxyproline ring provide a second hypothesis that account for the stability of the triple helix.

The most extensive proof for the stability was obtained from model peptides based on homo- and heterotrimeric triple helices. The influence of asymmetry of the triple helix on its stability has been shown. It was hypothesized that water-mediated hydrogen bonding does occur at the surface of the triple helix, which is facilitated by the asymmetric packing of the triple helix.

Collagen triple helices aggregate through a self-assembly process into ordered structures, ultimately into fibrils. Depending on the fibril model used, the existence of microfibrils is accepted or not. Because of many reports proving the existence of microfibrils (electron microscopy and AFM), the microfibril should be considered a structural entity. The aggregation of the triple helices into the microfibril is thought to occur from hydration forces, although the involvement of other non-covalent interactions as hydrophobic and electrostatic interactions has also been reported as a possible explanation.

The existence of a subfibrillar structure, between the microfibril and fibril seems obscure, but some structural evidence has been obtained from the observation of different morphologies of collagen fibrils. The common view is that subfibrils consist of aggregated microfibrils in a structure that up to date has not been unraveled.

The collagen fibril is an important structural entity in tissue. The structure can be described as an aggregate of triple helices in microfibrils, which possibly aggregate in subfibrils, which finally organise into a fibril. An alternative model originates from observations of the liquid-like behaviour of collagen triple helices within the fibril as observed in solid state NMR. Structural analysis by AFM and electron microscopy seem to underline the first model, although recently it was claimed that both the liquid-like and the more crystalline behaviour are co-existing in fibrils.

Fibril formation from collagen triple helices, a process called fibrillogenesis, can be induced *in vitro*, and has been extensively studied. The aggregation is an entropy-driven process, with the intermediate structures involved in fibrillogenesis contributing to the control over the fibril diameter. The presence of telopeptides on the triple helices increases the rate of triple helix aggregation as well as controls the diameter of the fibril. Despite the elaborate study of the fibrillogenesis process, the exact mechanism behind the process has not been unraveled completely.

2.4.2 Mechanical

The Young's modulus of a collagen triple helix has been determined via various methods at 3-6 GPa. Reversible stretching of the triple helix has been described to occur by deformation of domains in the triple helix sequence, which lack proline or hydroxy-proline residues.

Only one example of the force-extension curve for a single collagen triple helix has been reported up to now. The results obtained do not represent the mechanical behaviour of a triple helix, because a procollagen triple helix, still containing its C- and N-terminal propeptide

sequences was tested. These sequences do not have a triple helix conformation and therefore might influence the overall mechanical properties by making the structure more flexible.

Deformation at the triple helix level can consist of elongation and sliding of triple helices, which both lead to an increase in the D-period. The elongation of the triple helix has been described by three structural models.

- Elastic elongation of sequences lacking (hydroxy)-proline residues in the triple helix
- Stretching of microkinks in the triple helix
- Opening of sacrificial bonds in the helix, which consist of ionic interactions

Next to elongation of the triple helix, slipping of triple helices has been described by two modes of deformation. In the first mode blocks of triple helices slip in their staggered organisation, which leads to an increase in the gap region of the D-period. The second mode consists of relative slipping of triple helices, which are laterally adjoining.

The mechanical properties of single collagen fibrils are unknown, but interpretations have been made based on X-ray diffraction studies of macroscopic collagen materials under load and extrapolations of macroscopic mechanical properties of collagen materials using a structural model. These approaches yielded estimations of the Young's modulus and the stress at break value of collagen fibrils. The stress-strain curve of a single collagen fibril obtained by loading and unloading of the fibril has not been reported.

Besides the elongation of triple helices and slipping of triple helices, slipping of microfibrils has been reported during loading of tendons and collagen fibres. During tensile testing of a single collagen fibril all three mechanisms mentioned are likely to occur.

Although the organisation of collagen fibrils within collagen fibres is complex, interesting information on the mechanical properties of triple helices and fibrils has been obtained. Due to the large difference in mechanical behaviour between rat tail tendon fibres and self-assembled fibres, caused by the difference in structural organisation of the fibrils within the fibre, the reported mechanical properties should be interpreted with care.

2.5 References

- 1 K. E. Kadler, *Protein Profile - Extracellular matrix I*, 1994, **1**, 519.
- 2 Y. L. Sun, Z. P. Luo, A. Fertala, and K. N. An, *Biochem. Biophys. Res. Comm.*, 2002, **295**, 382.
- 3 C. H. Lee, A. Singla, and Y. Lee, *Int. J. Pharm.*, 2001, **221**, 1.
- 4 K. S. E. Cheah, *Biochem. J.*, 1985, **229**, 287.
- 5 J. B. Weiss and S. Ayed, in 'An introduction to collagen', ed. J. B. Weiss and M. I. V. Jayson, Churchill Livingstone, Edinburgh, 1982.
- 6 P. M. Zavlin, V. N. Izmailova, M. A. Sakvarelidze, and G. P. Yampol'skaya, *Russian Journal of Applied Chemistry*, 1993, **66**, 259.
- 7 F. H. Silver, J. W. Freeman, and G. P. Seehra, *J. Biomech.*, 2003, **36**, 1529.
- 8 D. E. Birk, E. I. Zycband, D. A. Winkelmann, and R. L. Trelstad, *Ann. N.-Y. Acad. Sci.*, 1990, **580**, 176.
- 9 D. L. Christiansen, E. K. Huang, and F. H. Silver, *Matrix Biol.*, 2000, **19**, 409.
- 10 F. H. Silver, I. Horvath, and D. J. Foran, *J. Theor. Biol.*, 2002, **216**, 243.
- 11 Z.-P. Luo, M. E. Bolander, and K.-N. An, *Biochem. Biophys. Res. Commun.*, 1997, **232**, 251.
- 12 J. P. Orgel, T. J. Wess, and A. Miller, *Structure*, 2000, **8**, 137.
- 13 D. L. Helseth and A. Veis, *J. Biol. Chem.*, 1980, **256**, 7118.
- 14 C. Meena, S. A. Mengi, and S. G. Deshpande, *Proc. Indian Acad. Sci.*, 1999, **111**, 319.
- 15 C. W. P. Foo and D. L. Kaplan, *Adv. Drug Del. Rev.*, 2002, **54**, 1131.
- 16 O. Akkus, 'Lecture - BIOE Tissue Mechanics', University of Toledo, OH, 2003.
- 17 J. A. Petruska and A. J. Hodge, *Proc. Natl. Acad. Sci. USA*, 1964, **51**, 871.
- 18 D. A. Slatter, C. A. Miles, and A. J. Bailey, *J. Mol. Biol.*, 2003, **329**, 175.
- 19 M. J. Capaldi and J. A. Chapman, *Biopolymers*, 1982, **21**, 2291.
- 20 J. P. R. O. Orgel, A. Miller, T. C. Irving, R. F. Fischetti, A. P. Hammersley, and T. J. Wess, *Structure*, 2001, **9**, 1061.
- 21 D. L. Helseth, J. H. Lechner, and A. Veis, *Biopolymers*, 1979, **18**, 3005.
- 22 Birkbeck College School of Crystallography, University of London, <http://www.cryst.bbk.ac.uk/>, 2003.
- 23 J. Bella, B. Brodsky, and H. M. Berman, *Structure*, 1995, **3**, 893.
- 24 R. S. Bhatnagar, C. A. Gough, J. J. Qian, and M. B. Shattuck, *Proc. Indian Acad. Sci.*, 1999, **111**, 301.
- 25 C. A. Miles and M. Ghelashvili, *Biophys. J.*, 1999, **76**, 3243.
- 26 J. Bella, M. Eaton, B. Brodsky, and H. M. Berman, *Science*, 1994, **266**, 75.
- 27 C. A. Miles and A. J. Bailey, *Micron*, 2001, **32**, 325.
- 28 R. Z. Kramer, J. Bella, P. Mayville, B. Brodsky, and H. M. Berman, *Nature structural biology*, 1999, **6**, 454.

- 29 G. N. Ramachandran, M. Bansal, and R. S. Bhatnagar, *Biochim. Biophys. Acta*, 1973,
300 **322**, 166.
- 30 J. V. Milchevsky, B. S. Zhorov, N. G. Esiova, and V. G. Tumanyan, *Journal of*
310 *biomolecular structure & dynamics*, 1999, **16**, 977.
- 31 S. Leikin, V. A. Parsegian, W.-H. Yang, and G. E. Walrafen, *Proc. Natl. Acad. Sci.*
320 *USA*, 1997, **94**, 11312.
- 32 S. Leikin, D. C. Rau, and V. A. Parsegian, *Proc. Natl. Acad. Sci. U. S. A.*, 1994, **91**, 276.
- 33 P. E. McClain and E. R. Wiley, *J. Biol. Chem.*, 1972, **247**, 692.
- 34 S. K. Holmgren, K. M. Taylor, L. E. Bretscher, and R. T. Raines, *Nature*, 1998, **392**,
350 666.
- 35 T. F. Linsenmayer, in 'Chapter 1 - Collagen', ed. E. D. Hay, Plenum Press, New York,
360 1991.
- 36 S. Habelitz, M. Balooch, S. J. Marshall, G. Balooch, and G. W. Marshall, *J. Struct. Biol.*,
370 2002, **138**, 227.
- 37 D. R. Baselt, J.-P. Revel, and J. D. Baldeschwieler, *Biophysical Journal*, 1993, **65**, 2644.
- 38 L. J. Gathercole, M. J. Miles, T. J. McMaster, and D. F. Holmes, *J. Chem. Soc. Faraday*
390 *Trans.*, 1993, **89**, 2589.
- 39 J. W. Smith, *Nature*, 1968, **219**, 157.
- 40 T. J. Wess, A. P. Hammersley, L. Wess, and A. Miller, *J. Mol. Biol.*, 1998, **275**, 255.
- 41 J. M. Chen, C. E. Kung, S. H. Fearheller, and E. M. Brown, *J. Prot. Chem.*, 1991, **10**,
420 535.
- 42 T. J. Wess, A. P. Hammersley, L. Wess, and A. Miller, *J. Struct. Biol.*, 1998, **122**, 92.
- 43 J. Woodhead-Galloway, in '5 - Two theories of the structure of the collagen fibril', ed.
440 D. W. L. Hukins, Verlag, Weinheim, 1984.
- 44 L. W. Jelinski and D. A. Torchia, *J. Mol. Biol.*, 1979, **133**, 45.
- 45 N. Kuznetsova, D. C. Rau, V. A. Parsegian, and S. Leikin, *Biophys. J.*, 1997, **72**, 353.
- 46 F. H. M. Nestler, S. Hvidt, J. D. Ferry, and A. Veis, *Biopolymers*, 1983, **22**, 1747.
- 47 N. Kuznetsova, S. L. Chi, and S. Leikin, *Biochem.*, 1998, **37**, 11888.
- 48 S. Leikin, D. C. Rau, and V. A. Parsegian, *Structural Biology*, 1995, **2**, 205.
- 49 E. M. Brown, G. King, and J. M. Chen, *J. Am. Leather Chemists Ass.*, 1997, **92**, 1.
- 50 J. Kastelic and E. Baer, Symposium of Society for Experimental Biology - Mechanical
510 Properties of Biological Materials, Cambridge University Press, Cambridge, 1980.
- 51 M. Gale, M. S. Pollanen, P. Markiewicz, and M. C. Goh, *Biophys. J.*, 1995, **28**, 2124.
- 52 M. C. Goh, M. F. Paige, M. A. Gale, I. Yadegari, M. Edirisinghe, and J. Strzelczyk,
530 *Physica A*, 1997, **239**, 95.
- 53 K. A. Piez and A. Miller, *J. Supramol. Struct.*, 1974, **2**, 121.
- 54 S. Yamamoto, J. Hitomi, M. Shigeno, S. Sawaguchi, H. Abe, and T. Ushiki, *Arch.*
550 *Histol. Cytol.*, 1997, **60**, 371.
- 55 R. R. Bruns, *J. Cell Biol.*, 1976, **68**, 521.

- 56 T. Nemetschek, R. Bowitz, and H. Nemetschek-Gansler, *Verh. Deutsche Ges. Path.*, 1975, **59**, 34.
- 57 M. Raspanti, T. Congiu, and S. Guizzarbi, *Matrix Biol.*, 2001, **20**, 601.
- 58 D. J. S. Hulmes, T. J. Wess, D. J. Prockop, and P. Fratzel, *Biophys. J.*, 1995, **68**, 1661.
- 59 V. Ottani, D. Martini, M. Franchi, A. Ruggeri, and M. Raspanti, *Micron*, 2002, **33**, 587.
- 60 D. J. S. Hulmes, *J. Struct. Biol.*, 2002, **137**, 2.
- 61 B. L. Trus and K. A. Piez, *Nature*, 1980, **286**, 300.
- 62 D. J. S. Hulmes and A. Miller, *Nature*, 1979, **282**, 878.
- 63 D. F. Holmes, C. J. Gilpin, C. Baldock, U. Ziese, A. J. Koster, and K. E. Kadler, *Proc. Natl. Acad. Sci. U. S. A.*, 2001, **98**, 7307.
- 64 N. Sasaki, N. Shukunami, N. Matsushima, and Y. Izumi, *J. Biomech.*, 1999, **32**, 285.
- 65 D. A. D. Parry, *Biophys. Chem.*, 1988, **29**, 195.
- 66 R. D. B. Fraser and T. P. McRae, *J. Mol. Biol.*, 1987, **193**, 115.
- 67 S. K. Sarkar, C. E. Sullivan, and D. A. Torchia, *Biochemistry*, 1985, **24**, 2348.
- 68 M.-M. Giraud-Guille, L. Besseau, and R. Martin, *J. Biomech.*, 2003, **36**, 1571.
- 69 T. Gutschmann, G.E. Fantner, M. Venturoni, A. Ekani-Nkodo, J.B. Thompson, J.H. Kindt, D.E. Morse, D. Kuchnir Fygenon, P.K. Hansma, *Biophys. J.*, 2003, **84**, 2593.
- 70 B. Öbrink, *Eur. J. Biochem.*, 1972, **25**, 563.
- 71 D. F. Holmes, R. B. Watson, J. A. Chapman, and K. E. Kadler, *J. Mol. Biol.*, 1996, **261**, 93.
- 72 F. H. Silver and R. L. Trelstad, *J. Biol. Chem.*, 1980, **255**, 9427.
- 73 D. F. Holmes, M. J. Capaldi, and J. A. Chapman, *Int. J. Biol. Macromol.*, 1986, **8**, 161.
- 74 B. R. Williams, R. A. Gelman, D. C. Poppke, and K. A. Piez, *J. Biol. Chem.*, 1978, **253**, 6578.
- 75 W. D. Comper and A. Veis, *Biopolymers*, 1977, **16**, 2113.
- 76 M. C. Goh, M. F. Paige, P. Markiewicz, I. Yadegari, and M. Edirisinghe, *ACS Symp. Series*, 1998, **694**, 94.
- 77 M. A. Lauffer, 'Entropy-driven processes in biology : polymerization of tobacco mosaic virus protein and similar reactions', Springer-Verlag, Berlin, 1975.
- 78 J. Parkinson, K. E. Kadler, and A. Brass, *Phys. Rev. E*, 1994, **50**, 2963.
- 79 J. Parkinson, K. E. Kadler, and A. Brass, *J. Mol. Biol.*, 1994, **247**, 823.
- 80 N. Kuznetsova and S. Leikin, *J. Biol. Chem.*, 1999, **274**, 36083.
- 81 K. E. Kadler, Y. Hojima, and D. J. Prockop, *Biochem. J.*, 1990, **268**, 339.
- 82 G. C. Wood, *Int. Rev. Conn. Tiss. Res.*, 1964, **2**, 1.
- 83 M. F. Paige, J. K. Rainey, and M. C. Goh, *Micron*, 2001, **32**, 341.
- 84 M. F. Paige and M. C. Goh, *Micron*, 2001, **32**, 355.
- 85 K. Kühn, *Coll. Rel. Res.*, 1982, **2**, 61.
- 86 B. d. C. Vidal, *Micron*, 2003, **34**, 423.
- 87 B. d. C. Vidal, *C.R. Acad. Sci. Paris - Life Sciences*, 1995, **318**, 173.

- 88 K. A. Hansen, J. A. Weiss, and J. K. Barton, *Trans. ASME*, 2002, **124**, 72.
 89 L. J. Gathercole and A. Keller, *Colston Papers*, 1975, **26**, 153.
 90 N. Sasaki and S. Odajima, *J. Biomech.*, 1996, **29**, 655.
 91 F. H. Silver, J. W. Freeman, I. Horvath, and W. J. Landis, *Biomacromol.*, 2001, **2**, 750.
 92 H. Hofmann, T. Voss, and K. Kühn, *J. Mol. Biol.*, 1984, **172**, 325.
 93 H. Utiyama, K. Sakato, K. Ikehara, T. Setsuiye, and M. Kurata, *Biopolymers*, 1973, **12**,
 53.
 94 K. Misof, G. Rapp, and P. Fratzl, *Biophys. J.*, 1997, **72**, 1376.
 95 P. Fratzl, K. Misof, I. Zizak, G. Rapp, H. Amenitsch, and S. Bernstorff, *J. Struc. Biol.*,
 1997, **122**, 119.
 96 J. B. Thompson, J. H. Kindt, B. Drake, H. G. Hansma, D. E. Morse, and P. K.
 Hansma, *Nature*, 2001, **414**, 773.
 97 K. E. Kadler, D. F. Holmes, H. Graham, and T. Starborg, *Matrix Biol.*, 2000, **19**, 359.
 98 N. Sasaki and S. Odijima, *J. Biomech.*, 1996, **29**, 1131.
 99 W. Folkhard, E. Mosler, W. Geercken, E. Knörzner, H. Nemetschek-Gansler, and T.
 Nemetschek, *Int. J. Biol. Macromol.*, 1987, **9**, 169.
 100 A. Schwartz, P. H. Geil, and A. G. Walton, *Biochim. Biophys. Acta*, 1969, **194**, 130.
 101 H. Riedl and T. Nemetschek, *Sitzungsber. Heidelberg Akad. Wiss. Math-Naturwiss.*, 1977,
5, 217.
 102 M. Raspanti, *Arch. Hist. Cytol.*, 2002, **65**, 37.
 103 D. H. Elliott, *Biol. Rev.*, 1967, **40**, 392.
 104 E. Gentleman, A. N. Lay, D. A. Dickerson, E. A. Nauman, G. A. Livesay, and K. C.
 Dee, *Biomaterials*, 2003, **24**, 3805.
 105 D. W. L. Hukins, in 'Chapter 8: Collagen orientation', ed. D. W. L. Hukins, Verlag,
 Weinheim, 1984.

CHAPTER 3

Tensile Testing of Single Collagen Fibrils, an Atomic Force Microscopy Approach

"Nil tam difficile est quin quarendo investigari possiet." - Horatius

(Abstract)

The combination of an atomic force microscope (AFM) with an inverted optical microscope was used to perform force spectroscopy measurements on single collagen fibrils. Using glass substrates partly coated with Teflon®, fibrils were attached with one end to the AFM cantilever and the other to the glass surface by epoxy glue droplets. The epoxy glue provides physical and covalent bonds of the fibril with the cantilever at one end and the glass surface at the other end. Force-distance AFM analysis of the glue revealed that this material was sufficiently stiff to perform adequate measurements with the fibril. By moving the fibril away from the surface and simultaneous monitoring of the deflection of the cantilever, which is a measure for the force, stress-strain curves of individual collagen fibrils were obtained.

3.1 Introduction

Collagen is the most abundant protein in mammals.^{1, 2} Despite extensive investigation of its macroscopic mechanical properties over four decades, it is still not possible to explain the mechanical properties from its underlying structure. Collagen fibrils are the principal, tensile stress-bearing components of connective tissue.³ The fibril has a diameter of ~ 100 -500 nanometre with a length up to the millimetre range⁴, which makes visualisation by optical microscopy and micro-manipulation possible. It has been shown that collagen fibrils can be easily micro-manipulated in an aqueous environment using glass micro-needles.⁵ For force spectroscopy experiments on single collagen fibrils, they have to be fixed with one end to a substrate and the other end to a force transducing element (FTE) (see Fig. 3.1).

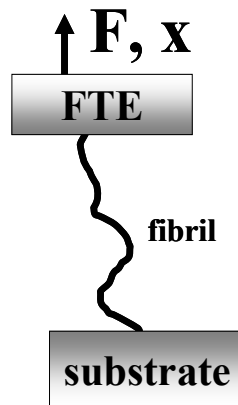


Figure 3.1 Schematic representation of a force spectroscopy experiment of a single collagen fibril.

Three important factors needed in this approach are: the force transducing element (FTE), the fixation procedure and modification of the substrate to enable micro-manipulation.

3.2 Force spectroscopy methods

Many approaches for force spectroscopy of microscopic structures have been developed. Three of these methods will be highlighted and their applicability for mechanical testing of collagen fibrils will be discussed.

In force spectroscopy, a trade-off has to be made between the dynamic range for measuring the force using the instrument, and the noise level. The required dynamic range is governed by the mechanical properties of the sample of interest and limitations of the applied instrument. The noise consists of electronic noise and the noise due to Brownian motion of the FTE, which is related to the spring constant of the used cantilever. By matching the estimated spring

constant of the fibril with that of the FTE, the noise level can be minimized and a linear response of the FTE can be obtained.

The force at break of a single collagen fibril was estimated at $30 \mu\text{N}$.⁶ From the stress at break value of non-treated self-assembled collagen fibres⁷, which are composed of aggregated collagen fibrils, the stress at break of a single collagen fibril of 200 nm in diameter was estimated at $0.15 \mu\text{N}$.⁸ When a fibril with a length of 100 μm is assumed to rupture at the same extension of the self-assembled fibre (24% strain), the spring constant of the fibril can be calculated from both estimations to be in the range of 10^{-3} to $10^0 \text{ N}\cdot\text{m}^{-1}$. The dynamic force range to determine the rupture force of a fibril at a suitable signal to noise ratio should be 10^{-5} to 10^{-8} N . The extension should range between 10^{-8} and 10^{-4} m . Three examples of force spectroscopy methods will be discussed below.

- Atomic force microscopy (AFM) has originally been developed for imaging single atoms and molecules on a surface.⁹ Its applications nowadays have been extended to force spectroscopy and nanomanipulation. Typical spring constants of the AFM cantilever range between 10^{-2} and $10^1 \text{ N}\cdot\text{m}^{-1}$.¹⁰
- Optical tweezers are based on the principle that micron-sized spheres in the focal point of a laser can be manipulated by movement of the focal point. When a fibrous protein is fixed between two beads, one bead can be held with an optical trap, while the second one is manipulated by a micropipette, for example. The optical trap is used to measure the force exerted on the protein, while the other bead is manipulated via the micropipette.^{10, 11} Typical spring constants related to this technique are 10^{-6} to $10^{-4} \text{ N}\cdot\text{m}^{-1}$.
- Glass needles (and micropipettes) have been applied in micro-manipulation systems, especially for cells (*in vitro* fertilization, for instance), but also in force spectroscopy. The bending of a glass needle with a known spring constant is monitored using an optical microscope. From the bending of the needle and the distance to the second fixation point, the stress-strain curve of a material fixed between the needle and a substrate can be calculated. Typical spring constants are 10^{-4} to $10^{-2} \text{ N}\cdot\text{m}^{-1}$, but values up to $10^2 \text{ N}\cdot\text{m}^{-1}$ are feasible by increasing the thickness of the glass needle.¹²

The spring constant of the fibril matches best with those of AFM cantilevers and glass needles. Application of optical tweezers is not suitable, because of the low spring constant of 10^{-6} to $10^{-4} \text{ N}\cdot\text{m}^{-1}$. The AFM methodology was chosen, because this facilitated high resolution imaging and mechanical testing within one set-up. Imaging of the fibril using AFM or electron microscopy (EM) techniques is essential to obtain the diameter of the fibril and to study its morphology.

When forces act on the AFM tip, the cantilever bends. This causes a deflection of the laser beam reflected from the back of the cantilever. The deflection is determined using a position detector (see Fig 3.2). Preliminary experiments showed that an AFM cantilever with a spring constant of $0.5 \text{ N}\cdot\text{m}^{-1}$ could be attached to a collagen fibril.

Unfortunately, it was found that the dynamic range of the position detector was too low to obtain a linear response. Therefore, a cantilever with a spring constant of $30\text{-}60\text{ N}\cdot\text{m}^{-1}$ was used. Using this cantilever, the focus of the laser bundle on the position detector remained in the linear region of the detector under the expected deflection range of the cantilever.

3.3 AFM set-up

A set-up containing an inverted microscope with an AFM on top of it was provided with a micrometer. The AFM tube is limited to a maximal extension of $4.0\text{ }\mu\text{m}$. Larger distances between the AFM tip and the surface are enabled by tilting the AFM head with a manual setscrew. The distance between the tip and the surface can now be determined using the micrometer, which is accurately measuring the height (Δh in Fig. 3.2) at the position of the setscrew. The AFM on top of the optical microscope blocked the light needed for illumination of the sample. An optical fibre was fixed under the AFM to illuminate the sample. A schematic representation of the used set-up is shown in Fig. 3.2.

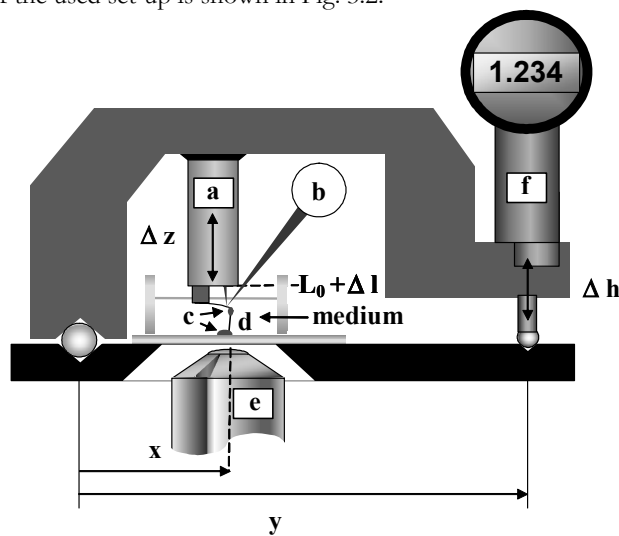


Figure 3.2 Schematic representation of the set-up containing an AFM on top of an inverted microscope. The fibril **d** was fixed via glue droplets **c** to the surface and to the cantilever. Increase of the distance between the AFM tip and the surface was performed over short ranges via tube **a** over lengths Δl , while the deflection of the cantilever was monitored via a laser at position detector (quadrant detector) **b**. The attached fibril was monitored using the inverted microscope of which objective **e** is shown. An optical fibre was used for illumination of the sample. With the lever rule $x:y$ the movement of the AFM tube over distances Δl is correlated to the height change Δh of the setscrew as determined by using the depicted micrometer **f** above it.

The travel of the AFM tube is linear with the applied voltage only for a distance of 530 nm. When the extension was increased, a non-linear deformation occurred. During forward and backward movement of the tube hysteresis was observed. In order to characterise this, a second position detector (quadrant detector) was positioned at the end of the AFM tube. A laser was focused on the detector to determine the z-position of the AFM tube independently. The difference between the applied saw-tooth function and the travel of the AFM was determined and used to correct the position of the base of the cantilever as a function of the applied voltage. Similarly, the response of the tube in the z-direction was determined at 530 nm·V⁻¹. Using a grid with known dimensions, the x and y movements of the AFM tube were calibrated as a function of the applied voltage. A response of 1600 nm·V⁻¹ in the x and 1938 nm·V⁻¹ in the y direction was obtained.

Collagen fibrils have typical lengths up to hundreds of micrometers. With an estimated strain at break of 10%, the AFM tip must at least be able to move over 25 μm distance. To enable the end-to-end distance of the fibril to exceed the maximal extension of the piezo tube of 4.0 μm, a setscrew was mounted as shown in Fig. 3.2. To accurately determine the extension of the AFM over larger distances by manual movement of the AFM head, a micrometer was used. The distance between AFM tip and surface as determined by the micrometer was calibrated. This was performed by calculating the ratio between translation of the setscrew (as shown by the micrometer) and the translation of the AFM tube for the same deflection signal. The ratio between the deflection sensitivity of both methods was calculated at 21.5 : 1.

3.4 Sample preparation

3.4.1 Fixation approach

The fixation of the fibril by one end to the force transducing element (FTE) and the other end to a substrate requires a method, which provides sufficient bonding strength and a high stiffness of the glue. Fixation can be performed using covalent and non-covalent bonds. Force spectroscopy experiments have shown that the force required for stretching of polymer chains ranges from ~0.1 to ~20 pN, whereas the force required for receptor-ligand bond dissociation falls in the range from ~2 to ~200 pN.¹³ The limiting force that can be determined using AFM, due to Brownian motion is ~10 pN. The force at break of the collagen fibril is estimated in the order of 0.15 μN⁸, which is 3-5 orders of magnitude higher than the reported bond dissociation forces. The fixation of a fibril therefore requires a large number of interactions. One way to provide this is by microscopic glue droplets, which should ensure a good fixation of the fibril to the substrate and FTE surface.

The glue has to meet the following demands: easy handling, sufficient time for manipulation (1 h), fixation time at room temperature within a few hours, stability when immersed in aqueous media, high stiffness and good binding of the glue with the fibril, substrate and cantilever. A number of glue types was examined for their applicability.

Cyanoacrylate glue was found to be unsuitable because of the rapid polymerization time (a few seconds) and its susceptibility to hydrolysis. Methacrylates that can be cured by UV-light (e.g. hydroxyethylmethacrylate) are inadequate because of possible chain scission and/or cross-linking of the fibril during the exposure to high intensity UV light, while curing the glue.^{14, 15} The most suitable choice was a two-component epoxy glue. This consists of a bis-epoxide and a tris-amine component that should be thoroughly mixed prior to use. The two components react via a ring opening reaction of the epoxide with the formation of an amine bond. The free amine functional groups of the collagen fibril can also participate in this reaction, resulting in a physically as well as chemically bound fibril. Possibly, also the hydroxyl functional groups of the glass substrate can participate in this reaction. The chemical reactions involved during the formation of covalent bonds between the glue, glass substrate and protein surface are schematically shown (Fig. 3.3).

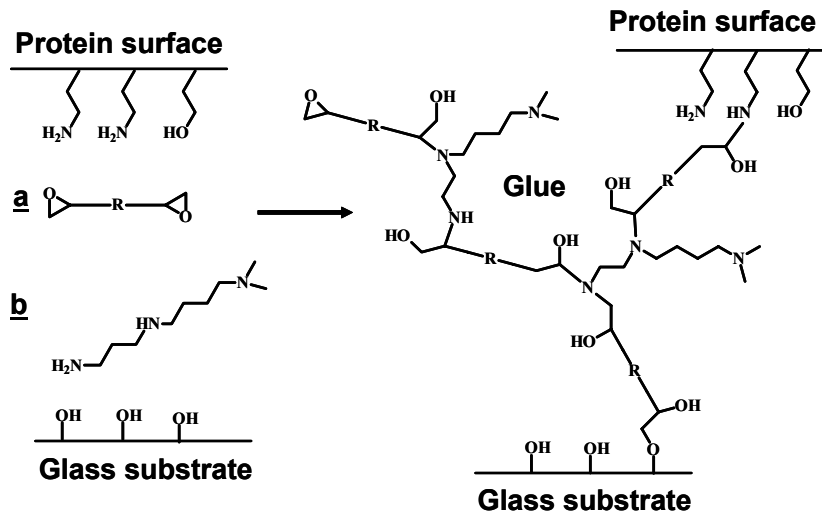


Figure 3.3 Chemical reactions involved in fixation of the glue and the attachment of the glue to the glass substrate and collagen fibril surface.

A schematic representation of the fibril, fixed in glue, is shown in Fig. 3.4.

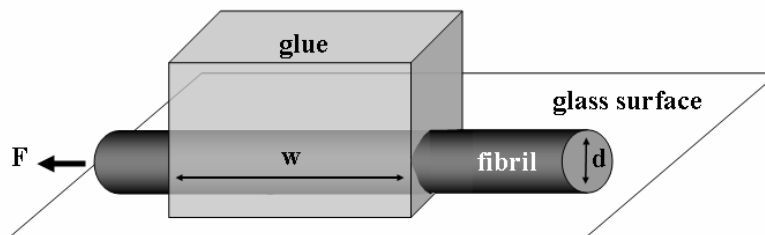


Figure 3.4 Schematic representation of fibril fixed in glue on a glass surface.

For a fibril with a diameter of 100 nm and a length w covered in epoxy glue, a contact area between glue and fibril was estimated to be at least half the surface area, because maximally half the fibril outer surface is in contact with the glass surface. A typical glue drop size was 50 μm in diameter, from which the area in contact with the fibril was calculated by:

$A = \frac{1}{2} \cdot (\pi \cdot d \cdot w)$. This value was equal to $7.9 \times 10^{-12} \text{ m}^2$. The force at break of the fibril was estimated to be 0.15 μN .⁸ When this force is applied to a surface of $7.9 \times 10^{-12} \text{ m}^2$ a shear stress of 0.18 MPa was calculated via: $\sigma = F \cdot A^{-1}$, which was well below the 18 MPa shear stress of the glue in aqueous media as reported by the supplier.¹⁶ This glue type therefore is expected to withstand this stress of 0.18 MPa. The glue can be manipulated for two hours and fixation is complete within 24 hours.

After fixation of the fibril to a glass surface the fibril should be fixed to the AFM cantilever. Therefore, a second surface is needed, to which the glue does not adhere. By coating part of the glass surface with Teflon, a non-adhesive surface is provided. A good interaction was needed between the glue and the fibril end located on Teflon. A cantilever was used from which the tip was removed by focused ion beam. The fixation procedure of one fibril end to the glass substrate and the other end to the AFM tip is schematically shown in Fig. 3.5.

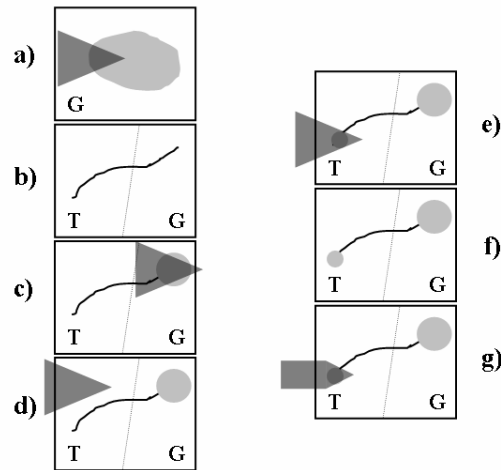


Figure 3.5 Schematic representation of the fixation of the fibril to glass and subsequently to the AFM cantilever on Teflon. The epoxy glue is thoroughly mixed and a triangular cantilever ($k: 0.5 \text{ N} \cdot \text{m}^{-1}$) is dipped into the glue **a)**. In **b)** a suitable fibril is selected, of which one end is located on the glass substrate and the other end on the Teflon coating. A drop of glue (diameter: $\sim 50 \mu\text{m}$) is deposited on the fibril end on glass in **c)**, then the cantilever is moved to the other fibril end located on Teflon in **d)**. A second deposition with the same cantilever is made on the fibril end located on Teflon in **e)**. The second drop has a diameter of $\sim 10 \mu\text{m}$ as shown in **f)**. The triangular cantilever is replaced for a rectangular one with a higher spring constant ($k: \sim 30 \text{ N} \cdot \text{m}^{-1}$) of which the tip was removed to provide a larger interaction surface for the glue droplet to adhere to. Finally, in **g)** the cantilever is brought in contact with the glue droplet on Teflon and left there for fixation for 18h.

After the fixation the fibril is carefully lifted from the surface as shown in Fig. 3.6.

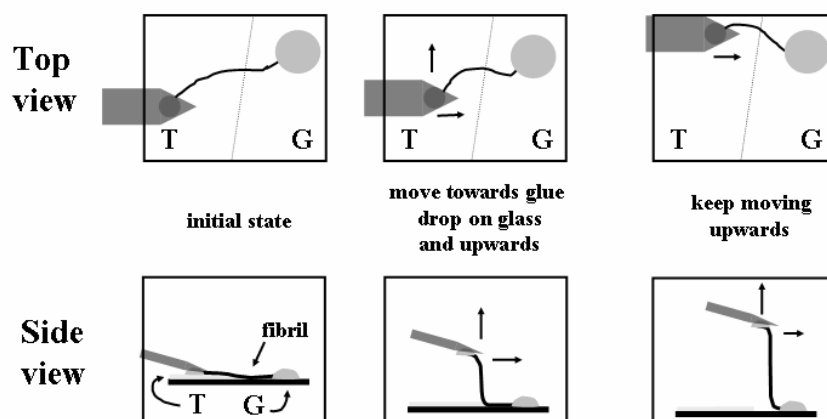


Figure 3.6 Schematic representation of the lift of the fibril after fixation from the Teflon-coated glass surface.

The fixation of the fibril to the cantilever and the glass/Teflon substrate was verified by lifting the fibril from the surface to a height corresponding to the length of the fibril (typically 100 μm), after which the deflection signal is determined. The stiffness of the glue droplet on the cantilever that fixed one fibril end was verified by recording a force-distance curve (Fig. 3.7b). This also defined the zero point of the height.

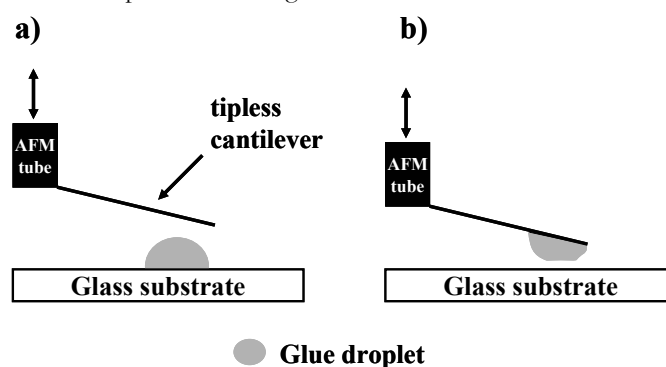


Figure 3.7 (a) Test of stiffness of a glue droplet on a glass substrate. (b) Test of stiffness of a glue droplet underneath the cantilever. Both experiments were performed using a tipless cantilever.

The shape of the force-distance curve provides information on the visco-elastic properties of the glue droplet, which is indicative of the fixation state. Deformation points to incomplete polymerization of the glue. It is essential to mix both components of the glue intensively for 15 min before applying it to the surface. In Fig. 3.8 two examples of part of a force-distance curve are shown of glue droplets showing proper and poor fixation, while the cantilever is in continuous contact with the surface (schematically shown in Fig. 3.7a).

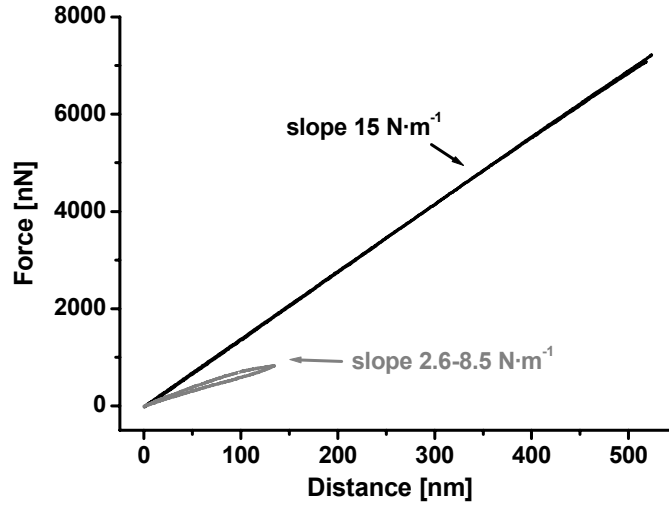


Figure 3.8 Part of the force-distance curve of a cantilever in continuous contact with a glue drop as shown in figure 3.7a. Loading rate top curve: $520 \text{ nm}\cdot\text{s}^{-1}$, bottom curve: $200 \text{ nm}\cdot\text{s}^{-1}$, tipless cantilever k : $27.6 \pm 1.8 \text{ N}\cdot\text{m}^{-1}$, epoxy glue Araldite® Precision, top 15 min intensive mixing of two components, bottom 2 min stirring of two components.

The stiffness of the glue should exceed that of the collagen fibril to exclude large deformation of the glue under the applied loads. From the force-distance curve of the fixed glue (Fig. 3.8, top curve) a stiffness of $15 \text{ N}\cdot\text{m}^{-1}$ was calculated. From the spring constant of the glue and the spring constant of the fibril a combined spring constant can be calculated using formula 3.1.

$$\frac{1}{k_{comb}} = \frac{1}{k_{fibril}} + \frac{1}{k_{cant.}} \quad (3.1)$$

With an estimated spring constant of the fibril between 0.1 and $1 \text{ N}\cdot\text{m}^{-1}$ as calculated in section 3.2, the combined spring constant will be between 0.099 and $0.938 \text{ N}\cdot\text{m}^{-1}$, as calculated according to formula 3.1. Therefore, the contribution of the glue to the stress-strain behaviour of the fibril will be almost 7%, which is negligible.

3.4.2 Teflon coating of glass substrate and collagen deposition

To carry out the desired measurements, a collagen fibril of good quality can be fixed firmly to a substrate with one end and the other end to the AFM cantilever. To achieve fixation of the fibril the following procedure was developed. First, fibrils were deposited on a suitable surface. In principle, a glass surface can be used for the attachment of one end of a fibril using an appropriate glue.

An excellent adhesion of the glue to the glass surface and fibril is essential and the glue should have adequate mechanical properties, which do not influence mechanical measurements of the fibrils. Furthermore, the other end of the fibril has to be attached to the cantilever using the same type of glue. Therefore, a droplet of glue has to be transferred from the surface to the cantilever. With the cantilever containing a droplet of glue, the other end of the fibril has to be picked up from the surface. This cannot be achieved using a glass surface, because the glue droplet at the cantilever will also stick to the glass surface. Therefore, a surface is required, which allows transfer of the fibril connected to the cantilever from the surface. The surface should possess a very low adhesion to the glue. In the previous discussion it was already mentioned that epoxy glue fulfils these requirements. The whole attachment procedure can thus be performed by using a glass surface, which is partly coated by Teflon. A sharp border between Teflon and glass is essential, with a transparent Teflon layer. Furthermore, a fibril should be positioned in such a way that part of the fibril is located on the glass surface, and the other part on the Teflon surface.

Using dispersions of collagen type I with a concentration of $20 \mu\text{g}\cdot\text{ml}^{-1}$ allowed the formation of isolated collagen fibrils, that were sufficiently long and homogeneous, as shown with optical microscopy, AFM and SEM.

Different procedures for coating glass with a fluorocarbon layer were evaluated. The boundary between the coating and the glass surface should be sharp (maximally $25 \mu\text{m}$ and detectable by optical microscopy). Teflon can be deposited by scratching a glass substrate with a heated Teflon stick.¹⁷ Teflon can also be applied from a spray can, with part of the surface covered by Scotch tape. After drying, the tape is removed leaving a blank surface and a coated area. An alternative method for coating glass is dip coating in (tridecafluoro-1,1,2,2-tetrahydrooctyl)-dimethylchlorosilane (TCFS), a fluorinated siloxane that forms a monolayer on glass with a high contact angle.^{18, 19} A fourth method consists of dip-coating glass in a Teflon AF solution.²⁰

The coated glass surfaces were studied by optical microscopy, AFM and SEM to determine the height of the coating, the width of the boundary between coating and substrate and its transparency. The Teflon deposition by scratching or spraying led to undefined layers, without sharp boundaries. Coating with TCFS resulted in a thickness gradient of the fluorinated surface over millimetres in width between bare glass and the coated area, probably due to diffusion of the volatile reagent. Dip-coating with Teflon AF resulted in a layer which was immediately visible. By AFM and SEM a layer thickness of $500 \pm 200 \text{ nm}$ and a boundary width of $6 \pm 2 \mu\text{m}$ was determined. Optical microscopy revealed a boundary width $<5 \mu\text{m}$. The hydrophobicity of the coated glass surface was determined by static water drop contact angle measurements. The contact angles of the bare glass and Teflon coated area were: $26 \pm 1^\circ$ (glass) and $117 \pm 3^\circ$ (Teflon), respectively.

The boundary between the glass surface and the Teflon coating was imaged by AFM in contact mode (Fig. 3.9a and 3.9b). Similar results were obtained by imaging in tapping mode. Collagen fibrils were deposited as discussed before on the partly Teflon coated glass discs from a dispersion containing $\sim 20 \mu\text{g}\cdot\text{ml}^{-1}$ of collagen. The resulting surface was imaged using contact mode AFM (Fig. 3.9a).

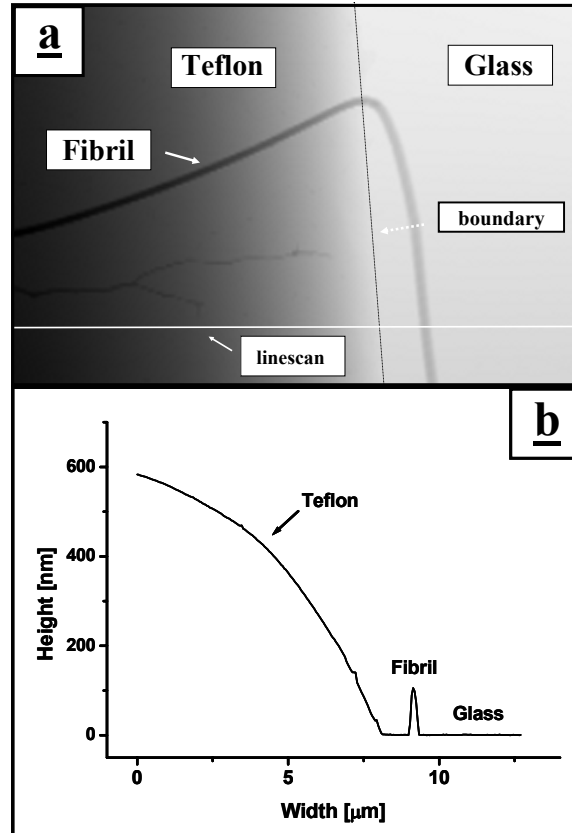


Figure 3.9 a) Contact mode AFM image of a collagen fibril crossing the Teflon/glass boundary. Image obtained at ambient conditions. Image size: $12.8 \times 7.8 \mu\text{m}$, cantilever k : $0.1 \text{ N}\cdot\text{m}^{-1}$, contact force $\sim 60 \text{ nN}$. Fibril diameter: $100 \pm 10 \text{ nm}$, Teflon coating thickness: $\sim 600 \text{ nm}$, boundary width to maximum height of Teflon: $\sim 8 \mu\text{m}$. **b)** Line-scan of contact mode AFM image, taken from top image. In the line scan profile the Teflon coating on glass, with a fibril located on the glass area can be designated.

After following the procedure presented in Figs. 3.5 and 3.6, an example of a successful fixation of one end of a collagen fibril to the glass substrate and of the other end to the AFM cantilever is shown in Fig. 3.10. In this case, a tip crash caused the cantilever to break off, without rupturing the fibril.

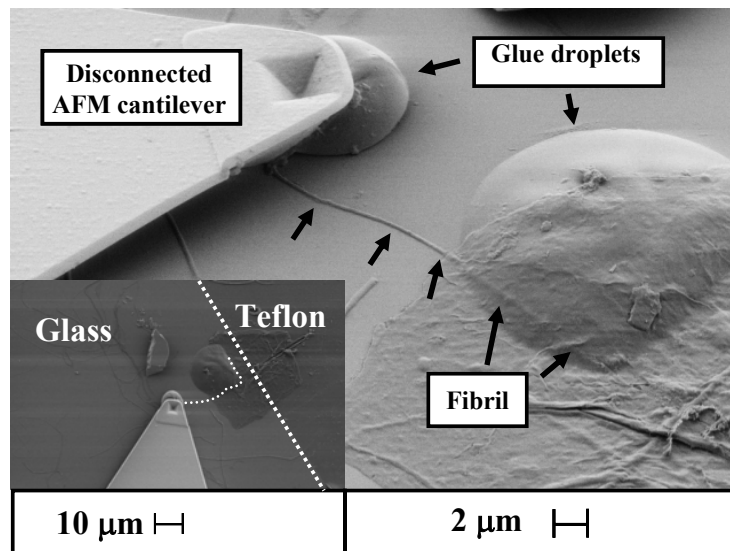


Figure 3.10 SEM image of a collagen fibril fixed between the AFM cantilever and the glass substrate by two glue droplets, magnification 2800 \times . In the inserted image at lower magnification (1000 \times) the Teflon/glass boundary is shown.

3.5 Tensile testing

Tensile testing of a single collagen fibril (fibril N1) of 214 ± 12 nm diameter and 119.0 ± 0.5 μm initial length was possible after fixation of the fibril to the AFM cantilever and the glass surface. After verification of the stability of the glue, the fibril was lifted to a height corresponding to a deflection signal of the AFM cantilever exceeding twice the noise level (~ 4 nN). This height was used as the initial fibril length in strain calculations. Possible small variations of the position of the fibril in the glue droplet on the glass surface in determining the total length of the fibril were assumed to be negligible. The fibril was extended over 2.3 μm from its initial length using the AFM tube. The resulting deflection data is shown in Fig. 3.11.

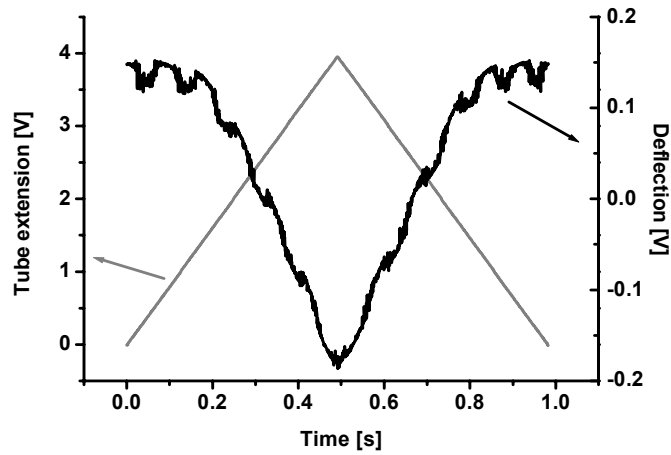


Figure 3.11 Deflection data from the tensile test of a single collagen fibril, obtained at ambient conditions. Cantilever k : $29.3 \pm 1.9 \text{ N}\cdot\text{m}^{-1}$, AFM tube extension rate: $8.0 \text{ V}\cdot\text{s}^{-1}$.

The noise pattern superimposed on the deflection signal is caused by an interference effect of the AFM laser, which could not be eliminated. The extension of the AFM tube is calculated after correction for non-linear behaviour and hysteresis of the AFM tube. The force-extension curve has been calculated from the corrected extension data and the cantilever deflection (Fig. 3.12).

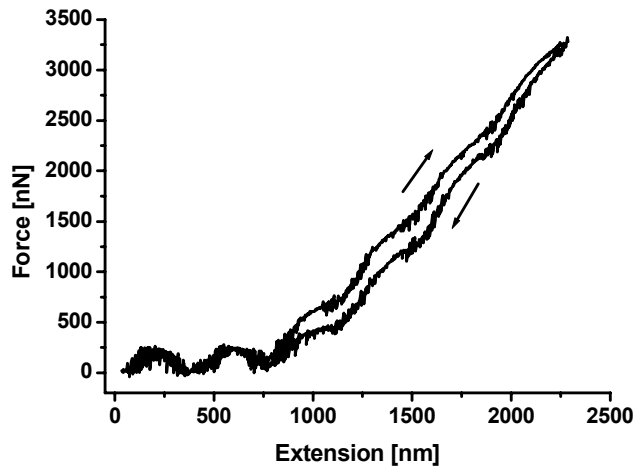


Figure 3.12 Force-extension curve of a single collagen fibril obtained at ambient conditions. Cantilever k : $29.3 \pm 1.9 \text{ N}\cdot\text{m}^{-1}$, extension rate: $4.6 \mu\text{m}\cdot\text{s}^{-1}$.

The strain was determined as the increase of the length with respect to the original length (formula 3.2) and the stress was calculated from the cross-sectional area of the fibril assuming a round shape as shown from formula 3.3.

$$\varepsilon = \frac{100\% \cdot (L - L_0)}{L_0} \quad (3.2)$$

$$\sigma = \frac{F}{A} \quad (3.3)$$

in which $A = (\frac{1}{4}\pi) \cdot d^2$
with d = diameter fibril

The initial 600 nm extension of the AFM tube does not result in a change in force and this region was discarded for the transformation of the force-distance results to the stress-strain curve (Fig. 3.13).

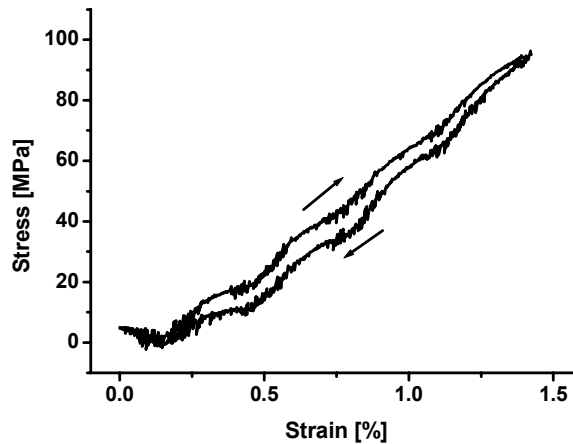


Figure 3.13 Stress-strain curve of a single collagen fibril obtained at ambient conditions. Cantilever k : $29.3 \pm 1.9 \text{ N}\cdot\text{m}^{-1}$, extension rate: $4.6 \mu\text{m}\cdot\text{s}^{-1}$.

The analysis of the mechanical properties of this collagen fibril will be discussed in chapter 4.

3.6 Conclusions

An AFM was positioned on top of an inverted microscope and a setscrew was used to tilt the head and thereby change the distance between the base of the cantilever and the surface. Calibration of the displacement of the AFM tube yielded a correction function for its non-linear behaviour and hysteresis. The setscrew was calibrated to enable controlled movement of the AFM head at distances over $4.0 \mu\text{m}$. Tensile testing of a single collagen fibril was enabled by fixing a fibril between a substrate surface and an AFM tip.

The fixation of the fibril was performed using epoxy glue droplets. The stiffness of the glue was much larger than that of the fibril and will not have to be taken into account when measuring the mechanical behaviour of the fibril. An apparent spring constant for the glue was calculated from the force-distance curve of the cantilever on a glue droplet, showing that the contribution of the glue to the stress-strain curve of the collagen fibril was negligible.

The interaction between the glue and the fibril is essential for a good fixation. Sufficient wetting of the fibril by the glue and covalent bonds between glue and fibril are expected. This was underlined by macroscopic tensile testing of self-assembled collagen fibres²¹ immersed in aqueous conditions, showing no displacement of the fibre fixed in the same epoxy glue.

The glass substrate was partially dip-coated with Teflon to obtain a bifunctional surface. On the Teflon-coated glass surface, collagen fibrils were deposited to an optimal density to enable micro-manipulation. Fibrils with one end located on the uncoated glass surface and the other end at the Teflon-coated area were fixed between the glass and the AFM tip using epoxy glue.

3.7 Acknowledgments

M.A. Smithers and A.M. Otter (Mesa⁺ Institute for Nanotechnology, University of Twente) are acknowledged for performing SEM analysis of the surfaces. F.B. Segerink (Optical Techniques group, Faculty of Science and Technology, University of Twente) is acknowledged for removal of the cantilever tips by FIB.

3.8 Experimental

3.8.1 Materials

The following materials have been applied: concentrated sulphuric acid (~96 w%), hydrogen peroxide (~30 w%) and concentrated hydrochloric acid (~37 w%) were obtained from Merck, Darmstadt, Germany. Acetone and toluene (AR stabilized) were obtained from Biosolve, Valkenswaard, the Netherlands. Phosphate buffered saline solution (PBS, B. Braun, Melsungen, Germany) at pH 7.4 containing 140 mM NaCl, 13 mM Na₂HPO₄ · 2H₂O and 2.5 mM NaH₂PO₄ · H₂O was used as received. (Tridecafluoro-1,1,2,2-tetrahydrooctyl)-dimethylchlorosilane was obtained from ABCR, Karlsruhe, Germany. Teflon spray TF 089 was obtained from CFS Products, Goes, the Netherlands. A Teflon stick (dimensions approximately: 10 x 2 x 1 cm) was obtained from Rubber b.v., Hilversum, the Netherlands.

A Perspex® ring (inner diameter: 20 mm, height: 4 mm and thickness: 3 mm) was prepared at the workshop of the Faculty of Science and Technology, University of Twente.

AFM images were analyzed using the program SPIP 1.9212, details at www.imagemet.com. The Mitutoyo ID-C112B micrometer was obtained from Mitutoyo, Veenendaal, the Netherlands.

3.8.2 Methods

Cleaning of glass discs

The glass discs (diameter: 15 mm, thickness: 0.3 mm, Knittel Gläser, Braunschweig, Germany) were immersed for 5 min in a mixture of 70 vol% of concentrated sulphuric acid and 30 vol% of a 30% solution of hydrogen peroxide. Afterwards, the discs were washed with demineralised water five times (10 min each), until the rinse water reached neutral pH. Subsequently, the discs were washed three times successively in acetone (5 min each), three times in toluene (5 min each) and stored under toluene. Prior to use the discs were dried at 130°C for 14 h.

Preparation of Teflon coated glass discs

The cleaned glass discs were manually partly dip-coated in a 6 w% solution of Teflon AF 1601S in Fluorinert® FC-75 (Dupont, Wilmington, DE) and dried horizontally for 14 h at ambient conditions under a cover.

Preparation of collagen dispersion

Bovine Achilles tendon collagen type I (3.1 g) obtained from Sigma-Aldrich (Steinheim, Germany) was swollen in hydrochloric acid (333 ml, 0.01M) for 14 h at 0°C. The resulting slurry was shred for 10 min at 0°C at 11000 rpm using a Braun MR 500 HC blender (Braun, Kronberg, Germany). The temperature was monitored and maintained below 5°C. The dispersion was filtered through a 74 µm filter (Belco 200 mesh, Vineland, NJ, USA). The dispersion was stored at temperatures below 5 °C and discarded after 6 months.

Collagen coated glass/Teflon surfaces

Glass discs partly coated with Teflon were incubated individually (to prevent scratching on the coating) for 10 min in a diluted collagen dispersion containing 1 ml of a dispersion (3.1 g collagen in 333 ml 1M HCl) and 150 ml of PBS (total concentration of collagen: ~22 µg per ml). Subsequently, the surfaces were washed in PBS for 10 min and subsequently three times in demineralised water (10 min each). Finally, the discs were dried at ambient conditions for 14 h under a cover.

Selection of suitable fibrils

The coated discs were examined with the inverted optical microscope at a magnification of 400x. Fibrils that crossed the glass-Teflon boundary completely, with at least 20 µm of their length on Teflon and a minimal total length of 50 µm were selected. Other selection criteria were: no other fibrils present within 20 µm of the end on Teflon and the fibril must not show inhomogeneities. Fibrils with structural abnormalities (dots on the fibril and branches overlapping other fibrils), as visualized by optical microscopy at 400x magnification, were excluded. The longest specimen present in one sample were selected. The final selection was made after tapping or contact mode imaging with the AFM. Fibrils containing microscopic

surface inhomogeneities and large diameter changes along their length, as shown by AFM imaging, were also discarded.

Movement of fibrils over the Teflon surface

Single collagen fibrils located on Teflon can be moved after non-covalent sticking of the fibril to the cantilever (coated sharp microlevers MSCT AUHW, type F, $k = 0.5 \text{ N}\cdot\text{m}^{-1}$, Veeco, Cambridge, UK). At ambient conditions, the cantilever was pressed on top of the fibril to a force of around 200 nN and moved up and down over 5 μm distance until the fibril stuck to the cantilever due to non-covalent interactions. The fibril was lifted from the surface and moved to a different location. By pressing the cantilever with the adhering fibril on the surface at a force of around 200 nN, the fibril was redeposited at a new location. After this movement, the fibril can be imaged in tapping mode only. Because of possible tip contamination, the cantilever was exchanged.

Preparation of the AFM for imaging

The cantilever (coated sharp microlevers MSCT AUHW, type F, $k = 0.5 \text{ N}\cdot\text{m}^{-1}$, Veeco, Cambridge, UK) was mounted in a home-build AFM ²², which was positioned on top of an inverted microscope (Zeiss Axiovert, Sliedrecht, the Netherlands). The laser was aligned to the quadrant cell detector. The AFM is connected to the computer, where the program spm44 was used for imaging (spm44 was developed at the Biophysical Techniques group, Faculty of Science and Technology, University of Twente).

AFM imaging in contact mode - at ambient conditions only

After mounting the cantilever F ($k = 0.5 \text{ N}\cdot\text{m}^{-1}$) and aligning the laser to the quadrant cell detector, force-distance curves were recorded. The base of the cantilever was displaced in vertical direction over 530 nm at $530 \text{ nm}\cdot\text{s}^{-1}$ using a saw-tooth function. The adhesion force between surface and tip was determined from the force-distance curve. A schematic force-distance curve is shown (Fig. 3.14).

By decreasing the distance of the tip to the surface, the cantilever was brought in continuous contact with the surface. The deflection sensitivity [$\text{nm}\cdot\text{V}^{-1}$] of the AFM was determined from the amplitude of the deflection signal (p-p), while the tip was in continuous contact with the surface. The deflection sensitivity was calculated from the deflection signal and the tube extension. Contact mode imaging was performed by scanning an area with a maximal size of 15.2 by 18.4 μm (x,y) at a resolution of 256 by 256 pixels, with a line frequency of $\sim 10 \text{ Hz}$. The height of the fibril was determined from line scans obtained in a scan direction orthogonally to the fibril axis. The D-period was determined from line scans parallel to the fibril axis. Imaging in contact mode typically was performed with scan forces of 100-300 nN.

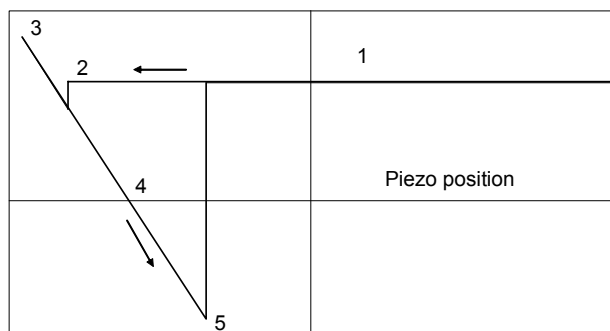


Figure 3.14 The deflection sensitivity was determined from the slope of line **3 - 5**, where the tip is in continuous contact with the surface. The full approach and retract curves as shown here consist of five regions. The tip approaches the surface between **1** and **2**. At some distance, the gradient of force overcomes the cantilever spring constant and the tip jumps into contact at **2**. Further movement up causes a deflection of the cantilever at **3**, during retraction the tip sticks usually much longer over **4** and snaps off when the spring constant overcomes the force gradient at **5**.^{23, 24}

AFM imaging in tapping mode - at ambient conditions and in aqueous media

Tapping mode is an imaging mode in which the tip is moved up and down close to its resonance frequency. Tapping mode leads to a large reduction in lateral forces during the imaging procedure.²⁵ Only at the lowest point of the sweep the tip is in contact with the surface. The reduction in amplitude due to the interaction is remained constant via a feedback loop that adjusts the vertical position of the tip.

At ambient conditions, a tapping frequency of ~ 105 kHz was used. The applied tapping amplitude was relatively high because a cantilever (type F, $k = 0.5 \text{ N}\cdot\text{m}^{-1}$) with a low spring constant was used. An amplitude of 400 to 800 nm was sufficient for the tip to escape from the contamination layer on the surface. The degree of the interaction with the surface is controlled by the set-point, which is equal to point 3 in Fig. 3.14. Typically, the reduction of the 'free' amplitude of the cantilever due to the interaction was set to 10-20 %. In tapping mode at ambient conditions a scan rate of 5-10 Hz was used.

When immersed in aqueous media, the resonance frequency for this cantilever has shifted to ~ 33 kHz. This is caused by an increase in effective mass and additional damping in the liquid. The applied amplitude was lower than at ambient conditions, because the interaction forces between the tip and surface are generally lower. The typical amplitude in liquid was around 50 nm. The applied amplitude reduction during scanning was 10-20 % of the 'free' amplitude. Tapping mode in liquid was performed at a scan rate of 2-5 Hz.

Determination of the full length of the collagen fibril

The height of the substrate was determined by bringing the cantilever in contact with the Teflon surface. Then, the fibril was lifted, until visually it was fully stretched without build-up of force. The length of the fibril (L_0 , see Fig. 3.15) was determined by extending the stretched fibril over 530 nm at 530 nm·s⁻¹ at increasing distance between the substrate and the cantilever, until a force value of 4 nN was observed. The noise due to Brownian motion of the cantilever with a typical spring constant of 30 N·m⁻¹ was 12 pN, according to the relation $F = (k_B \cdot T \cdot k)^{1/2}$, obtained from $\frac{1}{2} \cdot k_B \cdot T = \frac{1}{2} \cdot k \cdot x^2$ with $k = F \cdot x^{-1}$.

Swelling of the collagen fibril

The fibril was imaged using AFM tapping mode at ambient conditions using the cantilever with a low spring constant (coated sharp microlevers MSCT AUHW, type F, $k = 0.5$ N·m⁻¹, Veeco, Cambridge, UK). From one of the images, the fibril height was determined at five random locations. The heights were taken from line scans scanned orthogonally to the fibril axis. Then, demineralised water was added and the fibril was equilibrated for 30 min. The fibril was imaged again in tapping mode at the same location and from this image at five random locations the height of the swollen fibril was determined again. The degree of swelling S was calculated by the following formula (formula 3.4):

$$S = 100\% \cdot \frac{D_{wet} - D_{dry}}{D_{dry}} \quad (3.4)$$

From the images, obtained at ambient conditions and in demineralised water, the degree of swelling was found to be 73 ± 15 %.

Experimental set-up prior to fibril fixation

When a suitable fibril was located, its structure was imaged using AFM imaging in contact or tapping mode. The glass disc partially coated with Teflon and containing deposited collagen fibrils was glued to a microscope slide (size: 76 x 26 mm, 1 mm thick, Menzel-Gläser, Braunschweig, Germany) using epoxy glue with a hardening time of ~1 h (Araldite Rapid, Bostik Findley Ltd., Staffordshire, UK) on three locations, ensuring that a small gap of around 0.1 mm remained between the glass disc and the microscope slide, to provide optimal transmission of light. Around the disc a Perspex ring was fixed, using the same epoxy glue, permitting free movement of the AFM head during micro-manipulation experiments.

Fixation of a collagen fibril to the glass surface and AFM cantilever

The collagen fibril was fixed at one end to the surface of the glass disc by an epoxy glue droplet (Araldite Precision, Bostik Findley Ltd., Staffordshire, UK). The other end of the fibril was located on the Teflon coating, which enabled the selective fixation to the AFM cantilever with high stiffness and a rectangular shape ($k = 32$ - 62 N·m⁻¹, NCH-W Nanosensors, Darmstadt, Germany), via a second glue droplet.

The glue droplets were deposited by another AFM cantilever with a triangular shape (coated sharp microlevers MSCT AUHW, F, $k = 0.5 \text{ N}\cdot\text{m}^{-1}$, Veeco, Cambridge, UK), which was exchanged after the glue process. The different steps of the procedure are schematically shown in Fig. 3.5.

Equal amounts of the two components of the epoxy glue with hardening time of $\sim 12 \text{ h}$ were intensively mixed for 15 min on a microscope slide with a Teflon spoon. A small drop was deposited on a clean microscope slide and smeared out using a cover glass. The AFM was positioned above the glue surface and the cantilever was dipped once into the glue. The AFM was removed shortly and using the optical microscope the sample containing the fibril was positioned such that it was centred in the field of view. Next, the AFM was put on top of the sample, and using the optical microscope, repositioned above the fibril. Once positioned above the fibril end on glass, the tip was moved down. A drop of glue (size: $30\text{-}50 \mu\text{m}$) was deposited on this end and the cantilever was moved towards a position above the other end of the fibril, located on Teflon. The cantilever, which still contained glue, was used to deposit a second, smaller drop of glue of $10\text{-}20 \mu\text{m}$ in size. If necessary, another dip in the macroscopic glue drop can be performed.

The triangular cantilever was exchanged for a cantilever with a high spring constant and a rectangular shape ($k = 32\text{-}62 \text{ N}\cdot\text{m}^{-1}$, NCH-W Nanosensors, Darmstadt, Germany), of which the tip was removed using focused ion beam removal (performed at the Mesa⁺ institute, University of Twente). After aligning the laser to the quadrant-cell detector, the resonance frequency of the cantilever was determined.

Usually, the spring constant of a cantilever is calculated from its Brownian motion. Due to the small amplitude of the cantilever used in our set-up, the spring constant could not be determined using this method. Instead, the spring constant was calculated from the determined resonance frequency of the cantilever. The following relations between the spring constant k , the resonance frequency f and the dimensions t (thickness), w (width) and L (length) of a rectangular cantilever are known.²⁶

$$k = \frac{E \cdot w \cdot t^3}{4 \cdot L^3} \quad (3.5)$$

in which $E = E$ -modulus of Si

$$f = \frac{\sqrt{k}}{2 \cdot \pi} \quad (3.6)$$

in which $m =$ cantilever mass

Formula 3.6 can be converted in formula 3.8 by using formula 3.5 and a different expression for the mass m of the cantilever according to formula 3.7.

$$m = V \cdot \rho \quad (3.7)$$

in which ρ = density

and $V = L \cdot w \cdot t$

$$f = \frac{t \cdot \sqrt{\frac{E}{\rho}}}{4 \cdot \pi \cdot L^2} \quad (3.8)$$

By using formula 8 as an expression of t , which is used for t in formula 3.5, expression 3.9 is obtained.

$$k = 16 \cdot \pi^3 \cdot \rho^{3/2} \cdot \frac{1}{\sqrt{E}} \cdot w \cdot f^3 \cdot L^3 \quad (3.9)$$

This formula shows the correlation between the spring constant k , the width and length of the cantilever and its resonance frequency. All other factors remain constant. From formula 3.5 and 3.8, it was calculated that the dominant contribution to the relative error in k and f , is the relative error in the thickness t of the cantilever. A direct proof based on the specifications of the supplier can be found in Appendix B.

The contribution of w and L to the error in k and f was calculated based on the cantilever's specifications. The following values were provided for the rectangular cantilever: spring constant $k = 36\text{-}62 \text{ N}\cdot\text{m}^{-1}$, resonance frequency $f = 322\text{-}384 \text{ kHz}$, thickness $t = 3.74\text{-}4.41 \text{ }\mu\text{m}$, width $w = 29\text{-}31 \text{ }\mu\text{m}$ and length $L = 122 \text{ }\mu\text{m}$.

From these values, a relative error in the width of 3.3% is determined, while the relative error in the length is estimated at 0.82% when assuming the same error in w as in L during the production of the cantilevers. The resonance frequency can be determined with an estimated accuracy of $\sim 1 \text{ kHz}$, equal to a relative error of 0.29% for a typical resonance frequency of 350 kHz. When these relative errors are used to calculate the relative error in the spring constant from formula 9, the total error in k is composed of once Δw , three times Δf and three times ΔL . Via this method the error in k was calculated to be 6.6%.

To calculate spring constant k of a new cantilever from the resonance frequency determined, the width and length of the cantilever are assumed to be constant. This way, the correlation $k = C \cdot f^3$ is obtained. For the variation in k and f , as provided by the supplier, a function was calculated, which was used to determine the spring constant from a known resonance frequency.

The factor C was calculated from the specifications by coupling the highest spring constant with the highest resonance frequency and *vice versa*. This resulted in a value for C of $1.087 \pm 0.012 \cdot 10^{-15} \text{ kg}\cdot\text{s}$. By calculating k values for various values of f in the specified range using factor C , Fig. 3.15 was obtained.

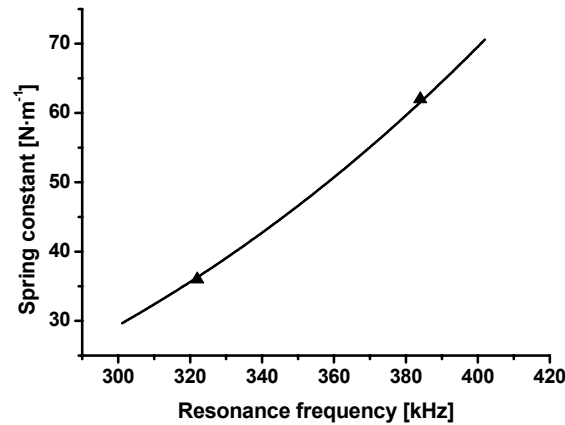


Figure 3.15 Correlation between the spring constant and the resonance frequency of the cantilevers according to the function $k = (1.087 \cdot 10^{-15} \text{ kg}\cdot\text{s}) \cdot f^3$. The range from the specifications of the cantilevers is shown in the graph.

The obtained function, which describes the correlation between the spring constant and the resonance frequency, was used to calculate the spring constants of the cantilevers from the known resonance frequencies.

The cantilever was positioned above the fibril end on Teflon and pressed on the surface with a force of around 10 μN . To avoid any movement of the microscope slide during the experiments, two magnets were attached to both ends of the microscope slide, just above two opposing magnets, which were located under the object table of the inverted microscope. In this state it was left for 20 h at ambient conditions.

The fibril was then lifted from the Teflon surface by moving the cantilever along the fibril length in the direction of the fibril end located on glass. Simultaneously, the distance between the tip and surface was increased gradually during the movement. The lifting of the fibril was monitored via the optical microscope, and was continued until no contact of the free fibril with the surface was visible. (Fig. 3.6)

Tensile testing of collagen fibrils.

The fixed fibril was moved upward at ambient conditions, until the deflection value exceeded twice the noise level, equal to a force of $\sim 4 \text{ nN}$. A saw-tooth loading pattern with an extension of 2.4 μm at an extension rate of 4.8 $\mu\text{m}\cdot\text{s}^{-1}$ was used to determine the mechanical properties of the fibril.

General transformation of data

From the obtained raw force-distance data one cycle was selected and the up and down curves were separated. The applied extension was corrected for the hysteresis of the tube and the non-linear behaviour of the tube. Then, the initial length of the fibril (L_0) was added to the determined extension values. The obtained values are schematically represented in Fig. 3.16.

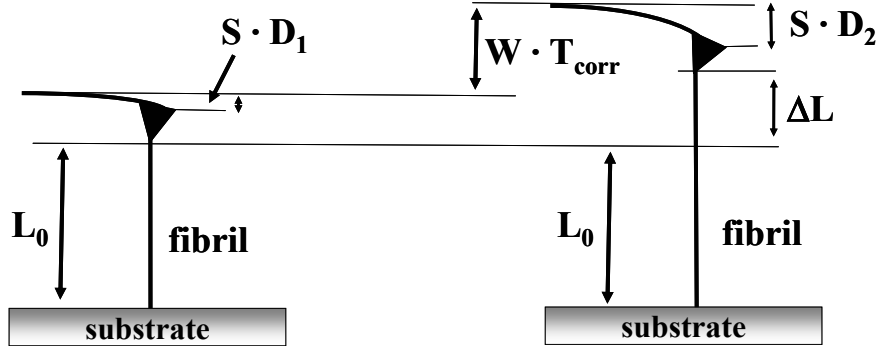


Figure 3.16 Schematic representation of the actual extension ΔL of the collagen fibril with the applied extension of the AFM tube $W \cdot T_{\text{corr}}$ and the bending of the AFM cantilever $S \cdot (D_2 - D_1)$.

The length increase ΔL [μm] was calculated from formula 3.10 with S (deflection sensitivity), k (cantilever stiffness), W (sensitivity of the tube), D (deflection) and T (tube extension values). The force values were calculated using formula 3.11:

$$\Delta L = W \cdot T_{\text{corr}} - S \cdot (D_2 - D_1) \quad (3.10)$$

$$F = (D_2 - D_1) \cdot (-1) \cdot k \quad (3.11)$$

From the length increase ΔL [μm] of the fibril, the strain ε [%] was calculated via formula 3.12 and from force F [nN] the stress σ [Pa] was calculated using formula 3.13:

$$\sigma = \frac{F}{A} \quad (3.12)$$

in which $A = (\frac{1}{4}\pi) \cdot d^2$

with d = diameter fibril

$$\varepsilon = 100\% \cdot \frac{\Delta L}{L_0} \quad (3.13)$$

SEM imaging of collagen fibrils

Using a Leo 1550 High Resolution SEM, the surface analysis was performed. When excessive charging of the surface was apparent, the sample was sputter-coated with an Au/Pd layer of 5 nm thickness.

Contact angle measurements

The coated glass discs were characterized by static water contact angle measurement using the sessile drop method. The measurements were performed with a Contact Angle Measurement System (Contact Angle System OCA 15 plus, Dataphysics, Filderstadt, Germany).

3.9 References

- 1 P. Fratzl, *Current Opinion in Colloid & Interface Science*, 2003, **8**, 32.
- 2 E. Gentleman, A. N. Lay, D. A. Dickerson, E. A. Nauman, G. A. Livesay, and K. C. Dee, *Biomaterials*, 2003, **24**, 3805.
- 3 N. Sasaki, N. Shukunami, N. Matsushima, and Y. Izumi, *J. Biomech.*, 1999, **32**, 285.
- 4 M. E. Nimni, 'Biochemistry', ed. M. E. Nimni, CRC Press, Boca Raton, FL, 1988.
- 5 T. Gutschmann, G.E. Fantner, M. Venturoni, A. Ekani-Nkodo, J.B. Thompson, J.H. Kindt, D.E. Morse, D. Kuchnir Fygenon, P.K. Hansma, *Biophys. J.*, 2003, **84**, 2593.
- 6 M. Raspanti, *Arch. Hist. Cytol.*, 2002, **65**, 37.
- 7 Y. P. Kato and F. H. Silver, *Biomaterials*, 1990, **11**, 169.
- 8 From the stress at break of the uncrosslinked fibre of 2.4 MPa and a diameter of 125 μm in PBS, the stress to break of a collagen fibril of 200 nm in diameter was calculated as follows. The cross-section of the fibre is $1.23 \cdot 10^{-8} \text{ m}^2$, while that of the fibril is $3.14 \cdot 10^{-14} \text{ m}^2$. By assuming a packing density of 50% of the fibrils in the cross-section of the fibre, $1.96 \cdot 10^5$ fibrils are found in one cross-section. The force at break of the fibre is calculated from the stress by multiplication with the cross-section. The force at break of a single collagen fibril will be $1/1.96 \cdot 10^5$ of this value, equal to 0.15 μN .
- 9 G. Binnig, C.F. Quate, C. Gerber, *Phys. Rev. Lett.*, 1986, **56**, 930.
- 10 M. L. Bennink, 'Force spectroscopy of single DNA-protein complexes - An optical tweezers study', University of Twente, Enschede, 2001.
- 11 S. M. Block and L. S. B. Goldstein, *Nature*, 1990, **348**, 348.
- 12 M. G. Poirier and J. F. Marko, *J. Muscle Res. Cell. Motility*, 2002, **23**, 409.
- 13 R. Merkel, *Phys. Rep.*, 2001, **346**, 343.
- 14 K. S. Weadock, E. J. Miller, L. D. Bellincampi, J. P. Zawadsky, and M. G. Dunn, *J. Biomed. Mater. Res.*, 1995, **29**, 1373.
- 15 T. Koide and M. Diato, *Dental Mat. J.*, 1997, **16**, 1.
- 16 Vantico, in 'Araldite® 2011 Toughened, Long Work Life Epoxy', 2003.
- 17 H. Schönherr, G.J. Vancso, *Polymer*, 1998, **39**, 5705.
- 18 Y. S. Lin and V. Hlady, *Coll. Surf. B: Biointerfaces*, 1994, **2**, 481.
- 19 T. G. Ruardij, 'Cellular Interactions with Chemical Gradient Surfaces', University of Groningen, Groningen, 1997.

- 20 S.-J. Ding, P.-F. Wang, X.-G. Wan, D.W. Zhang, J.-T. Wang, W.W. Lee, *Mater. Sci. Engin.*, 2001, **B83**, 130.
- 21 Y. P. Kato, D. L. Christiansen, R. A. Hahn, S.-J. Shieh, J. D. Goldstein, and F. H. Silver, *Biomaterials*, 1989, **10**, 38.
- 22 K. O. v. d. Werf, C.A.J. Putman, B.G. de Groot, F.B. Segerink, E.H. Schipper, N.F. van Hulst, J. Greve, *Rev. Sci Instrum.*, 1993, **64 (10)**, 2892.
- 23 A. L. Weisenhorn, P. Maivald, H.-J. Butt, and P. K. Hansma, *Phys. Rev. B*, 1992, **45**, 11226.
- 24 H. Schönherr, 'From Functional Group Ensembles to Single Molecules: Scanning Force Microscopy of Supramolecular and Polymeric Systems', Twente, Enschede, 1999.
- 25 F. Moreno-Herrero, P.J. de Pablo, J. Colchero, J. Gómez-Herrero, A.M. Baró, *Surf. Sci.*, 2000, **453**, 152.
- 26 D. Sarid, in 'Chapter 1 - Mechanical properties of levers', ed. D. Sarid, Oxford University Press, New York, 1991.

CHAPTER 4

Mechanical Properties of Single Collagen Type I Fibrils

"Niets doet de natuur doelloos." - Aristoteles

(Abstract)

The tensile properties of single collagen type I fibrils from bovine Achilles tendon origin were measured with an atomic force microscope (AFM,) combined with an optical microscope. The stress-strain curves of fibrils tested at ambient conditions did not change after repeated loading with stresses up to around 90 MPa. Irreversible lengthening of individual fibrils was observed when exceeding this stress value. The stress-strain behaviour of collagen fibrils immersed in aqueous media did not change after cyclic loading with stresses up to around 20 MPa. Again, when exceeding this stress value, permanent deformation of the fibril was observed. The tensile behaviour of fibrils placed in demineralised water and various aqueous buffers (pH 5.4-7.4), including buffers containing calcium ions, loaded with rates between 0.02 and 20 $\mu\text{m}\cdot\text{s}^{-1}$, was similar up to a stress of 7 MPa. The influence of bending of the fibril on its stress-strain curves was investigated in a first approximation using a finite element model for isotropic materials with an elastic behaviour. Following this approach, it was concluded that this influence was minimal.

A fibril with an initial length of 72 μm was tensile tested to rupture in a stepwise manner. A stress at break of 69 MPa was determined. A second fibril was extended in a stepwise manner to three times its original length without rupture to occur. From the stress-elongation curve a maximal stress of 123 MPa was determined. Both fibrils showed a similar stress-elongation curve. During cyclic loading with stepwise increase of the relative elongation, a residual stress was built up in the fibrils. Irreversible deformations up to three times the original length of the fibril did not lead to a permanent change of the collagen D-period (67 nm repeat). This finding underlines the stress-induced permanent lengthening mechanism of the fibril via sliding of microfibrils.

4.1 Introduction

Collagen is the most abundant protein in mammals, and is a generally accepted biomaterial in cardiovascular constructs, suture material and ligament replacement. The protein is an essential component of tendons and ligaments, bone, cartilage, skin, blood vessels, heart valves and eyes.^{1, 2} Despite the important function of collagen in the human body and its widespread application in biomaterials, the relation between the structure and the mechanical properties are still poorly understood.

Currently, around 25 different types of collagen have been described, of which type I is the most abundant.³ The types differ in α -amino acid sequence and quaternary structure. Only type I to V form fibrous supramolecular structures. Type I collagen is composed of a number of substructures, that self-associate in a hierarchical fashion towards the macroscopic structure. One example is the Achilles tendon, which is built almost exclusively from collagen type I. The structure has five levels of aggregation (Fig. 4.1). The aggregation of the peptide chain towards the fibril has been intensively studied. Two identical peptide chains and a distinct third one assemble into a triple helix. The chains have a repeating triplet sequence, consisting of a glycine, (hydroxy)-proline and a third amino acid.^{4, 5} The helical structure is stabilized by intra-helical hydrogen bonding, sometimes via bound water molecules. Both the C- and N-terminal residues of the protein chain are composed of non-helical telopeptides. (Non)-covalent interactions between the three strands in this region result in additional stabilization to prevent unwinding of the triple helix.^{4, 5} Five triple helices aggregate into a microfibril in a staggered organisation.⁴⁻⁶ Hundreds of microfibrils aggregate into a fibril.^{3, 7} The staggered organisation of triple helices in the microfibrils leads to a characteristic periodic structure (D-period), which can be detected by X-ray diffraction, electron microscopy or AFM.^{1, 8-10} Collagen fibrils are secreted by fibroblasts in the direction of the biomechanical forces.¹¹ The collagen fibril is involved in biomechanical processes between cells and the extra-cellular matrix, providing structural stability and distribution of mechanical stress.¹ The aggregation of triple helices towards fibrils is an entropy-driven process.^{3, 7} The subfibril as shown in Fig. 4.1 has not been identified as a single entity in self-assembly experiments^{6, 12} and its internal structure has not been clarified.

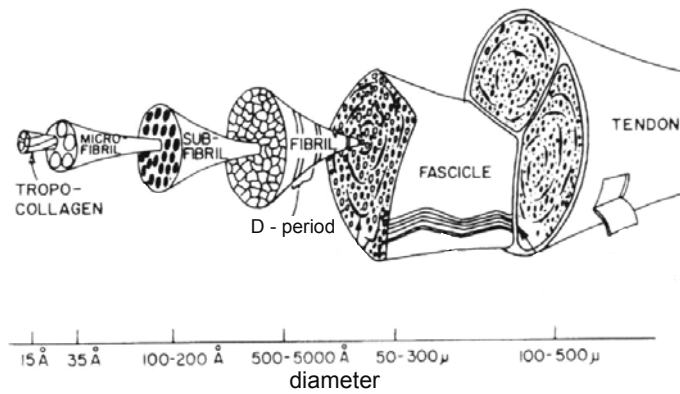


Figure 4.1 Hierarchical aggregation of collagen triple helices into fibrils and ultimately a tendon. The figure is taken from Kastelic et al., 1980.¹² Reprinted and adapted from *Symposium of Society for Experimental Biology - Mechanical Properties of Biological Materials, Symposium XXXIV*, author: J. Kastelic and E. Baer, *Deformation in tendon collagen*, 1980, with permission from Cambridge University Press. The image was published earlier in *Connective Tissue Research*, J. Kastelic, A. Galeski and E. Baer, "The multicomposite structure of tendon", vol. 6, p. 11-23, 1978, reproduced by permission of Taylor & Francis, Inc, <http://www.taylorandfrancis.com>.

The structure-property relationship of collagen is far from being completely understood. At present, single crystals of triple helices have not been obtained. Therefore, the structure of collagen has not been unraveled at atomic resolution yet.^{5, 13} To unravel the relation between the collagen structure and its macroscopic mechanical behaviour, it is essential to have information about the mechanical properties of the substructures. The current understanding of the stress-strain behaviour of collagen-based materials on a microscopic scale is based upon results from tensile testing in combination with X-ray diffraction. The stress-strain behaviour of a rat tail tendon (RTT) is shown as an example (Fig. 4.2).

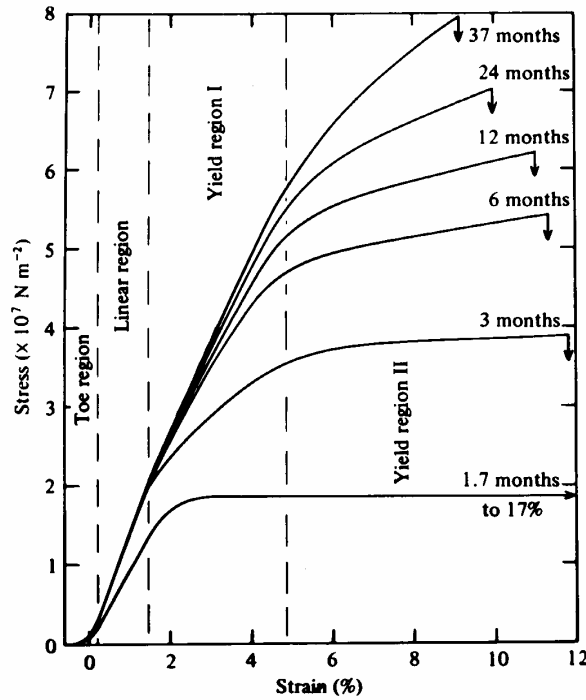


Figure 4.2 Stress-strain behaviour of a rat tail tendon (RTT) in neutral saline, as function of age with four distinct regions highlighted. Strain rate: $8\% \cdot \text{min}^{-1}$. Reprinted from Biorheol., D.F. Betsch and E. Baer, *Structure and Mechanical Properties of Rat Tail Tendon*, vol. 17, p. 83-94, ©1980, with permission from IOS Press.⁶

The toe region is attributed to straightening of the tendon's crimp structure. The linear region corresponds to elastic deformation of collagen fibrils and the Young's modulus is determined from its slope. In yield region I deformation was thought to occur via slipping of microfibrils or microfibril clusters. For yield region II an additional mechanism comes into play, involving slipping of triple helices within the microfibril (resulting in a change in D-period and even removal of the banding pattern). The removal of the banding pattern remained after unloading for RTT of immature rats, while the RTT of the oldest specimen regained their D-period.¹⁴ More details on the change in the D-period during loading of fibrils in collagen fibrous structures can be found in chapter 2.

The stress-induced structural changes of a bovine Achilles tendon in saline at each level of the hierarchy (see Fig. 4.1) were investigated by means of X-ray diffraction. The tendon was loaded at various constant stress values and the change in collagen D-period was recorded. During loading of the tendon, creep occurs. The D-period change is calculated from the stabilized D-period value after this creep. The stress-induced change in the 67 nm repeat of the fibrils constituting the tendon was defined as the strain in the fibril structure.

The strain in a collagen fibril can be described by three modes: triple helix elongation, increase in the gap region (together with the overlap region this represents the bands comprising the D-period) and relative slipping of laterally adjoining triple helices along the fibril axis. It was found that the first mode is the major contributor to the fibrillar strain. By assuming that the tendon's cross-sectional area is composed of a bundle of fibrils (Fig. 4.1), the stress on the individual fibrils was calculated.¹³ From the stress-strain curve of a fibril a Young's modulus of 430 MPa was determined. At 4% strain of the fibril a stress value of approximately 20 MPa was calculated.

The number of triple helices per cross-section was calculated by assuming the packing of triple helices into a microfibril as described by the Hodge and Petruska model¹⁵ and further aggregation of these microfibrils in a fibril. In this way, the number of triple helices in the cross-sectional area of the tendon was determined, which allowed the calculation of the stress on individual triple helices. The corresponding strain was determined by monitoring the distance between neighboring amino acids along the helical axis by X-ray diffraction.¹⁶

The water content of collagen-based materials has a large influence on the mechanical properties. This was studied by stepwise dehydration of rat tail tendons. The shape of the stress-strain curve changed significantly and the stress at break increased dramatically (Fig. 4.3).⁶

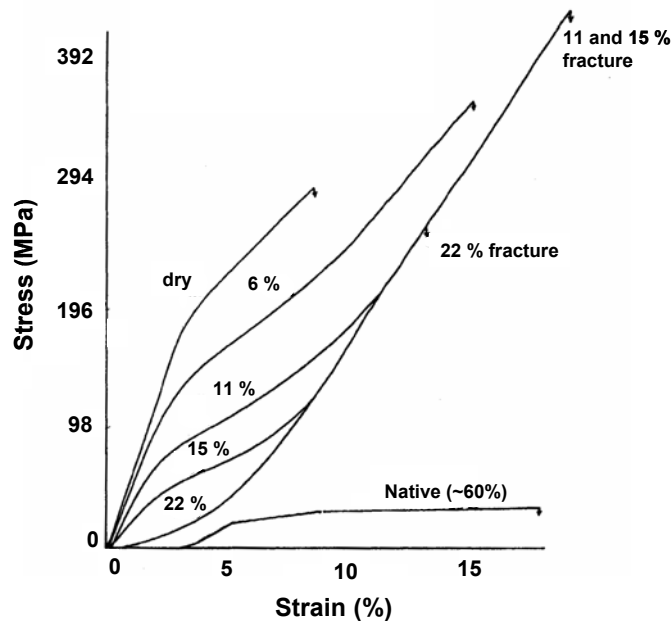


Figure 4.3 Stress-strain behaviour of a rat tail tendon (RTT) as a function of water content of the tissue. Rat tail tendons were taken from 3 month old rats. Percentages refer to relative humidity. Reprinted and adapted from Biorheol., D.F. Betsch and E. Baer, "Structure and Mechanical Properties of Rat Tail Tendon", vol. 17, p. 83-94, ©1980, with permission from IOS Press.

A dry rat tail tendon (RTT) shows a stress at break of 290 MPa with a Young's modulus of 5.8 GPa and a high strain modulus of 1.4 GPa. The mechanical properties of native RTT (3 months of age) in saline reveal a stress at break of 39 MPa and a Young's modulus of 1.4 GPa. This shows a significant decrease in stiffness and stress at break value by wetting of the RTT.⁶

Recently, force spectroscopy techniques have been developed, which open new perspectives for unraveling internal structures and micro-mechanical properties of individual collagen fibrils.^{17, 18} These techniques have also been applied in the investigation of the mechanical behaviour of triple helices and their aggregates. The mechanical behaviour of collagen triple helix aggregates¹⁹ and a single triple helix²⁰ were studied by force spectroscopy using an AFM and optical trap, respectively. Mechanical loading of undefined triple helix aggregates revealed the presence of sacrificial bonds. The experiments were performed via non-specific binding of triple helices to the AFM tip and the substrate. More sacrificial bonds reform during repetitive pulls and more energy dissipation was observed when the experiments were performed using a NaCl containing HEPES buffer medium, supplied with CaCl₂.¹⁹

In the study presented here, the high force resolution of the AFM was taken advantage of in measuring the tensile behaviour of single collagen fibrils. A home-build AFM²¹ was positioned on top of an inverted microscope. Collagen type I fibrils from bovine Achilles tendon origin were fixed between a glass surface and the AFM cantilever using microscopic glue droplets (details: chapter 3).

4.2 Results and discussion

4.2.1 Tensile testing of collagen fibrils at ambient conditions

4.2.1.1 Results reversible tensile testing

A suspension of collagen fibrils was deposited on a glass surface partly coated with Teflon. Fibrils crossing the Teflon-glass border were glued to the glass surface and the AFM cantilever, respectively, using small droplets of epoxy glue. The epoxy glue did not adhere to Teflon, which allowed lifting of the collagen fibril from the Teflon surface (details: chapter 3). Fibrils used in the experiments had a length between 50 and 200 μm and a diameter between 50 and 200 nm (details: Appendix C). The fibril was stretched by increasing the height of the AFM manually, while the force acting on the AFM cantilever was measured. The initial length of the collagen fibril was defined as the length at which the measured force exceeded a value of 4 nN, equal to twice the noise level. A schematic representation of the set-up is shown in Fig. 4.4.

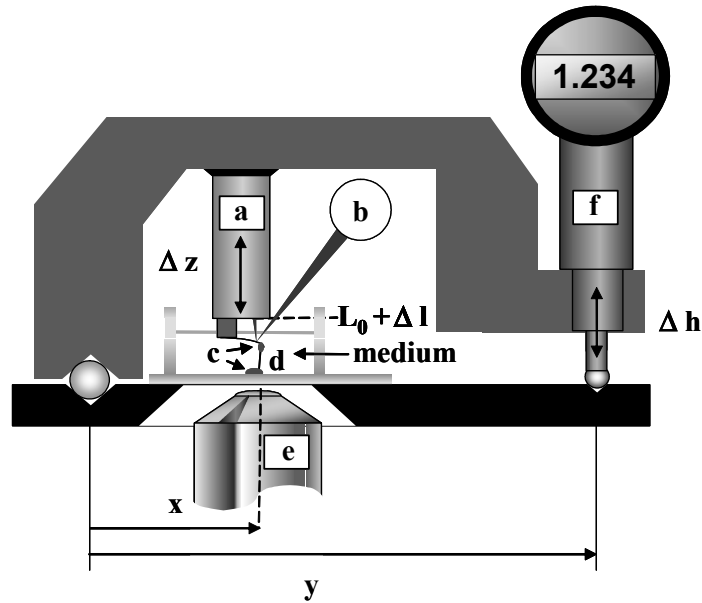
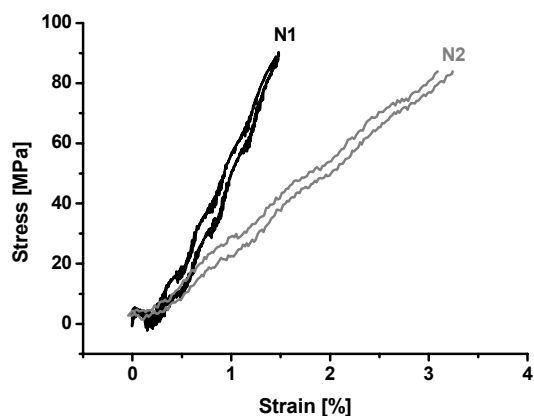


Figure 4.4 Schematic representation of the set-up containing the AFM on top of the inverted microscope. The fibril **d** was fixed via glue droplets **c** to the surface and to the cantilever (scale is not correct). Increase of the distance between the AFM tip and the surface was performed over short ranges via tube **a** over lengths Δl , while the deflection of the cantilever was monitored via a laser at position detector (quadrant detector) **b**. The attachment procedure was monitored using the inverted microscope of which objective **e** is shown. An optical fibre was used for illumination of the sample. With the lever rule **x:y** the movement of the AFM tube over distances Δl is correlated to the height change Δh of the setscrew as determined by using the depicted micrometer **f** above it.

A non-treated collagen fibril (fibril N1, details: table Fig. 4.5) with a length of 119 μm and a diameter of 214 nm was loaded cyclically to a stress of approximately 90 MPa at ambient conditions, with a maximal extension of 2.3 μm and an extension rate of 0.3 $\mu\text{m}\cdot\text{s}^{-1}$. The consecutively recorded stress-strain curves were fully overlapping, which revealed reversible mechanical behaviour. In Fig. 4.5 a single stress-strain curve of fibril N1 has been depicted. The hysteresis was 4.5×10^{-12} J.

A second non-treated collagen fibril (fibril N2, details: table Fig. 4.5) with a length of 57 μm and a diameter of 181 nm was mechanically tested using a similar protocol with a maximal extension of 1.9 μm and an extension rate of 0.4 $\mu\text{m}\cdot\text{s}^{-1}$. The resulting stress-strain behaviour of fibril N2 was also found to be fully reversible (Fig. 4.5). The hysteresis was 4.1×10^{-12} J.



Fibril	L_0 (μm)	d (nm)	ext. rate ($\mu\text{m}\cdot\text{s}^{-1}$)	cant. ($\text{N}\cdot\text{m}^{-1}$)	$\varepsilon^\#$ (%)	$\sigma^\#$ (MPa)	$E^\#$ (GPa)
N1	119 ± 0.5	214 ± 12	0.3	29.3 ± 1.9	1.4	91	7.2
N2	57 ± 0.5	181 ± 5	0.4	25.8 ± 1.7	3.3	84	2.7

Figure 4.5 Stress-strain curves of single collagen fibrils at ambient conditions. The conditions and obtained mechanical properties are shown in the table. Table details: $\varepsilon^\#$: strain at maximally applied stress $\sigma^\#$; $E^\#$: the modulus was determined between the onset of the stress increase and the maximally applied stress.

A small difference between the up and down curve of fibril N2 can be observed at the maximum stress value. This difference is due to a small error in the correction of the AFM tube hysteresis and non-linear behaviour. The fitted functions for the up and down curve do not intersect. The error in the fitted functions at this height is around 6%, which accounts for the difference between the curves. The noise pattern superimposed on the deflection signal of both curves is caused by an interference effect of the AFM laser. For stress calculations a circular cross-section of the collagen fibril was assumed.

From tapping mode AFM images at ambient conditions, the ratio between the width at half height and the height of the fibrils ($n=9$) was determined at 2.6 ± 1.0 to 1. The tip radius was reported at <20 nm according to the supplier. This suggests that the shape of the fibrils on the surface is oval or flattened, as was observed earlier in the Hansma lab.²² In this article a highly reversible flexibility of the fibril towards lateral compression was reported. The shape of the cross-section of a free standing collagen fibril is unknown, but due to the symmetry of the system a circular cross-section is most likely.

Due to the applied configuration of the collagen fibril, in which the fibril is elongated with two bending points, the obtained stress-strain curves might be influenced by the bending of the fibril. In a first approximation a finite element model was used for isotropic materials with an

elastic behaviour. Via this approach, the influence of bending on the stress-strain curve of a model system was investigated and compared to the results as presented here. It was found that using this model, the influence of bending on the stress-strain curve of a single collagen fibril was minimal (details: Appendix to chapter 4).

4.2.1.2 Comparison with literature

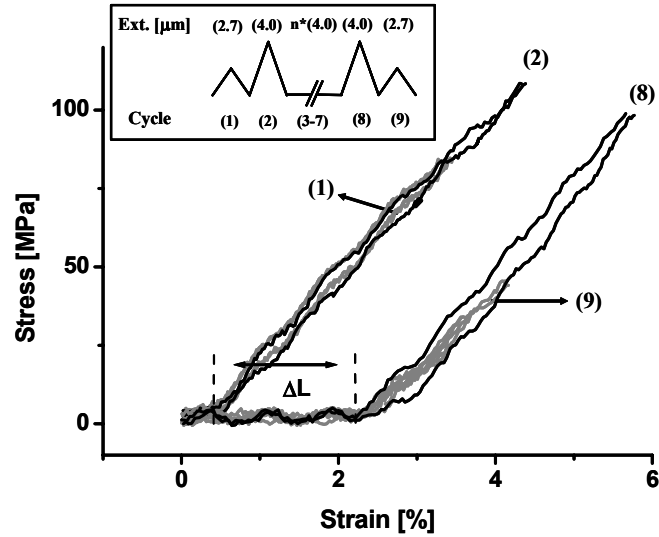
The stress-strain curves of fibrils N1 and N2 revealed a similar shape, but with a different Young's modulus of 7.2 GPa (fibril N1) and 2.7 GPa (fibril N2), respectively. This may be due to differences in environmental conditions during the measurements. The tensile testing was not performed in a climate controlled atmosphere, which may lead to differences in hydration level of the collagen fibril. Mechanical properties of collagenous materials are known to be strongly dependent on the water content (see Fig. 4.3).⁶

Self-assembled collagen fibres, formed by extrusion of a cold, acidic collagen solution from bovine hide origin into a neutral medium at room temperature, are composed of aggregated collagen fibrils.²³ In the dry state the non-treated fibres have a Young's modulus of 4.8 ± 0.5 GPa, with a stress at break of 370 ± 25 MPa and a strain at break of $22 \pm 5\%$.^{24, 25} In comparison, the Young's modulus of a dry rat tail tendon (RTT) is 5.8 GPa and the stress and strain at break were 290 MPa and 8.6 %, respectively (Fig. 4.3).⁶ The stress-strain curve of the RTT has two different slopes with a Young's modulus of 5.8 GPa, while at higher strain values from 3.0 to 8.6% the modulus was 1.4 GPa.⁶

The mechanical properties of single collagen fibrils N1 and N2 at ambient conditions are similar to those of the RTT and the self-assembled fibres. From the results on mechanical testing of single collagen fibrils N1 and N2 at a strain of 1.4 and 3.3%, respectively, as described before, a linear stress-strain curve with a slope of 5 ± 3 GPa was obtained.

4.2.1.3 Results irreversible tensile testing

Up to a stress value of ~ 90 MPa the stress-strain curves of the fibrils did not change during repetitive cyclic loading. Fibril N2 (fibril N2, details table of Fig. 4.5) was first loaded to a stress value of around 70 MPa (cycle 1, extension 2.7 μm , see Fig. 4.6), which is fully reversible as in the foregoing experiment. After unloading, the applied extension was increased to 4.0 μm (cycle 2), which also increased the maximal stress to 110 MPa (Fig. 4.6). At this stress value, permanent deformation occurred. The loading of the fibril at this extension was repeated another six times (only cycles 2 and 8 are shown in Fig. 4.6). Finally, the fibril was loaded using an extension of 2.7 μm (cycle 9), the same as applied in the first cycle. This showed that during the six cycles with an extension of 4 μm at a stress value above 90 MPa, a permanent deformation of in total 1.1 μm had occurred.



Fibril	L_0 (μm)	ΔL (μm)	d (nm)	ext. rate ($\mu\text{m}\cdot\text{s}^{-1}$)	cant. ($\text{N}\cdot\text{m}^{-1}$)	$\epsilon^\#$ (%)	$\sigma^\#$ (MPa)	S^\ddagger (GPa)
N2	57 ± 0.5	1.1	181 ± 5	0.6-1.1	33.0 ± 2.2	4.3	110	2.6

Figure 4.6 Mechanical behaviour of collagen fibril N2 when loaded to stress values at around 110 MPa, which led to irreversible lengthening of the fibril. Extension rate: $0.6 \mu\text{m}\cdot\text{s}^{-1}$ (cycle 1 and 9, in grey), $1.1 \mu\text{m}\cdot\text{s}^{-1}$ (cycle 2 to 8, in black), obtained at ambient conditions. Insert shows the cycles, with corresponding extensions. The conditions and obtained mechanical properties are shown in the table. ΔL was determined from the onset of curves 2 and 8 in Fig. 4.6, because between curve 2 and 8 permanent deformation had taken place. Table details: $\epsilon^\#$: strain at maximally applied stress $\sigma^\#$ (cycle 2); S^\ddagger : the slope was determined between the onset of the stress increase and the maximally applied stress.

In the consecutive steps, permanent lengthening of the fibril occurred in every step to a final length of $58 \pm 0.5 \mu\text{m}$. The measured maximal stress values decreased slightly from 110 to 99 MPa from cycle 2 to 8. Despite the permanent lengthening of the fibril under the applied stress, the slope of each cycle remained the same. It is unclear why in the upward and/or downward curve of cycles 2 and 8 the permanent deformation is not apparent. This phenomenon was also observed for other collagen fibrils, which were mechanically tested at ambient conditions (data not shown here, details Appendix C).

Permanent deformation was found to occur at values above 90 MPa, which leads to lengthening of the fibril. The lengthening of the fibril might lead to displacement of microfibrils within the fibril, which could alter the mechanical properties when the fibril becomes too thin.

Theoretically, the lengthening of the fibril might lead to a change in interactions between the microfibrils within the fibrils, which might change the mechanical properties. The slope of the

stress-strain curves did not change after permanent deformation had taken place. This may indicate that increased interaction between the microfibrils did not take place, or that changes in the interactions between microfibrils did not take place. SEM analysis of fibrils after rupture showed that no necking had occurred at the broken ends (Fig. 4.7).

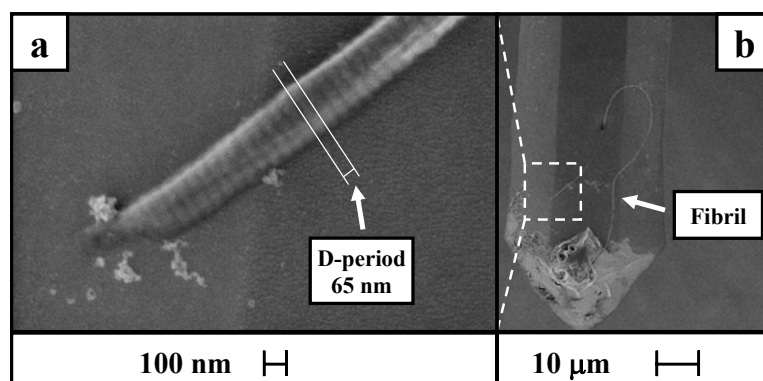


Figure 4.7 SEM image (b) of collagen fibril N5/G2 (details: appendix C) after rupture, which occurred during a tensile test experiment (details: Fig. 5.6, chapter 5). The fibril is fixed to an AFM cantilever, magnification: 1000 \times . In the second SEM image (a) at higher magnification (52000 \times), the broken end of the fibril is visible, revealing a retained D-period and absence of necking during rupture of the fibril.

The observation that no necking occurred during tensile testing of collagen fibrils suggests that the permanent deformation was spread homogeneously over the fibril.

The permanent deformation most likely occurs via sliding of microfibrils. Furthermore, the collagen D-period, which is originating from the organisation of triple helices in the microfibril, was retained. This suggests that the orientation and corresponding interactions between microfibrils essentially do not change during permanent deformation.

4.2.2 Tensile testing of collagen fibrils placed in aqueous media

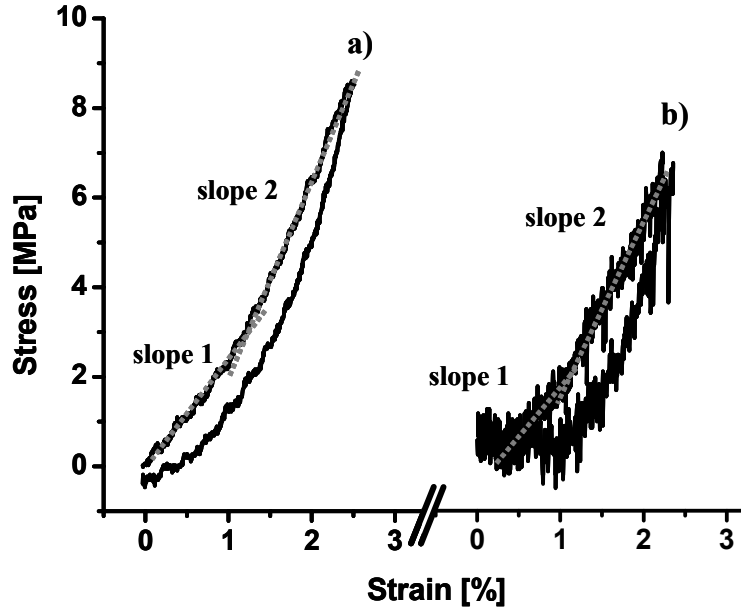
Collagen fibril N1 (details in table, Fig. 4.5) that was tensile tested up to stresses of around 150 MPa at ambient conditions (data not shown here, details in Appendix C) had undergone permanent deformation to a length of 126 μm . The fibril was then equilibrated in phosphate buffer at pH 7.4 at room temperature for 30 min. The fibril was loaded to a maximal stress of 9 MPa with a maximal extension of 3.1 μm at an extension rate of 0.6 $\mu\text{m}\cdot\text{s}^{-1}$. The obtained stress-strain behaviour was fully reversible and a hysteresis of 3.6×10^{-13} J was calculated from the curve presented in Fig. 4.8 (curve a).

No significant difference in the stress-strain curve was observed, when switching the buffer to PBS (pH 7.4), HEPES buffer (pH 6.9), CaCl_2 containing HEPES buffer (pH 6.9) or to demineralised water.

In a recent paper¹⁹, large differences in mechanical behaviour of aggregated collagen triple helices in the presence of calcium and sodium ions, compared to a medium containing only sodium ions have been reported. These results were obtained from force spectroscopy experiments on collagen triple helices supported on a glass surface placed in HEPES buffer with and without CaCl₂. Single or aggregated collagen triple helices located on the surface showed an interaction with the AFM tip and by pulling the tip a force-distance curve was obtained.

In our experiments, single collagen fibrils did not show a large influence of the ions in the applied medium on the mechanical properties. The inter-helical ionic interactions within the non-defined aggregates of collagen triple helices¹⁹ apparently are in a distal range which is ideal for calcium to bind. Since the collagen fibrils did not show an improvement of mechanical properties by calcium ions, it can be suggested that the triple helices in the fibril are organised in a different way. The ionic interactions that might influence the mechanical properties of the fibril apparently are not influenced by the presence of calcium ions.

Because fibril N1 had been subjected to different stresses with permanent deformation, a control experiment was performed. A new fibril (fibril N3, details table Fig. 4.8) was fixed between the glass surface and the AFM tip. This fibril had a length of 44 μm and a diameter of 188 nm. The fibril was loaded to a maximal stress of 7 MPa at a maximal extension of 1.0 μm at an extension rate of 0.2 $\mu\text{m}\cdot\text{s}^{-1}$ in MES buffer at pH 5.4. The obtained stress-strain curve was fully reversible with a hysteresis of 1.8×10^{-14} J as calculated from the curve presented in Fig. 8 (curve b). The difference in energy dissipation between fibril N1 (3.6×10^{-13} J) and fibril N3 (1.8×10^{-14} J) can be explained from the difference in fibril diameter and initial length. When the hysteresis is calculated per volume the value for fibril N1 is only 1.8 times larger than that of fibril N3, which suggests that indeed the difference in geometry causes the large difference in energy dissipation values. The shape of the stress-strain curve of the two fibrils immersed in different aqueous media was similar.



Fibril	L_0 (μm)	d^* (nm)	ext. rate ($\mu\text{m}\cdot\text{s}^{-1}$)	cant. ($\text{N}\cdot\text{m}^{-1}$)	$\epsilon^\#$ (%)	$\sigma^\#$ (MPa)	E^\ddagger (MPa)
N1	125.7 ± 0.5	370 ± 20	0.6	29.3 ± 1.9	2.5	8.6	240^\times 450^\times
N3	44 ± 0.5	188 ± 23	0.2	23.0 ± 1.5	2.3	6.7	310 380

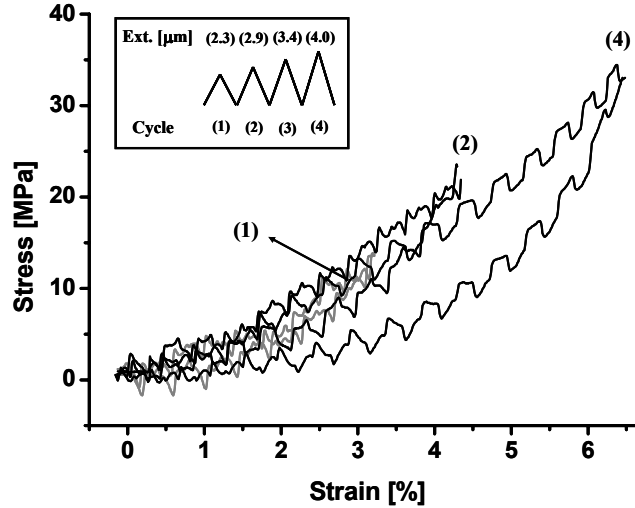
Figure 4.8 Fully reversible stress-strain curves of a collagen fibril in phosphate buffer at pH 7.4 (fibril N1, graph a) and MES buffer pH 5.4 (fibril N3, graph b), room temperature. The conditions and obtained mechanical properties are shown in the table. Table details: *: swollen fibril; $\epsilon^\#$: strain at maximally applied stress $\sigma^\#$; E^\ddagger : the initial slope was determined at stress values up to 3.1 ± 0.1 MPa, the second slope was determined at stress values higher than 3.1 ± 0.1 MPa. \times : slope was determined for a fibril that experienced permanent deformation.

The mechanical properties of collagenous materials are loading rate dependent.²⁶ In order to study whether the mechanical properties of collagen fibrils are also loading rate dependent, collagen fibril N1 (details in table, Fig. 4.5) was loaded to a stress of 10 MPa at extension rates between 0.02 and 20 $\mu\text{m}\cdot\text{s}^{-1}$ in PBS (pH 7.4), HEPES buffer (pH 6.9) or CaCl_2 containing HEPES buffer (pH 6.9), or in demineralised water. At these stress levels permanent deformation is absent. No effect of the applied extension rate on the stress-strain behavior was observed. Also, no effect of the applied medium on the observed mechanical properties was observed (details: Appendix C).

Apparently, the range of extension rates applied during tensile testing of single collagen fibrils (0.02 to $20 \mu\text{m}\cdot\text{s}^{-1}$) was too narrow to observe an effect. The influence of the strain rate on the modulus of a rat tail tendon (RTT) according to Knörzer *et al.*²⁷ was significant at strain rates exceeding $100 \text{ \%}\cdot\text{s}^{-1}$. The highest extension rate in our experiments was $20 \mu\text{m}\cdot\text{s}^{-1}$, which is equal to a strain rate of $16 \text{ \%}\cdot\text{s}^{-1}$, at which no influence of the loading rate is expected, according to the article.²⁷

Even though the two fibrils had a different history, the similarity in shape of the stress-strain curve shows that the history had no significant influence on the mechanical properties. These results also revealed that the effect of the pH on the mechanical properties was negligible in the range between 5.4 and 7.4. The shape of the stress-strain curve however, was different from that observed at ambient conditions. The curve for fibrils at ambient conditions showed a Hookean stress-strain relation, while the curves obtained for fibrils in aqueous media have an increasing slope with increasing strain. Apparently, the type of interactions between triple helices and microfibrils in a fibril, which are important for the mechanical behaviour of the fibril are strongly influenced by swelling of the fibril in aqueous media, leading to a different deformation behaviour when stress is applied.

At high stresses, permanent deformation of collagen fibrils was observed at ambient conditions. To investigate if this phenomenon also occurs for fibrils in aqueous media, a new collagen fibril (fibril N4, details table in Fig. 4.9) with a diameter of 182 nm and an initial length of $72 \mu\text{m}$ was fixed and loaded to a stress value of 18 MPa and extension of $2.3 \mu\text{m}$ at an extension rate of $0.46 \mu\text{m}\cdot\text{s}^{-1}$ in MES buffer at pH 5.4 (Fig. 4.9). Subsequently, the extension applied in the cyclic loading pattern was increased in 3 steps to a final extension of $4.0 \mu\text{m}$ at an extension rate of $0.91 \mu\text{m}\cdot\text{s}^{-1}$ in the 4th cycle (Fig. 4.9).



Fibril	L_0 (μm)	ΔL (μm)	d^* (nm)	ext.rate ($\mu\text{m}\cdot\text{s}^{-1}$)	cant. ($\text{N}\cdot\text{m}^{-1}$)	$\epsilon^\#$ (%)	$\sigma^\#$ (MPa)	S^\ddagger (GPa)
N4	72 ± 0.5	0.3	182 ± 9	0.46 - 0.91	26.6 ± 1.8	6.5	35	250 - 790

Figure 4.9 Tensile testing of collagen fibril N4, which resulted in permanent deformation. At stress values above 20 MPa, irreversible lengthening of the collagen fibril was observed. Cycle 1 with an extension of 2.3 μm is shown in grey and cycle 3 with an extension of 3.4 μm was omitted for clarity. MES buffer, pH 5.4, room temperature. The conditions and obtained mechanical properties are shown in the table. Table details: *: swollen fibril; $\epsilon^\#$: strain at maximally applied stress $\sigma^\#$ (curve 4); S^\ddagger : the slopes were determined from curve 4; the initial slope was determined at stress values up to 5 MPa and the final slope was calculated at stress values higher than 18 MPa.

The noise pattern superimposed on the deflection signal of both curves is caused by an interference effect of the AFM laser. The stress-strain curve at the highest extension (cycle 4, Fig. 4.9) showed a maximal stress of 35 MPa at a strain of 6.5 %. In this stress-strain curve up to a stress value of 5 MPa the slope was 250 MPa, which increased to a slope of 790 MPa at stress values above 18 MPa. The permanent deformation of the fibril was $\sim 0.3 \mu\text{m}$ after the last three cycles. The maximal stress applied during the last cycle was 35 MPa.

To study the influence of previous permanent deformation of fibrils, accomplished in a particular aqueous medium, on the subsequent mechanical behaviour of this fibril, the medium was exchanged and the fibril was loaded again to permanent deformation. The media used were PBS (pH 7.4), HEPES buffer (pH 6.9), CaCl_2 containing HEPES buffer (pH 6.9) or demineralised water. The applied medium was changed when fibril N2 (fibril N2, details Figs. 4.5 and 4.6) was permanently lengthened between 1 and 6 μm (details table Appendix C).

The stress-strain curves obtained by loading the fibril placed in PBS (pH 7.4), HEPES buffer (pH 6.9), CaCl₂ containing HEPES buffer (pH 6.9), and in demineralised water to stress values up to 55 MPa, showed that the stress-strain behaviour was not significantly influenced by permanent deformation, neither by the applied medium.

To enable extensions large enough to rupture the fibril, the entire AFM head was lifted using a calibrated setscrew over height Δh (see Fig. 4.3), because the maximal extension of the fibril using the AFM tube is limited to 4.0 μm (details: chapter 3). While the fibril was loaded with a sawtooth pattern ($\Delta l = 4.0 \mu\text{m}$ at $0.74 \mu\text{m}\cdot\text{s}^{-1}$), the AFM head was lifted in steps of 3 μm every third cycle (see Fig. 4.10). Only the marked second cycle (Fig. 4.10) was used in the analysis of the mechanical data.

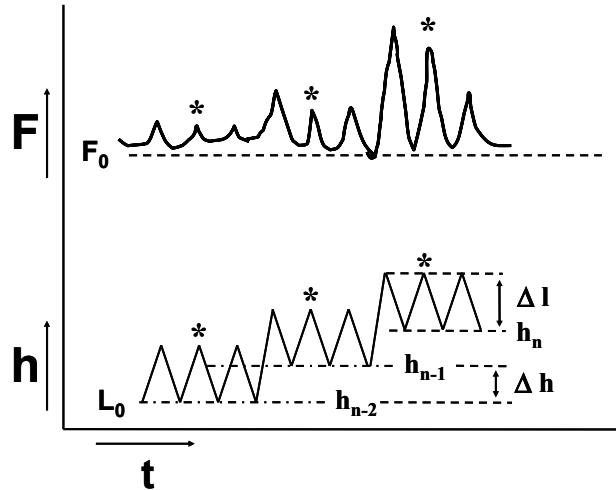
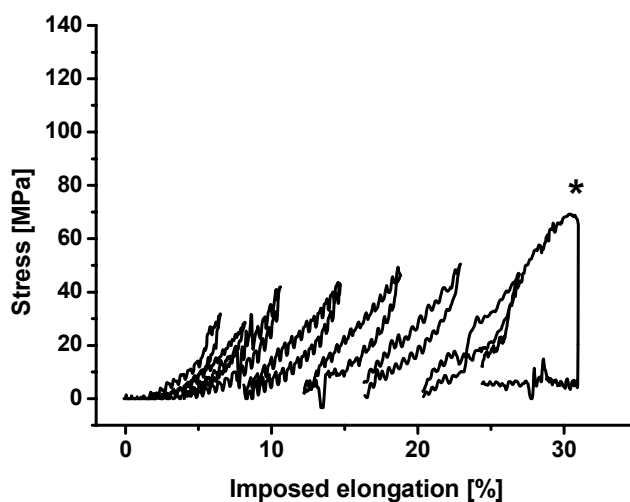


Figure 4.10 Schematic representation of the methodology for tensile testing of a collagen fibril via a stepwise height increase. The height was increased by 3.0 μm , after each third cycle, during continuous cyclic loading over an extension of 4.0 μm at an extension rate of $0.74 \mu\text{m}\cdot\text{s}^{-1}$. The cycling was started at a certain height, where the force on the fibril was $\sim 4 \text{ nN}$. After three cycles at h_{n-2} the height is increased over 3.0 μm to h_{n-1} , where $h_{n-1} = h_{n-2} + \Delta h$. In the analysis, only the second cycle at each height was used.

Collagen fibril N4 (fibril N4, details table in Fig. 4.9) was used for the experiments as depicted in Fig. 4.10. The resulting stress-elongation behaviour of fibril N4 in MES buffer at pH 5.4 is shown in Fig. 4.11. The same experiment was performed using a new fibril (fibril N5, details table in Fig. 4.12) with a length of 101 μm and a diameter of 201 nm, which was immersed in phosphate buffer at pH 7.4 and tensile tested following the same procedure as shown in Fig. 4.10. The resulting stress-elongation behaviour of fibril N5 has been depicted in Fig. 4.12. The imposed elongation in this experiment is normalized at 0% elongation using the initial length. The increase in the relative elongation was calculated from two parameters.

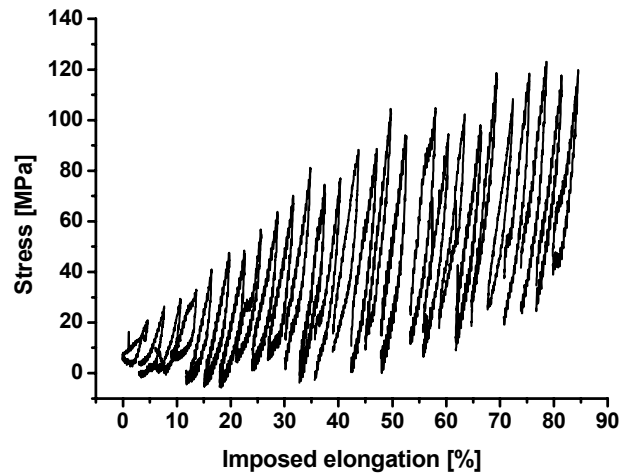
First, from the stepwise height increase (3 μm) the length at the start of three loading cycles is calculated. Then, the additional extension from the cyclic loading over 4 μm was added to the imposed elongation, already established at the start of the three loading cycles.

The imposed elongation, which is calculated via this method, does not represent strain, because during the cycles, stress relaxation via permanent lengthening occurs. In doing these experiments full stress relaxation of the fibril was not allowed. The fibril was extended over 4 μm at a rate of 0.1 Hz and after three cycles (equal to 30 s) an extra manually applied extension over 3 μm was added. In this approach, it is assumed that the initial length for these three cycles remains constant.



Fibril	L_0 (μm)	d^{\equiv} (nm)	ext. rate ($\mu\text{m}\cdot\text{s}^{-1}$)	cant. ($\text{N}\cdot\text{m}^{-1}$)	σ_{max} (MPa)
N4	72 ± 0.5	182 ± 9	0.74	26.6 ± 1.8	69

Figure 4.11 Stress-elongation curves of collagen fibril N4 using the protocol described in Fig. 4.10. Performed in MES buffer, pH 5.4. In the last cycle, rupture of the fibril was observed. The stress values were corrected for the assumed diameter change of the fibril. The conditions and obtained mechanical properties are shown in the table. Table details: \equiv : swollen fibril; σ_{max} : stress at break.



Fibril	L_0 (μm)	$d \equiv$ (nm)	ext. rate ($\mu\text{m}\cdot\text{s}^{-1}$)	cant. ($\text{N}\cdot\text{m}^{-1}$)	$\sigma^\#$ (MPa)
N5	101 ± 0.5	201 ± 9	0.74	28.3 ± 1.9	123 ± 3

Figure 4.12 Stress-elongation curves of collagen fibril N5 obtained using the protocol described in Fig. 4.10. Phosphate buffer, pH 7.4, at room temperature. The stress values were corrected for the assumed diameter change of the fibril. The conditions and obtained mechanical properties are shown in the table. Table details: \equiv : swollen fibril; maximally applied stress $\sigma^\#$.

One of the main characteristics of both curves is a gradual increase of the residual stress. The amount of residual stress is an indication of the relative rate of stress relaxation during loading of the fibril, compared to the extension rate. The residual stress values at the start of each cycle in the stress-elongation curves of fibril N4 and N5 as shown in figure 4.11 and 4.12, respectively, were determined and related to the corresponding relative elongation values (Fig. 4.13).

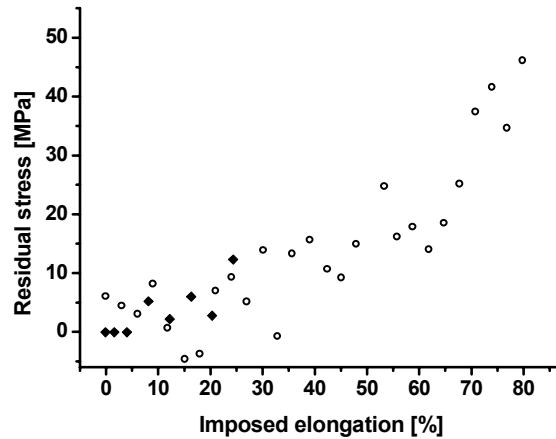


Figure 4.13 Residual stress at the start of each cycle plotted against the corresponding relative elongation. Open circles (○) represent values obtained for fibril N4 (details: Fig. 4.10), diamonds (◆) represent values obtained for fibril N5 (details: Fig. 4.11).

Two collagen fibrils were tensile tested using the protocol as depicted in Fig. 4.10. From the resulting stress-elongation curves and the residual stress at each corresponding relative elongation value a number of observations was made.

- The shape of the overall stress-elongation curve of both fibrils was similar up to ~30% elongation. Furthermore, the individual stress-elongation cycles up to ~30% elongation were also similar in shape. Apparently, the history of the fibril does not influence its mechanical behaviour.
- Up to ~30% relative elongation in the individual cycles, no residual stress was observed.
- Above ~30% relative elongation for both fibrils a residual stress was observed, which increased at increasing relative elongation. This suggests that the stress relaxation occurs at a lower rate than the rate of extension of the fibril in the individual cycles.
- At the start of various cycles of the stress-elongation curves, a residual stress of the previous cycle was present, after the cycle the residual stress has decreased, indicating permanent lengthening of the fibril.

4.2.3 Comparison with literature

The mechanical properties of collagen fibrils N1 and N3, which were determined in a regime without permanent deformation, will be compared to the mechanical properties of collagen fibrils in a bovine Achilles tendon, as reported in literature.¹³ The shape of the stress-strain curve of the two fibrils immersed in different aqueous media was similar as shown in Fig. 4.8. From the curves at low stress values up to 3.1 MPa, a Young's modulus of 280 ± 50 MPa was determined, while at stress values higher than 3.1 MPa, a slope of 420 ± 50 MPa was found.

From a X-ray diffraction study of deformation and stress in an Achilles tendon in saline during tensile testing, a stress-strain curve of a collagen fibril in the tendon was calculated, based on a structural model. The obtained stress-strain curve showed a Hookean behaviour. The calculated Young's modulus of a collagen fibril was 430 MPa. At a strain of 4%, the stress in the fibril was 20 MPa.¹³

The Young's modulus reported in the X-ray diffraction study is of the same magnitude as the Young's modulus of 280 ± 50 MPa, obtained for single collagen fibrils N1 and N3 at stress values between 0 and 3 MPa.

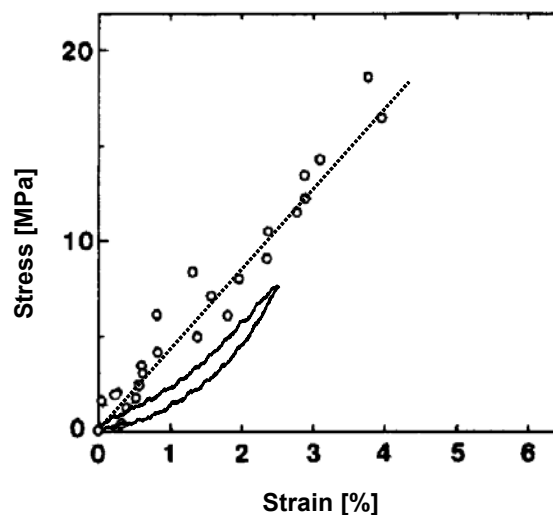


Figure 4.14 Stress-strain curve of collagen fibril N1 placed in phosphate buffer as depicted by the solid line. This was compared to the stress-strain curve of a collagen fibril (depicted by the open circles (○)), that was obtained by X-ray diffraction during loading of a bovine Achilles tendon in saline. Reprinted and adapted from *J. Biomech.*, N. Sasaki and S. Odajima, "Elongation Mechanism of Collagen Fibrils and Force-Strain Relations of Tendon at Each Level of Structural Hierarchy", vol. 29(9), p. 1131-1136, ©1996, with permission from Elsevier.

The stress-strain behaviour of a single collagen fibril placed in aqueous media is different from that derived from the X-ray diffraction study of a tendon under stress (Fig. 4.14). The stress-strain curves obtained for single collagen fibrils showed a non-Hookean behaviour, while the fibrils in an Achilles tendon as determined by X-ray diffraction showed a linear stress-strain behaviour. This difference might be explained by the methodology of applying and calculating the strain values of a fibril within a bovine Achilles tendon by X-ray diffraction. Each strain value is calculated from the relative change in the D-period as determined by X-ray diffraction. When the tendon was loaded, creep was observed. The change in D-period after the creep had stopped was used to calculate the strain at the applied stress. The change in the D-period during the occurrence of creep and the corresponding stress-strain behaviour of the fibril was not taken into account in this experiment.

During tensile testing of single collagen fibrils, such as fibril N1, the mechanical behaviour was determined from the immediate response of the fibril to an applied load.

Tensile testing of single collagen fibrils as shown here, resulted in a stress to break value of 69 MPa for fibril N4 (Fig. 4.11), while fibril N5 (Fig. 4.12) persisted at a stress of 123 MPa. Based on the ultimate tensile strength of fibrous collagen structures, the stress at break of a collagen fibril was estimated at 1 GPa.²⁸ In another report, an estimate for the maximal stress at break of individual fibrils was reported at 147-294 MPa, based on the calculation of the collagen content in a tendon.²⁹

In our experiments only two fibrils were tensile tested. The observed range of stress values are within the range reported in literature. The values reported in literature though, were obtained by extrapolation of the mechanical behaviour of macroscopic collagen materials towards the micro-mechanical behaviour of its collagen substructures. These interpretations are model-based and can lead to large deviations in mechanical properties.

The mechanical properties of rat tail tendon (RTT) fibres have been related to the mechanical properties of the collagen fibrils, which constitute the fibre.³⁰ The stress-strain curve of the RTT fibre placed in saline contains a non-linear toe region, which relates to uncrimping of collagen fibrils in the fibre. The linear region of the curve, where the modulus of the fibre was calculated from, represents straightening and loading of the fibrils in the fibre.³⁰ From the stress-strain curve as shown in Fig. 4.15 a stress at break of 54 ± 11 MPa and a modulus in the linear region of 500 ± 45 MPa was determined.

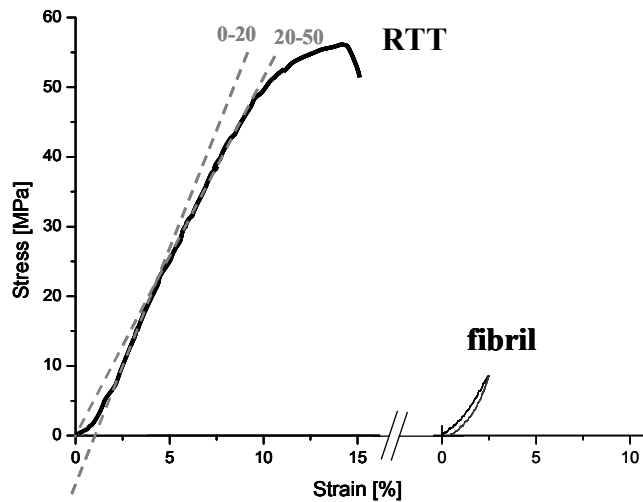


Figure 4.15 Stress-strain curve of a RTT fibre placed in saline, taken from Pins *et al.* The slopes of the stress-strain curves at 0-20 MPa and 20-50 MPa have been included. For comparison, the stress-strain curve of single collagen fibril N1 placed in phosphate buffer as shown also in Fig. 4.8a has been added. Reprinted and adapted from *Mater. Sci. Eng. C*, G.D. Pins and F.H. Silver, "A self-assembled collagen scaffold suitable for use in soft and hard tissue replacement", vol. 3, p. 101-107, ©1995, with permission from Elsevier.

The modulus of 500 ± 45 MPa, obtained from the linear region (3-20 MPa) of the stress-strain curve of a RTT fibre, corresponds well to the modulus of 420 ± 50 MPa, which was calculated for the single collagen fibrils at stress values between 3 and 7 MPa. For comparison, the stress-strain curve of fibril N1 is included in Fig. 4.15.

This result suggests that the linear region of the stress-strain curve of a RTT fibre indeed represents the extension of fibrils constituting the fibre. At increased extension of the RTT fibre, when exceeding the linear region at the yield point, the slope reduces, suggesting permanent deformation. This reduction in the slope of the curve starts at a stress of 20 MPa. This value correlates well to the observed stress value of 20 MPa for collagen fibrils placed in aqueous media, which represents the limiting stress value where permanent deformation sets in. It suggests that permanent deformation of RTT fibres can be directly correlated to permanent lengthening of the fibrils in the fibre. When increasing the extension of the RTT fibre even further at a stress of 54 ± 11 MPa, rupture occurred. For collagen fibril N4 a stress at break value of 69 MPa was determined, while fibril N5 persisted when it was loaded to a stress value of 123 MPa. These results suggest that the stress at break value of a collagen fibril is within range of that of a RTT fibre. Based on these findings, the correlation between the rupture mechanism of a RTT fibre and the rupture mechanism of the fibrils it is built from seems plausible.

From the stress-strain curves of a rat tail tendon (RTT) as shown in Fig. 4.2, permanent deformation of fibrils occurs, starting at the yield point at a stress value of around 20 MPa. Slipping of microfibrils has been reported as the deformation mechanism acting in the first yield region.¹⁴ This is based upon the observation that the banding pattern of the fibrils (D-period) showed tilting. In the second yield region, the slipping of microfibrils continues, but the triple helices in the microfibrils also slip, leading to a change in the D-period.¹⁴ The D-period banding pattern can completely disappear due to this damage.⁸

It is found that during mechanical testing of collagen fibrils at stress values below 20 MPa the fibril undergoes fully reversible deformation. During elastic deformation of a collagen fibril, reversible deformation and/or reversible displacement of microfibrils might occur. The deformation of microfibrils can be explained from reversible deformation and/or reversible displacement of triple helices. At stress levels exceeding 20 MPa, permanent deformation was observed, which might occur via irreversible displacement of microfibrils and/or irreversible displacement of triple helices. This is in good correspondence with the yield point in the stress-strain curve of a RTT (Fig. 4.2) at a stress value of 20 MPa. The collagen D-period of the fibrils after permanent deformation up to three times their original length was found to be unchanged as observed by SEM and AFM imaging of the tensile tested fibrils (details: Appendix D) This finding suggests an intact inner structure of the collagen microfibrils, which excludes irreversible displacement of triple helices as a possible mechanism. Irreversible displacement of microfibrils is the proposed mechanism for permanent deformation that corresponds to our findings.

4.3 General conclusions

Tensile testing of single collagen fibrils was enabled by fixation of a collagen fibril to an AFM cantilever and a glass substrate by small glue droplets. From the stress-strain curves of non-treated collagen fibrils N1 and N2 at ambient conditions, Young's moduli of 7.2 and 2.7 GPa were determined. The large difference between the two values was attributed to variation in moisture content of the fibrils. When exceeding a maximal stress of around 90 MPa, permanent lengthening of the fibrils was observed.

Reversible mechanical loading of collagen fibrils N1 and N3 in aqueous media was possible up to stress values of around 20 MPa. A Young's modulus of 280 ± 50 MPa and a modulus of 420 ± 50 MPa at higher stress values above 3 MPa were determined from the stress-strain curves. It was observed that the applied medium (demineralised water, PBS, Na⁺ and Ca²⁺ containing HEPES buffer) had no significant effect on the mechanical properties. The applied loading rate between 0.02 and 20 $\mu\text{m}\cdot\text{s}^{-1}$ did not result in a significant difference in stress-strain behaviour.

The influence of bending on the stress-strain curves of collagen fibrils was investigated using a finite element model for isotropic materials with an elastic behaviour. The results obtained via this model suggest that the influence of bending of the fibril on the obtained stress-strain curves is minimal (details: Appendix to chapter 4).

Permanent deformation of fibrils immersed in aqueous media was observed upon exceeding a stress value of around 20 MPa. Tensile testing of single collagen fibrils to stress values beyond 20 MPa in four different media (demineralised water, PBS, Na⁺ and Ca²⁺-containing HEPES buffer) yielded comparable stress-strain curves.

The length of two collagen fibrils was increased stepwise to enable extensions above 10%. The resulting stress-elongation behaviour of these two fibrils was found to be highly comparable. The overall shape of the stress-elongation curves was comparable, but also the shape of the individual stress-elongation cycles.

The residual stress at the start of each cycle increased while going to higher relative elongation values. This residual stress suggests that stress relaxation of the fibrils occurs at a lower rate than the extension rate of the cycles. Up to ~30% relative elongation no residual stress was observed. Above 30% relative residual stress was observed, which increased at higher relative elongations. It was found that permanent deformation at relative elongations up to 200% does not have a significant influence on the stress-elongation behaviour of collagen fibrils.

4.4 Acknowledgement

M.A. Smithers (Mesa⁺ institute for Nanotechnology, University of Twente) is acknowledged for performing SEM analysis of the surfaces. F.B. Segerink (Optical Techniques group, Faculty of Science and Technology, University of Twente) is acknowledged for removal of the cantilever tips by FIB.

4.5 Experimental

4.5.1 Materials

A phosphate buffered saline solution (PBS, pH 7.4, B. Braun, Melsungen, Germany) containing 140 mM NaCl, 13 mM Na₂HPO₄·2H₂O and 2.5 mM NaH₂PO₄·H₂O was used as received. MES buffer contained 0.05 M 2-[morpholino]ethanesulfonic acid (Sigma-Aldrich, Steinheim, Germany) and was adjusted to pH 5.4 with 1M NaOH or 1M HCl. The buffered Na⁺-HEPES and Ca²⁺-HEPES solutions (sodium chloride, calcium chloride and 2-[4-(2-hydroxyethyl)-1-piperaziny]-ethanesulfonic acid obtained from Merck, Darmstadt, Germany) were prepared as described by Thompson *et al.*¹⁹ and adjusted to pH 7.4 with 1M NaOH or 1M HCl. The phosphate buffer with a pH 7.4 contained a 54 mM Na₂HPO₄·2H₂O solution and a 13 mM NaH₂PO₄·H₂O solution and was adjusted to pH 7.4 with 1M NaOH or 1M HCl (sodium biphosphate and sodium dihydrogenphosphate obtained from Merck, Darmstadt, Germany).

4.5.2 Methods

Preparation of collagen dispersion

Bovine Achilles tendon collagen type I (3.1 g) obtained from Sigma-Aldrich (Steinheim, Germany) was swollen in hydrochloric acid (333 ml, 0.01M) for 14 h at 0°C. The resulting slurry was shredded for 10 min at 0°C at 11000 rpm using a blender (Braun MR 500 HC, Kronberg, Germany), while the temperature was kept below 5°C. The dispersion was filtered through a 74 µm filter (Belco 200 mesh, Vineland, NJ). The collagen dispersion mainly consisted of collagen fibrils, as observed by SEM imaging of undiluted drops of the dispersion on glass (J.A.J. van der Rijt, unpublished results).

Sample preparation

Glass discs with a diameter of 15 mm and thickness: 0.3 mm (Knittel Gläser, Braunschweig, Germany) were manually partly dipcoated in a 6 wt% solution of Teflon AF 1601S in Fluorinert FC-75 (Dupont, Wilmington, DE) and dried horizontally for 14 h at ambient conditions. The partly Teflon-coated glass discs were individually immersed for 10 min in a diluted collagen type I dispersion containing 1 ml of the dispersion and 150 ml PBS (total concentration of collagen: 22 µg collagen per ml). Subsequently, the surfaces were washed in PBS for 10 min and subsequently three times in demineralised water (10 min each). Finally, the discs were dried at ambient conditions for 14 h.

Fixation methodology

Fixation of the fibrils to the substrate at one end and to the AFM cantilever at the other end is described in Chapter 3 of this thesis.

Tensile testing of collagen fibrils.

The fibril glued to the tip of the AFM cantilever by one end and by the other end to the glass surface was immersed in the desired medium and left to equilibrate for 15 min. The AFM cantilever with the fibril fixed to it was moved upward until the deflection value exceeded twice the noise level, equal to a force of approximately 4 nN. A saw-tooth loading pattern with increasing extension between 530 and 3710 nm was used to determine the mechanical properties of the fibril. The extension rate was varied from 0.10 to 0.74 µm·s⁻¹.

SEM imaging of collagen fibrils

Using a Leo 1550 High Resolution SEM, the surface analysis was performed. When excessive charging of the surface was apparent, the sample was sputter-coated with an Au/Pd layer of 5 nm thickness.

4.6 References

- 1 P. Fratzl, *Current Opinion in Colloid & Interface Science*, 2003, **8**, 32.
- 2 E. Gentleman, A. N. Lay, D. A. Dickerson, E. A. Nauman, G. A. Livesay, and K. C. Dee, *Biomaterials*, 2003, **24**, 3805.
- 3 M. Venturoni, T. Gutschmann, G. E. Fantner, J. H. Kindt, and P. K. Hansma, *Biochem. Biophys. Res. Comm.*, 2003, **303**, 508.
- 4 T. J. Wess, A. P. Hammersley, L. Wess, and A. Miller, *J. Mol. Biol.*, 1998, **275**, 255.
- 5 J. P. Orgel, T. J. Wess, and A. Miller, *Structure*, 2000, **8**, 137.
- 6 D. F. Betsch and E. Baer, *Biorheol.*, 1980, **17**, 83.
- 7 J. Parkinson, A. Brass, G. Canova, and Y. Brechet, *J. Biomech.*, 1997, **30**, 549.
- 8 E. Baer, A. Hiltner, and D. Jarus, *Macromol. Symp.*, 1999, **147**, 37.
- 9 S. Leikin, D. C. Rau, and V. A. Parsegian, *Proc. Natl. Acad. Sci. U. S. A.*, 1994, **91**, 276.
- 10 T. J. Wess and J. P. Orgel, *Thermochim. Act.*, 2000, **365**, 119.
- 11 M. E. Nimni, 'Biochemistry', ed. M. E. Nimni, CRC Press, Boca Raton, FL, 1988.
- 12 M. C. Goh, M. F. Paige, M. A. Gale, I. Yadegari, M. Edirisinghe, and J. Strzelczyk, *Physica A*, 1997, **239**, 95.
- 13 N. Sasaki and S. Odijima, *J. Biomech.*, 1996, **29**, 1131.
- 14 J. Kastelic and E. Baer, Symposium of Society for Experimental Biology - Mechanical Properties of Biological Materials, Cambridge University Press, Cambridge, 1980.
- 15 J. A. Petruska and A. J. Hodge, *Proc. Natl. Acad. Sci. USA*, 1964, **51**, 871.
- 16 N. Sasaki and S. Odajima, *J. Biomech.*, 1996, **29**, 655.
- 17 H. B. Li, W. A. Linke, A. F. Oberhauser, M. Carrion-Vazquez, J. G. Kerkvliet, H. Lu, P. E. Marszalek, and J. M. Fernandez, *Nature*, 2002, **418**, 998.
- 18 P. M. Williams, S. B. Fowler, R. B. Best, J. L. Toca-Herrera, K. A. Scott, A. Steward, and J. Clarke, *Nature*, 2003, **422**, 446.
- 19 J. B. Thompson, J. H. Kindt, B. Drake, H. G. Hansma, D. E. Morse, and P. K. Hansma, *Nature*, 2001, **414**, 773.
- 20 Y. L. Sun, Z. P. Luo, A. Fertala, and K. N. An, *Biochem. Biophys. Res. Comm.*, 2002, **295**, 382.
- 21 K. O. v. d. Werf, C.A.J. Putman, B.G. de Grooth, F.B. Segerink, E.H. Schipper, N.F. van Hulst, J. Greve, *Rev. Sci Instrum.*, 1993, **64 (10)**, 2892.
- 22 T. Gutschmann, G.E. Fantner, M. Venturoni, A. Ekani-Nkodo, J.B. Thompson, J.H. Kindt, D.E. Morse, D. Kuchnir Fyngenson, P.K. Hansma, *Biophys. J.*, 2003, **84**, 2593.
- 23 D. L. Christiansen and F. H. Silver, *Biomimetics*, 1992, **1**, 265.
- 24 K. Takaku, T. Ogawa, T. Kuriyama, and I. Narisawa, *J. Appl. Pol. Sci.*, 1996, **59**, 87.
- 25 K. Takaku, T. Kuriyama, and I. Narisawa, *J. Appl. Pol. Sci.*, 1996, **61**, 2437.
- 26 S. M. Cusack, A., *J. Mol. Biol.*, 1979, **135**, 39.

- 27 E. Knörzer, W. Folkhard, W. Geercken, C. Boschert, M. H. J. Koch, B. Hilbert, H. Krahl, E. Mosler, H. Nemetschek-Gansler, and T. Nemetschek, *Arch. Orthop. Trauma Res.*, 1986, **105**, 113.
- 28 M. Raspanti, *Arch. Hist. Cytol.*, 2002, **65**, 37.
- 29 D. H. Elliott, *Biol. Rev.*, 1967, **40**, 392.
- 30 G. D. Pins and F. H. Silver, *Mater. Sci. Eng. C*, 1995, **3**, 101.

APPENDIX TO CHAPTER 4

Effect of bending of a collagen fibril during tensile testing

A4.1 Introduction

Tensile testing of a single collagen fibril was enabled by fixation of one fibril end to a glass substrate by a droplet of epoxy glue and the other end to an AFM cantilever using a second drop of epoxy glue. Originally, the fibrils were deposited on a partially Teflon coated glass surface. After fixation of the fibril, as described before, the fibril was lifted from the surface using the AFM cantilever until the fibril was straight above the fixation point on the surface and a force of $\sim 4\text{nN}$ (equal to a stress of 0.13 MPa for a fibril with a diameter of 200 nm) was exerted on the fibril. The change in configuration of the fibril is shown in Fig. A4.1.

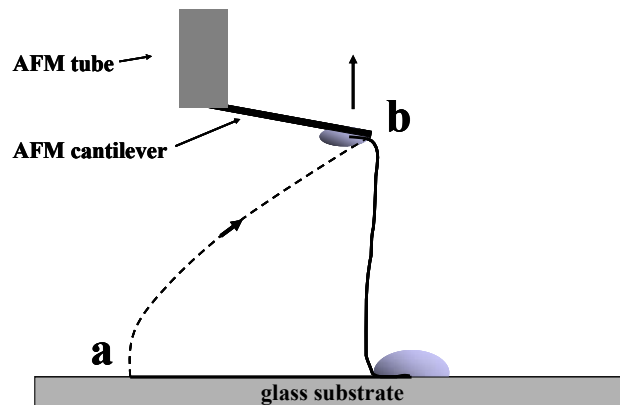


Figure A4.1 (a) Schematic representation of initial configuration of the fibril deposited on the substrate. (b) Configuration of the fibril during tensile testing. A schematic picture of the displacement of the fibril from the initial to the final position is represented by the dashed line.

The tensile testing experiment was started after the fibril was placed in configuration **b**. In configuration **b** when the fibril was fully stretched a tensile testing experiment was performed. The mechanical properties of the collagen fibril were derived from the obtained stress-strain curves.

In these calculations, it is assumed that the fibril has a geometry similar to an uniaxial tensile test. The total length of the fibril is assumed to be equal to the distance between the fixation points on the cantilever and on the glass surface.

In reality, the fibril is elongated perpendicular to the original orientation of the fibril (Fig. A4.1). This implies that near the fixation points the fibril is highly bent. The influence of bending of the fibril on the stress-strain curves was investigated in more detail.

The possible influence of bending of a collagen fibril on the corresponding stress-strain curves via the applied tensile testing approach is discussed below.

- What is the shape of the fibril during reversible loading in the applied configuration? The length of the fibril used in the calculations was obtained from the distance between the AFM cantilever and the glass surface. When a significant segment of the fibril length is involved in the curvature of the bend, the actual length of the fibril is higher than that used in the calculations.
- What are the stress levels in the fibril, originating from the bending process? The bending of the fibril will lead to stress concentrations near the fixation points of the fibril ends.
- What is the influence of bending of the fibril on the mechanical properties derived from the stress-strain curves? During loading of the fibril the stress should be equally distributed over the fibril to ensure that the configuration in which the fibril was tensile tested can be compared to an uniaxial tensile testing experiment.
- What is the influence of the Young's modulus of the fibril on the effect of bending on the stress-strain curves?

A4.2 Methods

To address these questions, the simultaneous bending and tensile testing of the fibril was modelled using finite element analysis. Finite element analysis is a tool used in mechanical engineering to describe and solve problems that occur during loading of complex material designs.

The collagen fibril has a typical thickness in the order of ~ 200 nm and a typical length of ~ 100 μm . The mechanical behaviour of the fibril during simultaneous bending and tensile testing was simulated by the bending and stretching of a sheet with a thickness of 0.2 mm, a width of 1 mm and a length of 100 mm, which ensures a similar length to width ratio as the fibril. Furthermore, the modulus was set to 300 MPa, which is equal to the obtained Young's modulus of collagen fibrils immersed in aqueous media (details: chapter 4).

The plate-shaped model has an initial length of 100 mm and lies in a straight geometry flat on a surface. Then, one of the fixation points is lifted upward until the distance between the clamps

is 95 mm. At that height, no tensile stress was calculated by the model in the middle of the fibril. The resulting stress in the sheet during further elongation, as well as the local stress near the fixation points, will be calculated based on the following model.

The stress in the sheet model was considered in two dimensions as shown in Fig. A4.2a. The deformation of the plate in this modelling experiment is described by the Mindlin theory.^{1, 2} The bending of a plate, including shear stresses in the plate, can be described using this model. Regarding the material model, a model that exactly describes the stress-strain behaviour of an oriented semi-crystalline fibre, while taking non-linear deformations into account, is currently not available. Therefore, a finite element model for isotropic materials under elastic deformations was used. The degree of bending of a plate over a radius R can be described by the model when R is minimally five times larger than the thickness of the plate. The Poisson ratio (ν) of the plate material was set to 0.3.

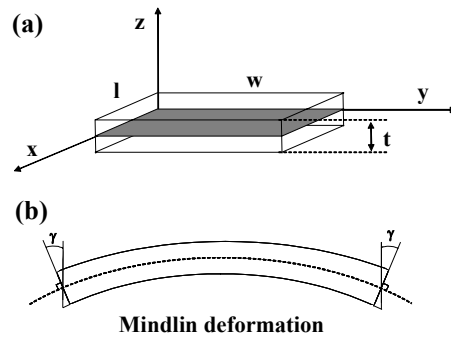


Figure A4.2 (a) Plate stress model coordinates, x : width, y : length, z : thickness. (b) Deformation of a plate according to the Mindlin theory.

The chosen finite element model can only provide a limited description of the effect of bending on the stress-strain behaviour of a plate, because of the constraints as discussed above. A model that exactly describes the stress-strain behaviour of an oriented semi-crystalline fibre, while taking non-linear deformations into account, is currently not available. Furthermore, to develop and use a more simplified 3-D isotropic model would demand long simulation times and a great effort, which is beyond the scope of this thesis. The results obtained by modelling of a plate during tensile testing in a bent configuration according to the Mindlin theory therefore can only provide an indication of the effect of bending on the stress-strain behaviour of a single collagen fibril.

A4.3 Results

The plate with a length of 100 mm, a width of 1 mm and a thickness of 0.2 mm was fixed at coordinates x,y,z : $(0,0,0)$ and $(100,0,0)$. The stress in the plate is calculated at 15 integration points in each of the 100 blocks with a size of $1 \times 1 \times 0.2$ mm ($l \cdot w \cdot t$), consisting of two equally sized triangular elements. During the experiment the fixation point at $(100,0,0)$ is transferred to coordinate $(0,0,95)$, which is directly above the first fixation point. The plate is elongated by moving the upper fixation points to coordinate $(0,0,105)$. The geometries of the plate with the upper fixation point at coordinates $(0,0,95)$ up to $(0,0,105)$ are shown in Fig. A4.3.

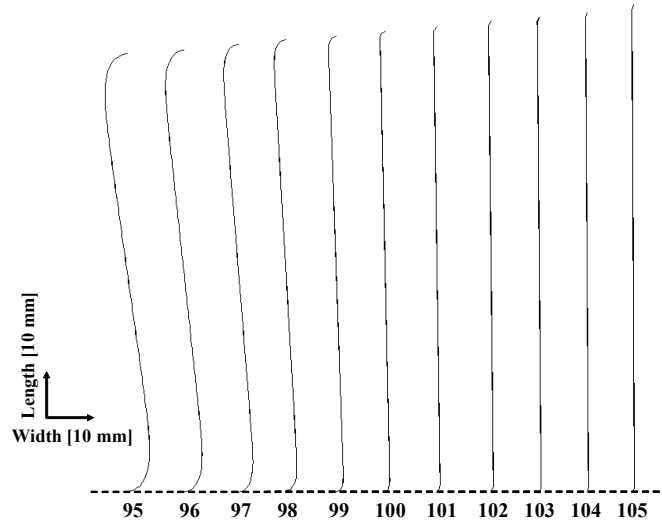


Figure A4.3. Plate geometry during translation of the second fixation point from the original position $(0,0,95)$ directly above the first fixation point up to a new position $(0,0,105)$.

From the geometry of the plate between 95 and 105 mm in height it can be concluded that a rapidly decreasing fraction of the total length of the plate is involved in the bending experiment. The bending of the plate occurs over a radius that is decreasing while increasing the distance between the fixation points.

For a better comparison with the experimental results obtained for collagen fibrils, two modelling experiments were performed. For a plate with a modulus of 300 MPa and a geometry ($t \cdot w \cdot l$) of $0.2 \times 1 \times 100$ mm the following elongation was performed.

In configuration **A**, the plate was elongated over 10 mm in the z -direction starting at $(0,0,95)$ to $(0,0,105)$. In configuration **B** the plate was elongated over 5 mm in the x -direction from $(100,0,0)$ to $(105,0,0)$ to obtain an uniaxial tensile test (Fig. A4.4). Two force-distance curves were obtained, which were significantly different in shape.

For configuration **B**, a linear force-distance curve starting at 100 mm length at zero force was obtained, which increased to a force of 3.0 N at a length of 105 mm. In configuration **A**, the force in the centre of the plate was found to increase gradually from 0.002 N at 94.6 mm length to 0.36 N at 100 mm and 2.84 N at 105 mm length (Fig. A4.5).

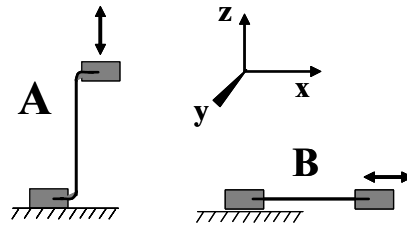


Figure A4.4 Two tensile testing configurations: configuration **A** contains two bending points and configuration **B** is performed as an uniaxial tensile test.

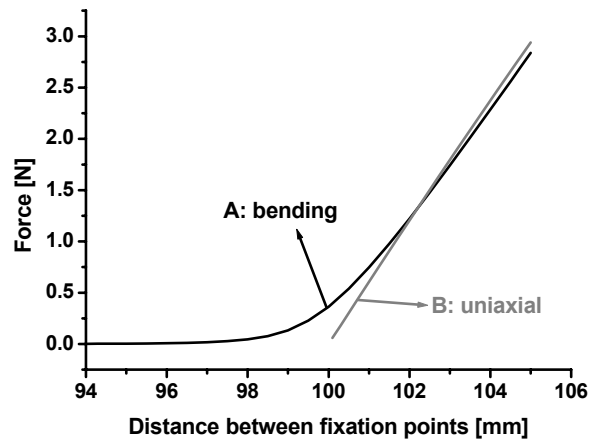


Figure A4.5 Force-distance curves of a plate with dimensions ($0.2 \times 1 \times 100$ mm), when tensile tested in configuration **A** and **B** as schematically depicted in Fig. A4.4.

To compare the mechanical behaviour of the plate as shown in Fig. A4.5 with the experimental results of single collagen fibrils immersed in aqueous media, the obtained force-distance curves have to be transformed into stress-strain curves. The stress-strain curve of a single collagen fibril starts at 0% strain. This value is correlated to the length of the fibril (actually, the distance between the fixation points) when a stress of 0.13 MPa (equal to a force of ~ 4 nN for a fibril with 200 nm diameter) was monitored, while extending the fibril over 500 nm distance at $0.1 \mu\text{m}\cdot\text{s}^{-1}$, during manual lifting of the fibril.

For the force-distance curve obtained for the plate in configuration A, a stress of 0.15 MPa limits the minimal stress that could be detected in the set-up used for the single collagen fibrils. Therefore, the zero strain level was set equal to a height of 97.5 mm for the plate. At that point an overall stress significantly higher than the noise level is acting on the plate.

The total length of the plate at 97.5 mm distance between the fixation points still is 100 mm, therefore, in the calculation of the strain, L_0 was 100 mm. The force-distance curve calculated for a plate in configuration B starts at 0% strain. For both configurations, in the calculation of the stress from the force on the centre of the plate and the cross-section, the decrease in the cross-section of the plate was calculated assuming a Poisson ratio of 0.3. The calculation of the strain represents an average value, calculated from the extension values obtained from the modelling experiment. The value can be considered equal to the strain in the plate within an error of $\sim 0.2\%$. The resulting stress-strain curves are shown in Fig. A4.6.

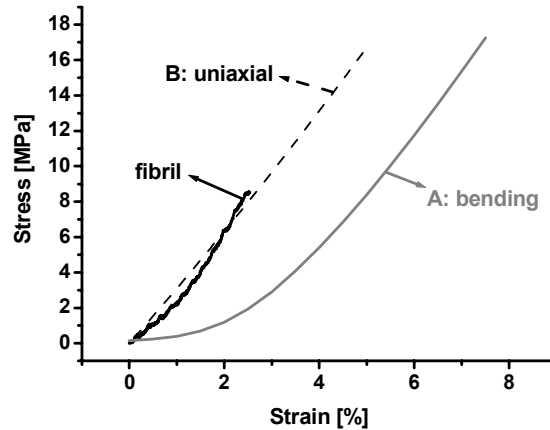


Figure A4.6 Stress-strain curve of a single collagen fibril immersed in an aqueous medium (black solid line). Modelled stress-strain curve of a plate with a Young's modulus of 300 MPa and initial dimensions of $0.2 \times 1 \times 100$ mm ($t \cdot w \cdot l$), tested in uniaxial configuration **B** (black dashed line) and modelled stress-strain curve of the same plate tensile tested in configuration **A**, which contains two bending points (grey solid line).

The stress-strain curves obtained by modelling of tensile testing of a plate in two configurations show a significant difference. The slope of the stress-strain curve of the plate tested in configuration B (uniaxial) is constant, while the slope of the stress-strain curve of the plate in configuration A (bending) gradually increases, until it is equal to the slope obtained in configuration B at $\sim 4.7\%$ strain. This finding suggests that when a plate is tensile tested in both configurations, the stress-strain curves have the same slope above 4.7% strain. The stress-strain curve in configuration A (bending) will be influenced by the bending of the plate up to that strain value and the modulus obtained for the stress-strain curve does not represent the Young's modulus.

When the stress-strain curve of a collagen fibril immersed in aqueous medium is compared to the stress-strain curves of the plate in both configurations, the shape of the stress-strain curve is highly similar to that of the plate tested in configuration B (uniaxial). Apparently, the stress-strain curve of a single collagen fibril is not influenced as strongly as suggested by the obtained modelling results. This suggests that the stress needed to create a sharp bend in the collagen fibril is lower than observed for the plate in the modelling experiments, probably because of

local plastic deformation in the fibril. For collagen fibrils during bending and subsequent elongation, large stresses are generated on the outside and inside of the bent fibril segment. Above a stress of around 20 MPa, collagen fibrils immersed in aqueous media were found to undergo permanent deformation. This process is also expected to occur for collagen fibrils in the applied tensile testing configuration, based on the calculated stress levels for the plate during bending. In principle, stress concentrations are expected to occur at the bending points in the fibril. Rupture of the fibril might be initiated at these locations. Imaging of ruptured collagen fibrils after tensile testing showed that the broken ends of the fibril were not located directly at the fixation point at the outside of the glue droplets.

When a plate is bent, the deformation of the plate on the outside consists of elongation, while the inside of the plate experiences compression. This leads to stress concentration in the ends of the plate near the fixation points. Because of the constraints set by the model, the stress values calculated on the outside and inside of the plate at the bending point cannot be directly compared to the values that would be generated during bending of a fibril.

Collagen fibrils tensile tested at ambient conditions showed a linear stress-strain behaviour with a Young's modulus of ~ 5 GPa (chapter 4). The modelled tensile test of the plate in configuration A and B was repeated with a Young's modulus of 5 GPa. The effect of bending of the plate on the stress-strain behaviour was similar as found for a plate with a Young's modulus of 300 MPa, as shown above. In Fig. A4.7 the stress-strain curves of both configurations are presented, together with the stress-strain curve obtained for a collagen fibril at ambient conditions.

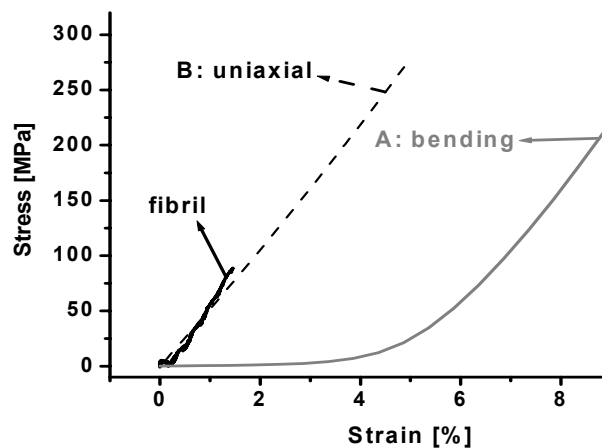


Figure A4.7. Stress-strain curve of a single collagen fibril at ambient conditions (black solid line). Modelled stress-strain curve of a plate with a Young's modulus of 5 GPa and initial dimensions of $0.2 \times 1 \times 100$ mm ($t \cdot w \cdot l$), tested in uniaxial configuration **B** (black dashed line) and modelled stress-strain curve of the same plate tensile tested in configuration **A**, which contains two bending points (grey solid line).

When both stress-strain curves are compared to that of the collagen fibril, the stress-strain curve of the plate tested in configuration B (uniaxial), resembles best with the curve of the fibril tested at ambient conditions. This result is the same as observed for the stress-strain curve of the plate with a Young's modulus of 300 MPa, when compared to the stress-strain curve of a collagen fibril immersed in an aqueous medium. This suggests that the modulus of the plate does not influence the difference in the force-distance curve or in the stress-strain curve, when tensile tested in configuration A (bending) or configuration B (uniaxial).

A4.4 Relevance of the modelling experiments for tensile tests with fibrils

As shown before, the applied model can only provide an indication of the influence of bending of the fibril during tensile testing on the obtained stress-strain curves. Also, the limited number of elements in the plate over which the stress is calculated limits the resolution of the bending radius of the plate.

The influence of bending on the stress-strain curve of an isotropic plate during elastic deformation as described by the model should be regarded as a worst case scenario. When for instance plastic deformation would be included, the bending of the plate would occur at even lower stress values than observed for the current model.

The influence of bending decreases, when the radius over which the bend occurs decreases, finally leading to a slope of the stress-strain curve, which is similar to that of the uniaxial stress-strain curve.

This can be observed from Fig. A4.5, in which the force-distance curves of the uniaxial and the bent configuration are compared. Up to a distance of around 102 mm between the fixation points, the two curves have a different slope, but beyond this distance the two curves almost overlap. This suggests that the uniaxial character of the force-distance curve obtained for the fibril in the bent configuration prevails from a certain elongation on. The shape of the plate at this elongation (102 mm) is shown in Fig. A4.3.

A4.5 Conclusion

The length of the fibril involved in bending, compared to the length of the fibril as calculated from the distance between the fixation points, can be estimated by the geometry of the plate during the modelling experiments. Since the tensile testing experiment in the bent configuration of the plate was assumed to start at a minimal overall stress of 0.13 MPa on the plate, the distance between the fixation points at zero strain was determined at 97.5 mm. The overall length at this point still is 100 mm. In the geometry image of the plate only a small segment is bent, while the major part is oriented as expected for an uniaxial tensile test.

It is envisaged that during bending of the plate at the fixation points a stress will be generated. When the finite element model was applied, tension and compression stress were observed in the bending points. These stresses are likely to also occur during bending of a collagen fibril. At stress values above 20 MPa, permanent lengthening of the collagen fibrils was observed, exceeding this stress level during tensile testing of the fibril might facilitate its bending.

Based on the similarity between the stress-strain curves of a single collagen fibril and the modelled uniaxial stress-strain curve of a proportionally similar plate with the same Young's modulus, the influence of bending of the fibril on its stress-strain curve was suggested to be small. The observed results based on a model experiment, assuming a uniform material with fully elastic deformation, showed a large influence of bending on the stress-strain curve.

Probably, the fibril undergoes a bend at very low stress values, an effect which is not observed during the applied tensile testing procedure. The remaining stress-strain behaviour is dominated by the uniaxial tensile test. This effect was also observed in the modelling experiments on the plate, although it occurred at a higher stress and strain levels. In the modelling experiments, the difference between the stress-strain curves obtained in the uniaxial and the bent configuration was observed between 0 and 5% strain. At larger elongation of the plate, both curves had a similar slope. The influence of bending on the shape of the stress-strain curve, as determined by the modelling experiments for a plate with a Young's modulus of 300 MPa and 5 GPa, was not changed due to the difference in modulus.

A4.6 Acknowledgements

Prof. dr. J. Huétink is acknowledged for discussion of the bending effect and facilitating the finite element modelling experiments. Dr. ir. T. Meinders is acknowledged for performing the finite element modelling experiments and discussion of the implications for the stress-strain behaviour of collagen fibrils.

A4.7 Materials and Methods

Modelling experiments were performed using the finite element code DIEKA, developed at the Huétink group, faculty of Engineering Technology, University of Twente.

A4.8 References

- 1 J. L. Batoz and P. Lardeur, *Int. J. Num. Meth. Eng.*, 1989, **28**, 533.
- 2 B. D. Carleer, 'Finite element analysis of deep drawing', University of Twente, Enschede, 1997.

CHAPTER 5

Chemical modification (cross-linking) of collagen fibrils - Influence on mechanical properties

"The meeting of two personalities is like the contact of two chemical substances; if there is any reaction, both are transformed." - Jung

(Abstract)

The influence of glutaraldehyde and a carbodiimide/N-hydroxysuccinimide (EDC/NHS)-mediated cross-linking of collagen fibrils on their mechanical properties was investigated. The tensile properties of a fibril immersed in phosphate buffer (pH 7.4) with an initial length of 126 μm , loaded to a maximal stress of around 15 MPa did not change upon glutaraldehyde cross-linking. The glutaraldehyde cross-linked fibril ruptured at a stress of 168 MPa. A collagen fibril with an initial length of 44 μm , which was cross-linked using EDC/NHS, ruptured at a stress of 87 MPa.

Glutaraldehyde cross-linked fibrils showed a rapid increase in residual stress in cyclic stress-elongation curves at increasing relative elongation. This suggests that the rate of stress relaxation is lower than the applied extension rate.

For EDC/NHS cross-linked fibrils, a different stress-strain behaviour was observed. Due to rapid stress relaxation, no residual stress was observed. Surface decoration of microfibrils during EDC/NHS cross-linking resulted in an even higher stress relaxation rate than observed for non-treated fibrils.

Glutaraldehyde cross-linked, non-treated and EDC/NHS cross-linked fibrils, all showed an increase in residual stress at higher relative elongation values. The reduced diameter during elongation was thought to cause a reduction in distance between the microfibrils. The enhanced strength and number of non-covalent interactions between microfibrils will hinder the irreversible microfibril displacement process. For glutaraldehyde cross-linking the increase in residual stress at higher relative elongation was increased even further by the presence of covalent bonds between microfibrils.

5.1 Introduction

Cross-linking of collagen is a process occurring in humans and animals, which stabilizes the internal structure. These natural cross-links are an important aspect of the ageing process. Cross-linking involves several enzymatically initiated condensation reactions. An example is the lysyl oxidase-mediated formation of aldehyde groups from lysine and hydroxylysine residues in the collagen triple helix, mainly located at the C- and N-telopeptides. An aldehyde functional group is formed, which is converted into an imine bond upon intramolecular condensation with a lysine residue of another polypeptide of the triple helix. Further condensation reactions and rearrangements lead to a variety of cross-links.^{1, 2} Covalent binding of the three polypeptide chains of the triple helix, will stabilize its quaternary structure. Natural cross-linking of collagen continues during the lifetime of humans and animals. As a consequence, the stiffness of tissue increases in time, as shown by the increasing modulus in the yield region of rat tail tendons at increasing age.³⁻⁵

Since the 1970s, collagen has been applied in biomaterial applications such as sutures, heart valve prostheses and ligament prostheses.^{6, 7} Cross-linking has proven an essential step in the manufacturing of biomaterials, because it prevents rapid biodegradation. Furthermore, cross-linked collagen materials will provoke a milder foreign body reaction upon implantation, compared to non-treated collagen.⁶ The cross-linking agent that has been extensively used for biomaterial fixation is glutaraldehyde. The glutaraldehyde cross-linking reaction of collagen polypeptide chains is schematically shown in Fig. 5.1a.

More recently, a number of disadvantages of the glutaraldehyde treatment were described, of which calcification of the resulting collagen structure after implantation was the most important one.⁸⁻¹⁴ The exact origin of calcification is still under debate, but initiation of calcium phosphate deposition at cellular remnants (phospholipids and proteins)¹⁵⁻¹⁷ and/or stress-induced damage¹⁸⁻²⁵ are the most likely causes. In the last decade, new cross-linking reagents have been developed, which have resulted in reduction of calcification.²⁶⁻²⁸ The mechanical properties of collagen-based materials cross-linked via different methods depend on the cross-linking agent and the degree of cross-linking. It is not yet possible to predict the effect of the cross-linking reagent on the mechanical properties of the resulting collagen structure. One example of a new cross-linking agent, which reduces calcification in collagen-based biomaterials, is 1-ethyl-3-(3-dimethyl aminopropyl) carbodiimide hydrochloride in combination with N-hydroxysuccinimide (EDC/NHS).^{29, 30} This 'zero-length' cross-linking reaction between collagen polypeptide chains is schematically depicted in Fig. 5.1b.^{31, 32}

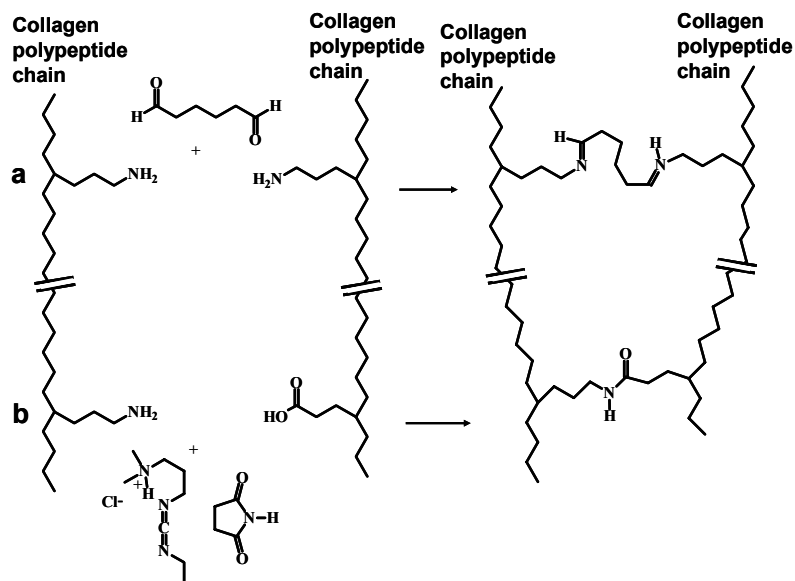


Figure 5.1 Cross-linking between two collagen polypeptide chains. The chains contain residues with carboxylic acid (aspartate or glutamate) or amine (hydroxylysine and lysine) functional groups. A cross-link can be formed via a glutaraldehyde spacer as shown in scheme **a** of the simplified graph. A condensation reaction between an aldehyde and an amine group forms an imine bond (also referred to as Schiff base). This imine bond is not stable over long time periods, therefore it is usually transformed into an amine bond by reduction using sodium cyanoborohydride. In scheme **b** a 'zero-length' amide cross-link is formed via the condensation reaction between an amine and a carboxylic acid group after EDC/NHS activation of the carboxylic acid group.

Glutaraldehyde cross-linking enables covalent binding of two amine groups of (hydroxy)-lysine residues at a distance of 1.3 nm. The distance between triple helices, calculated from the distance between the polypeptide backbone of the α -amino acid chains in two adjacent triple helices, is reported to be 0.15-0.18 nm (Fig. 5.2). The distance between microfibrils as calculated from the triple helix backbone is 1.3-1.7 nm (Fig. 5.2).³³ Therefore, glutaraldehyde cross-linking is thought to generate intra- and inter-triple helical cross-links as well as inter-microfibrillar cross-links.

Using EDC/NHS, cross-linking takes place after activation of carboxylic acid groups and subsequent reaction with amine group functionalized residues. Only intra- and inter-triple helical cross-linking are expected to occur after reaction of collagen with EDC/NHS.

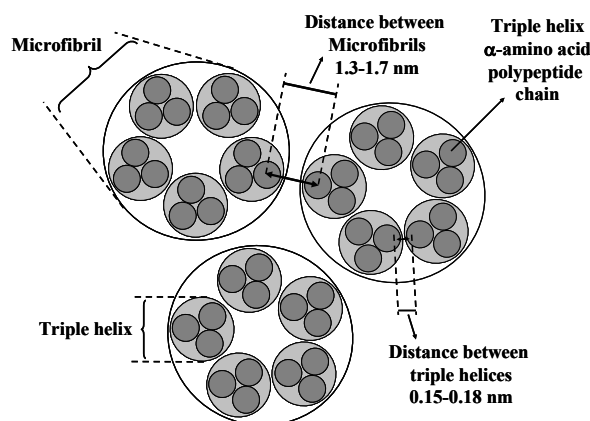


Figure 5.2 Schematic representation of the organisation of three collagen α -amino acid polypeptide chains into a triple helix and the assembly of five triple helices in a microfibril. The shortest distance between triple helices (0.15-0.18 nm) and microfibrils (1.3-1.7 nm), as calculated from the polypeptide backbone of the α -amino acid polypeptide chains in the triple helix, is shown in the figure.

It is known from studies on self-assembled collagen fibres that their mechanical properties can alter significantly upon cross-linking. The stress at break of wet fibres increased from 2.4 MPa for non-treated fibres, to 44 MPa for glutaraldehyde cross-linked fibres. The Young's modulus of the wet fibres also increased from 13 MPa to 314 MPa for non-treated and glutaraldehyde treated fibres, respectively.³⁴

The structure of collagen has been studied for decades. Spectroscopic, X-ray diffraction - and degradation studies revealed an organisation starting with collagen triple helices, which self-assemble via microfibrils, fibrils, and fibres into the macroscopic structure.³⁵ The relation between the mechanical properties of the macroscopic structure and its constituting elements is still obscure. Even less understood is the influence of cross-linking on the mechanical properties of substructures such as triple helices, microfibrils and fibrils. The effect of cross-linking on the macroscopic structure can be determined by mechanical testing. The influence of cross-linking of the substructures on the mechanical properties of the macroscopic collagen structure has not been studied.

In chapter 3 of this thesis it has been shown that single collagen fibrils can be fixed between an AFM cantilever and a substrate by epoxy glue droplets. The fibril can be lifted from the Teflon surface, because the epoxy glue does not adhere to Teflon. Mechanical testing of non-treated collagen fibrils is described in chapter 4. Mechanical tests of collagen fibrils placed in aqueous media showed that permanent deformation occurred at stress values above 20 MPa. The mechanical behaviour of the fibrils did not change when different media (PBS (pH 7.4), HEPES buffer (pH 6.9), CaCl₂ containing HEPES buffer (pH 6.9) or demineralised water) and extension rates (0.02 - 20 $\mu\text{m}\cdot\text{s}^{-1}$ using the same media) were applied.

By applying a stepwise elongation of a non-treated fibril a stress at break of 69 MPa was determined (details: Chapter 4). In this chapter the mechanical properties of single collagen fibrils cross-linked either with glutaraldehyde or EDC/NHS will be investigated and compared with the mechanical properties of non-treated fibrils.

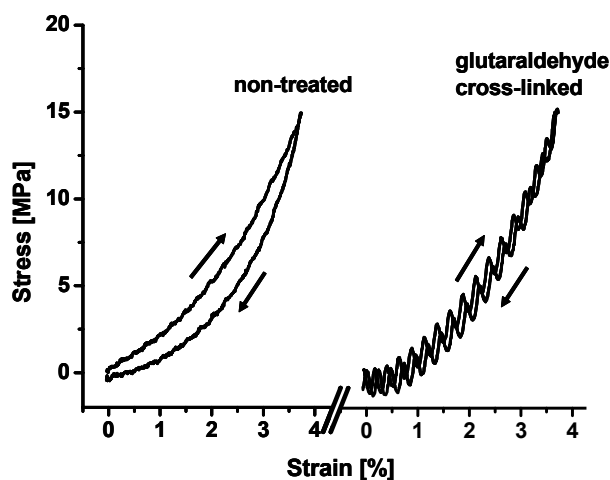
5.2 Results and discussion

5.2.1 Optimization of cross-linking conditions using a collagen fibre system

To ensure optimal cross-linking conditions for the cross-linking of collagen fibrils, the cross-linking of self-assembled collagen fibres³⁶ (typical diameter of 100 μm) with either glutaraldehyde or EDC/NHS was investigated. The reduction of the number of amine groups per 1000 amino acid residues as measured by the TNBS method³⁷, was used to assess the degree of cross-linking in time. For cross-linking with glutaraldehyde, an optimal cross-linking was obtained after reacting the fibres with 0.25 vol% glutaraldehyde in phosphate buffer at pH 7.4 for 2 h at room temperature. This resulted in a reduction of free amine groups from 28/1000 to 4/1000. The highest cross-linking density for the reaction with EDC/NHS was obtained using a molar ratio of EDC and NHS of 3.3, and a molar ratio of EDC to free carboxylic acid groups of collagen of at least 200, and a reaction time of 4 h in 0.05 M MES buffer at pH 5.4. These cross-linking conditions resulted in a reduction of free amine groups from 28/1000 to 8/1000. The optimal conditions for the cross-linking of collagen fibres were also used for the cross-linking of a single fibril.

5.2.2 Stress-strain behaviour of fibrils at low strain before and after glutaraldehyde cross-linking

A single collagen type I fibril (fibril N1, details in table of Fig. 5.3) from bovine Achilles tendon origin with a diameter of 370 nm and an initial length of 126 μm was fixed in the AFM set-up to enable mechanical testing (details: chapter 3). The fully stretched fibril (immersed in phosphate buffer, pH 7.4) was tensile tested by cyclic loading with a maximal extension of 4.0 μm at an extension rate of 0.8 $\mu\text{m}\cdot\text{s}^{-1}$, which led to a maximal stress of 15 MPa. In Fig. 5.3 the resulting stress-strain curves are depicted. A fully reversible stress-strain behaviour was observed. Subsequently, the medium was exchanged with a 0.25 v% solution of glutaraldehyde in the same phosphate buffer. The fibril was left to equilibrate and to cross-link for a period of 2 h and the medium was not refreshed. The fibril (new coding: fibril G1, details in table of Fig. 5.3) was loaded with an extension of 4.0 μm at an extension rate of 0.8 $\mu\text{m}\cdot\text{s}^{-1}$, leading to a maximal stress of 15 MPa.



Fibril	L_0 (μm)	d^{\equiv} (nm)	ext. rate ($\mu\text{m}\cdot\text{s}^{-1}$)	cant. ($\text{N}\cdot\text{m}^{-1}$)	$\varepsilon^{\#}$ (%)	$\sigma^{\#}$ (MPa)	E^{\ddagger} (MPa)
N1	126 ± 0.5	370 ± 20	0.8	29.3 ± 1.9	3.7	14.9	200 - 610
G1	126 ± 0.5	370 ± 20	0.8	29.3 ± 1.9	3.7	15.3	160 - 700

Figure 5.3 Experimental conditions and mechanical properties of a single collagen fibril before and after cross-linking by glutaraldehyde, obtained from stress-strain curves at stress values up to 15 MPa. Non-treated (N1, details: appendix C), phosphate buffer, pH 7.4. Glutaraldehyde cross-linked (G1, details: appendix C), 0.25 v% glutaraldehyde in phosphate buffer, pH 7.4 for 2 h. The medium was not refreshed. Both experiments were performed at room temperature. Experimental details and obtained mechanical properties are shown in the table. Table details: \equiv : swollen fibril; $\varepsilon^{\#}$: strain at maximally applied stress $\sigma^{\#}$; E^{\ddagger} : the initial slope was determined at stress values up to 2.3 ± 0.6 MPa and the final slope was calculated at stress values higher than 7.0 ± 0.1 MPa.

The noise pattern superimposed on the deflection signal, which is especially apparent in the curve of the cross-linked fibril, is caused by an interference effect of the AFM laser. The values of the slopes of the stress-strain curves are shown in the table of Fig. 5.3. The slopes for cross-linked and non-treated fibrils were similar.

It has previously been observed for self-assembled collagen fibres that cross-linking with glutaraldehyde increases the stiffness.^{34, 36} An increase of the high strain modulus from 13 to 340 MPa was observed after cross-linking with glutaraldehyde. The modulus was calculated by drawing a best-fit secant line at the upper region of the stress-strain curve to obtain an average stiffness. For the non-treated fibres the stress at break was 2.4 ± 0.5 MPa, while for the glutaraldehyde cross-linked fibres a stress at break of 37 ± 8 MPa was determined. The slopes therefore were determined at stress values between 0.4 and 2.4 MPa for non-treated and between 10 and 37 MPa for glutaraldehyde cross-linked fibres.^{34, 36} Self-assembled fibres consist of random aggregates of fibrils. Our results show that at single fibril level no difference

in the modulus between cross-linked and non-treated fibrils was observed (Fig. 5.3). This suggests that the stress-strain behaviour of cross-linked and non-treated self-assembled collagen fibres will be influenced by the interaction between fibrils.

As shown in the introduction of chapter 4 (see Fig. 4.2), natural cross-linking of rat tail tendons (RTT) had no significant influence on their initial modulus, as determined from the linear region in the stress-strain curve (determined from 3-20 MPa).³ Only the stress at break value was found to increase significantly at increasing age of the rat. This suggests that the influence of cross-linking of single collagen fibrils on their mechanical properties, can only be observed at higher stress and strain values.

5.2.3 Stress-strain behaviour of glutaraldehyde cross-linked fibrils at high relative elongation

As mentioned in chapters 3 and 4, the maximal extension of the AFM tube is limited to 4.0 μm . As shown previously in chapter 3, further extension of the fibril to rupture was enabled by lifting the entire AFM head using a calibrated setscrew over height Δh . While the fibril was continuously loaded with a sawtooth pattern ($\Delta l = 4.0 \mu\text{m}$ at $0.8 \mu\text{m}\cdot\text{s}^{-1}$), the AFM head was manually lifted in steps of 3 μm every third cycle (see Fig. 5.4). Only the second cycle (marked with an asterisk) was used in the analysis of the mechanical properties of the fibril. This selection was made because during the loading part of the first curve the height is being changed manually, which might influence the observed mechanical behaviour.

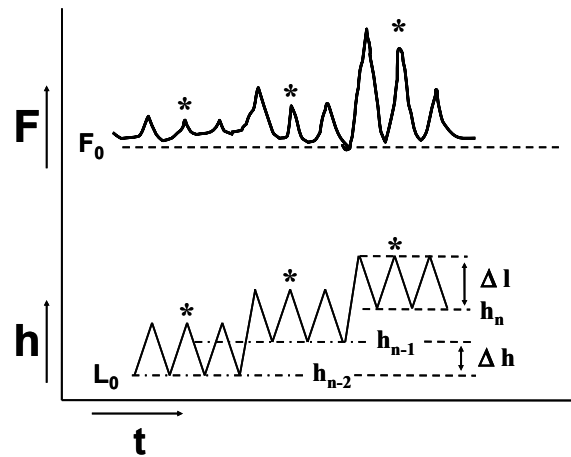


Figure 5.4 Schematic representation of the methodology for tensile testing of a collagen fibril via a stepwise height increase. The height was increased by 3.0 μm , after each third cycle, during continuous cyclic loading over an extension of 4.0 μm at an extension rate of $0.74 \mu\text{m}\cdot\text{s}^{-1}$. The cycling was started at a certain height, where the force on the fibril was $\sim 4 \text{ nN}$. After three cycles at h_{n-2} the height is increased over 3.0 μm to h_{n-1} , where $h_{n-1} = h_{n-2} + \Delta h$. In the analysis, only the second cycle at each height was used.

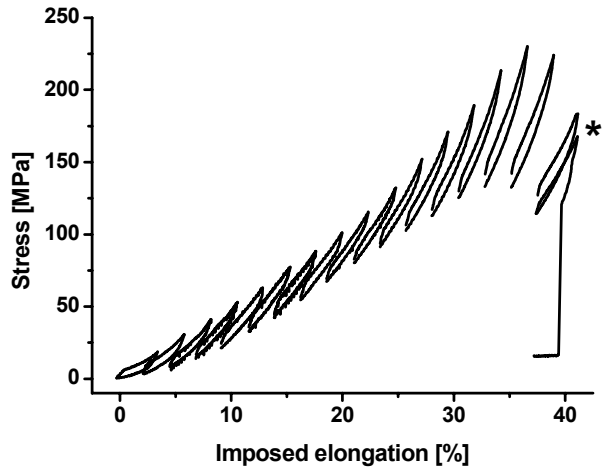
The collagen fibril (fibril G1, details in table of Fig. 5.3), which was cross-linked with glutaraldehyde and tensile tested to a stress value of 15 MPa, was used for the experiment as depicted in Fig. 5.4. The resulting stress-elongation behaviour is shown in Fig. 5.5.

A second fibril N5 (fibril N5, details: chapter 4 and appendix C), with an initial length of 101 μm and an original diameter of 201 nm, was used after being extended in length from 101 to 192 μm during tensile tests described in chapter 4. Because no rupture had occurred after extending the non-treated fibril over 190% in length, the fibril was also immersed in a 0.25 v% glutaraldehyde solution in phosphate buffer at pH 7.4 for 2 h. Subsequently, fibril G2 (previously N5, now G2, details: chapter 4 and appendix C) was stressed to break using the method shown in Fig. 5.4. The resulting stress-elongation behaviour of this fibril is depicted in Fig. 5.6.

The permanent deformation of the fibril during mechanical testing over these large extensions was expected to result in a decrease in fibril diameter. This may lead to a change in the internal structure of the fibril. The diameter of the fibril after the imposed elongation was calculated assuming a Poisson ratio of 0.5. The stress values for both fibrils were corrected for the decrease in diameter, which has been verified experimentally (details: appendix A).

The imposed elongation in this experiment is normalized at 0% elongation using the initial length. The increase in relative elongation was calculated from two parameters. First, from the stepwise height increase (3 μm) the length at the start of three loading cycles was calculated. The additional extension from the cyclic loading over 4 μm was added to the relative elongation at the start of the three loading cycles.

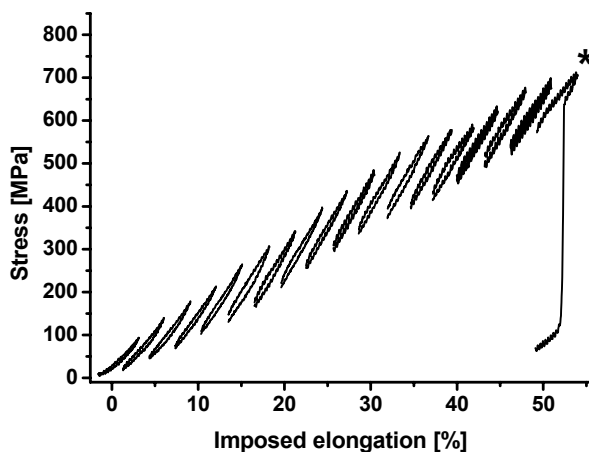
The imposed elongation, which is calculated via this method, does not represent strain, because during the cycles stress relaxation via permanent lengthening occurs. During the experiments, full stress relaxation of the fibril was not allowed. The fibril was extended over 4 μm at a rate of 0.1 Hz, and after three cycles (equal to 30 s) an extra manually applied extension of 3 μm was added. In this approach, we assume that the initial length for these three cycles is constant.



Fibril	L_0 (μm)	d^{\equiv} (nm)	ext. rate ($\mu\text{m}\cdot\text{s}^{-1}$)	cant. ($\text{N}\cdot\text{m}^{-1}$)	σ_{max} (MPa)
G1	129 ± 0.5	370 ± 20	0.74	29.3 ± 1.9	168

Figure 5.5 Experimental conditions and mechanical properties of fibril G1 obtained by tensile testing, according to the method depicted in Fig. 5.4. Cross-linked in 0.25 v% glutaraldehyde phosphate buffer, pH 7.4 for 2h at room temperature. The medium was not refreshed during the experiment. Table details: \equiv : swollen fibril; the stress at break value (σ_{max}) is shown in the table. The stress values were corrected for the assumed diameter change of the fibril.

The stress-elongation curves of collagen fibril G2 should be interpreted with care, because this fibril was pre-elongated over 2.9 times its original length (equal to 190% imposed elongation), prior to its cross-linking.



Fibril	L_0 (μm)	d^{\equiv} (nm)	ext. rate ($\mu\text{m}\cdot\text{s}^{-1}$)	cant. ($\text{N}\cdot\text{m}^{-1}$)	σ_{max} (MPa)
G2	$290 \pm 0.5^{\wedge}$	119^{\wedge}	0.74	28.3 ± 1.9	714

Figure 5.6 Experimental conditions and mechanical properties of fibril G2 obtained by tensile testing according to the method depicted in Fig. 5.4. Cross-linked in 0.25 v% glutaraldehyde in phosphate buffer, pH 7.4 for 2h at room temperature. The medium was not refreshed during the experiment. \wedge : Pre-elongated fibril, the length and diameter after 190% pre-elongation are shown. Table details: \equiv : swollen fibril; the stress at break value (σ_{max}) is shown in the table. The stress values were corrected for the assumed diameter change of the fibril.

Fibril G1 was first cyclically loaded to a stress of 230 MPa, without rupture to occur. Rupture of the fibril was observed at a stress of 168 MPa at slightly higher relative elongation. Fibril G2 ruptured at a maximal stress of 714 MPa. The mechanical properties of fibrils G1 and G2 will only be compared in a qualitative way. Pre-elongation of fibril G2 by 190% will reduce the diameter of the fibril (details: appendix A).

For all fibrils that were tensile tested according to the stepwise elongation protocol, only the residual stress at the beginning of the second cycle is discussed. The shape of the stress-elongation curves of fibril G1 are comparable to those of fibril G2, despite the pre-elongation of the latter. In both cases, initially (at low elongation values) the residual stress at the beginning of the second cycle is low. Already after around 5% elongation, the residual stress at the beginning of the second cycle increased significantly, a process which continued until rupture occurred. The rapid increase of the residual stress level at the beginning of the second cycle suggests a lower relaxation rate than the applied extension rate. The residual stress values at the start of each second cycle in the stress-elongation curves of fibril G1 and G2 were determined and plotted against the imposed elongation values (Fig. 5.7).

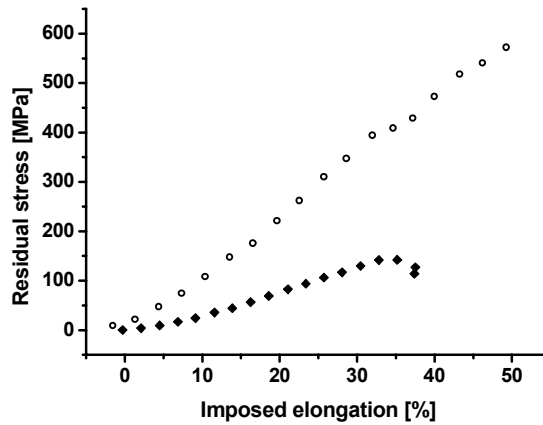


Figure 5.7 Residual stress at the start of each second cycle plotted against the corresponding imposed elongation. Diamonds (◆) represent values obtained for fibril G1 (details Fig. 5.5), open circles (○) represent values obtained for fibril G2 (details Fig. 5.6).

The residual stress-elongation curves of fibrils G1 and G2 show that for both fibrils the residual stress increases at low imposed elongation. The difference in residual stress between fibrils G1 and G2 might be caused by a difference in mutual distances between triple helices and microfibrils that constitute the fibril, because of a difference in pre-strain. This process might have resulted in an increase in cross-linking efficiency. A higher cross-linking efficiency would cause a higher stiffness of pre-strained fibril G2, compared to fibril G1. Furthermore, the stress-relaxation of the fibril via microfibril slipping will be more hindered in fibril G2, compared to fibril G1, because of the possibly increased number of inter-microfibrillar cross-links.

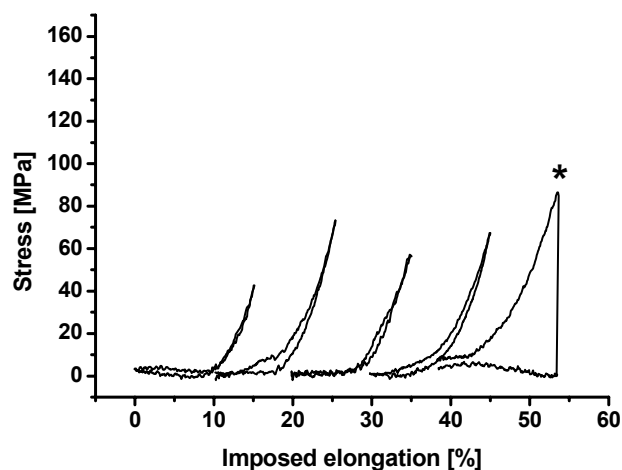
Alternatively, at decreasing distance between the microfibrils, the influence of decoration of the microfibril surface by dangling ends of glutaraldehyde molecules that reacted only at one side with lysine and hydroxylysine residues might increase. Possibly, decoration of the microfibril influences the irreversible displacement of microfibrils via alteration of the non-covalent interactions between the microfibrils. Because the strength of these interactions are dependent on the distance between interacting residues, a decrease in the distance between the microfibrils by pre-strain might improve the strength of these interactions.

For a quantitative comparison of the hindering of microfibril slipping of both fibrils, the stress relaxation process should have been left to equilibrate to stress values below 20 MPa. Due to the applied methodology, this information could not be obtained from the experimental results.

5.2.4 Stress-strain behaviour of EDC/NHS cross-linked fibrils at high relative elongation

Although glutaraldehyde has been widely acknowledged for its excellent cross-linking efficacy, release of the cytotoxic reagent from treated tissue, possible carcinogenicity of the compound and its role in the cause of calcification has led to the development of alternative cross-linking reagents. A well-known alternative reagent is EDC/NHS, which activates the carboxylic acid groups of aspartate and glutamate residues in the polypeptide chains of the triple helices, to facilitate a condensation reaction with amine containing (hydroxy)-lysine residues. The tissues treated with this reagent are biocompatible and a large reduction in calcification compared to glutaraldehyde cross-linked tissue has been observed.²⁹ Collagen fibrils were cross-linked using EDC/NHS and subsequently tensile tested, according to the method shown in Fig. 5.4.

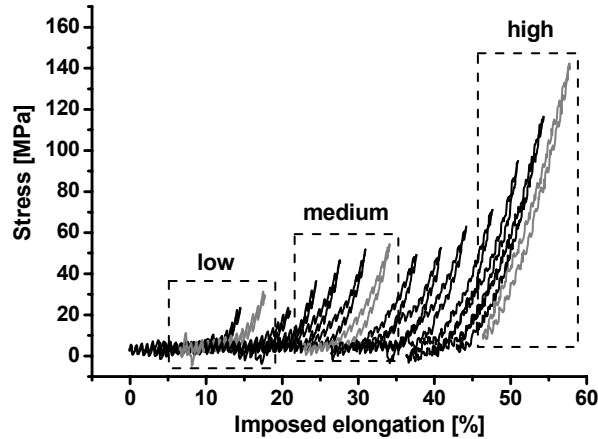
Collagen fibril EN1 (previously N3, now EN1, details table in Fig. 5.8) with a diameter of 188 nm and an initial length of 42 μm was cross-linked using EDC/NHS, and subsequently tensile tested according to the method schematically shown in Fig. 5.4. A second fibril (originally N6, now EN2, details: table Fig. 5.9) with a diameter of 243 nm and an initial length of 31 μm was tensile tested in the same manner. The resulting mechanical behaviour of fibrils EN1 and EN2 is shown in Figs. 5.8 and 5.9, respectively.



Fibril	L_0 (μm)	d^{Ξ} (nm)	ext. rate ($\mu\text{m}\cdot\text{s}^{-1}$)	cant. ($\text{N}\cdot\text{m}^{-1}$)	σ_{max} (MPa)
EN1	44 ± 0.5	188 ± 23	0.74	23.0 ± 1.5	87

Figure 5.8 Mechanical properties of fibril EN1, obtained by tensile testing according to the method depicted in Fig. 5.4. Cross-linking was performed with 6.8 mM EDC and 2.0 mM NHS in 0.05 M MES buffer for 4 h, pH 5.4 at room temperature. The medium was not refreshed during the experiment. Table details: Ξ : swollen fibril; the stress at break value (σ_{max}) is shown in the table. The stress values were corrected for the assumed diameter change of the fibril.

For fibril EN2 the stress values up to 58% imposed elongation were measured. At this relative elongation value the limit of the linear regime of the position detector of the AFM was reached. The deflection, correlating to the stress on the fibril is limited by this detector (details: Chapter 3). To extend the force range during the measurement, the location of the laser spot on the detector was manually changed, which might have influenced the measurement. Therefore, the data from 58% relative elongation up to rupture was not included in the stress-elongation curve (Fig. 5.9).



Fibril	L_0 (μm)	$d^{\#}$ (nm)	ext. rate ($\mu\text{m}\cdot\text{s}^{-1}$)	cant. ($\text{N}\cdot\text{m}^{-1}$)	$\sigma^{\#}$ (MPa)
EN2	31 ± 0.5	243 ± 52	0.74	28.5 ± 1.9	143

Figure 5.9 Mechanical properties of fibril EN2, obtained by tensile testing according to the method depicted in Fig. 5.4. Cross-linking was performed with 6.8 mM EDC and 2.0 mM NHS in 0.05 M MES buffer for 4 h, pH 5.4 at room temperature. The medium was not refreshed during the experiment. Table details: \equiv : swollen fibril; the maximally applied stress ($\sigma^{\#}$) is shown in the table. The stress values were corrected for the assumed diameter change of the fibril.

For all fibrils that were tensile tested according to the stepwise elongation protocol, only the residual stress at the beginning of the second cycle is discussed. When comparing the shape of the stress-elongation curves for each second cycle of both fibrils, the individual cycles are similar. Over almost the full relative elongation range no residual stress was observed at the start of the second cycles. The fast stress-relaxation is most probably caused by rapid permanent deformation. Both fibrils EN1 and EN2 show stress-elongation cycles with a non-linear increasing slope. The observation that the initial stress for each second cycle is zero for all relative elongation values suggests that permanent lengthening of the fibril occurred in the first cycle. At each imposed elongation value, the fibril was cyclically loaded three times, before increasing the imposed elongation value by 3 μm (details: Fig. 5.4). For all fibrils that were tensile tested according to this protocol, only the second cycle is discussed.

This selection was made, because during the loading part of the first curve the height is being changed manually, which might influence the observed mechanical behaviour.

When the raw data of the first cycles of the stress-elongation curves of fibrils EN1 and EN2 was analyzed, these cycles were found to have a significantly higher energy dissipation, compared to that of the second cycle. In some of the first cycles, a distinctive yield point was observed. For example, the 4th cycle of Fig. 5.8 is selected. This cycle represents the second cycle of the applied triplet. The raw data of all three cycles is shown in Fig. 5.10. When the same analysis was performed for glutaraldehyde cross-linked and non-treated fibrils the first cycle also showed a higher energy dissipation than the second cycle, but a distinctive yield point was not observed.

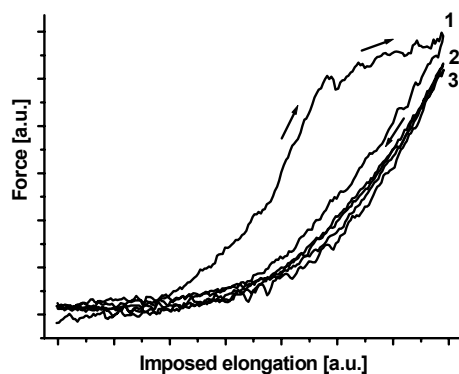


Figure 5.10 Three cycles of the force-imposed elongation curve of fibril EN1. The second cycle represents the 4th cycle of the stress-elongation curve (Fig. 5.8).

In the stress-elongation curves of EDC/NHS cross-linked fibrils, the residual stress at the start of the second cycle was almost zero. Still, a trend towards higher residual stress values at high relative elongation was apparent, especially from Fig. 5.9. When the curves at low, medium and high imposed elongation are compared, the change in the shape of the curve towards higher residual stress values is clear (Fig. 5.11).

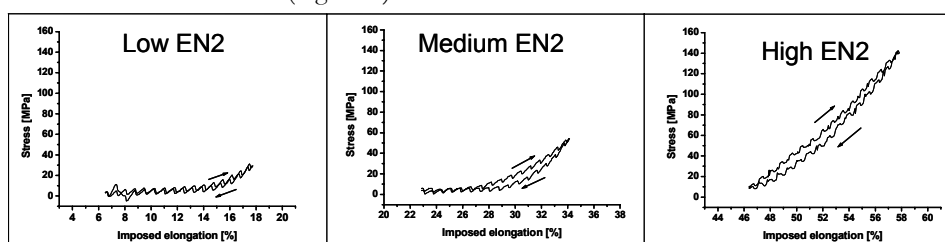


Figure 5.11 Stress-elongation curves of the second cycles during stepwise elongation of EDC/NHS cross-linked collagen fibril EN2 at three different imposed elongation values, taken from Fig. 5.9.

When these stress-elongation curves of the second cycles during stepwise elongation of EDC/NHS cross-linked fibrils are compared to those of the stress-elongation curves of non-treated collagen fibrils at the same imposed elongation values, a difference is observed. The curves of the non-treated fibrils showed an almost constant slope, which was equal to the maximal slope of the stress-elongation curves of the EDC/NHS cross-linked fibril as shown in Fig. 5.11.

The difference in the shape of the stress-elongation curves can only be explained from EDC/NHS-mediated cross-linking and surface decoration of the collagen triple helices and microfibrils in the fibril. Usually, cross-linking leads to stiffening of collagenous materials. In this case the slope of the stress-elongation curves was lower than that of the non-treated fibrils, which suggests that the fibril has softened. Therefore, surface decoration of the microfibril and triple helix surface by N-hydroxysuccinimide esters of aspartate and glutamate residues, which had not been involved in a condensation reaction with lysine and hydroxylysine residues, seems to be a dominant factor for the difference in mechanical behaviour between EDC/NHS cross-linked and non-treated fibrils. The conversion of aspartate and glutamate residues into N-hydroxysuccinimide esters during decoration of the microfibril and triple helix surface might lead to a change in the non-covalent interactions between microfibrils and triple helices, due to the reduced number of free carboxylic acids at the surface of the microfibrils and triple helices.

5.2.5 Comparison of mechanical properties of non-treated and glutaraldehyde and EDC/NHS cross-linked fibrils

Despite the limited number of fibrils tested ($n=2$) for glutaraldehyde and EDC/NHS cross-linked and non-treated fibrils, distinctive differences between the stress-elongation curves were observed. The most important parameter that distinguishes the three fibril types is the residual stress. For non-treated and EDC/NHS cross-linked fibrils up to $\sim 30\%$ relative elongation values, no residual stress was observed at the beginning of the second cycle. This in contrast to the glutaraldehyde cross-linked fibrils, which showed an increase of the residual stress already at $\sim 0\%$ relative elongation (Fig. 5.12).

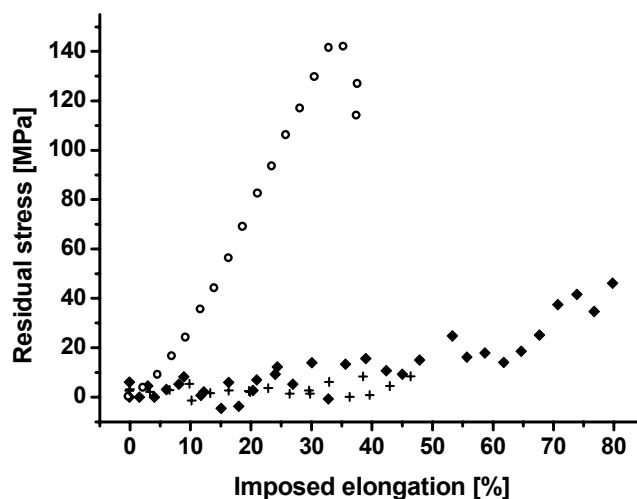


Figure 5.12 Residual stress at the start of each second cycle as a function of the imposed elongation. The residual stress is determined from the stress value at the start of each second cycle. Open circles (○) represent values obtained for fibril G1 (details: Fig. 5.4), diamonds (◆) represent values obtained for fibrils N4 and N5 (details: chapter 4), plus signs (+) represent values obtained for fibrils EN1 and EN2.

The nature of differences in residual stress for glutaraldehyde cross-linked fibrils, as compared to EDC/NHS and non-treated fibrils, may be explained by the cross-links introduced via glutaraldehyde. Glutaraldehyde is capable of forming inter-microfibrillar cross-links. In chapter 4 it was already postulated, based on the mechanical behaviour of non-treated fibrils, that irreversible displacement of microfibrils is the dominant mechanism for the permanent deformation of fibrils. Rapid permanent deformation prevents the build-up of residual stress in the fibrils before the next second cycle is applied. Because in glutaraldehyde cross-linked fibrils this deformation mechanism may be hindered by cross-links, more residual stress after each second cycle as a function of the imposed elongation will be introduced.

Above ~30% relative elongation values both non-treated, as well as EDC/NHS cross-linked fibrils showed an increase in the residual stress. For glutaraldehyde cross-linked fibrils a residual stress was observed already at ~0% relative elongation and increased significantly with higher relative elongation values. The increase of residual stress while going to higher relative elongation values was observed for EDC/NHS and glutaraldehyde cross-linked and non-treated fibrils. This seems to be a generally occurring mechanism.

During elongation of the fibrils, the diameter of the fibril will be reduced, when a constant volume is assumed. The distance between microfibrils in the fibril will decrease due to this process, which will increase the strength and number of non-covalent interactions between the microfibrils.

Stress relaxation of collagen fibrils via permanent deformation was postulated to occur via irreversible displacement of microfibrils. When this process is hindered by stronger interactions between the microfibrils a higher residual stress is present in the fibril.

In glutaraldehyde cross-linked fibrils next to non-covalent interactions between the microfibrils, covalent bonds between microfibrils have been generated. These covalent bonds will hinder the slipping of microfibrils, leading to impeded stress relaxation. This leads to higher residual stress values in the fibrils at lower relative elongation, compared to non-treated and EDC/NHS cross-linked fibrils.

A second, complementary mechanism can be hypothesized when the non-covalent interactions between the microfibrils are inhomogeneously spread over the microfibril's outer surface. Possibly, domains with a high concentration of functional groups capable of forming non-covalent bonds between microfibrils are present on the outer surface. The relative elongation of the fibrils leads to permanent deformation via sliding of the microfibrils. When the domains with a strong interaction are brought in close proximity via irreversible displacement of microfibrils, a higher stress is needed to continue this slipping process. This will result in the increase of the residual stress of the fibrils at higher imposed elongation values.

5.3 Conclusions

A non-treated collagen fibril was mechanically loaded to a stress value of maximally 15 MPa before, and after glutaraldehyde cross-linking. It was found that glutaraldehyde cross-linking does not affect the slope of the stress-strain curve at strain values up to 3.7%.

Loading to higher stress values was enabled via stepwise elongation of the glutaraldehyde cross-linked fibrils. For glutaraldehyde cross-linked fibril G1 (details: appendix C) with an initial length of 126 μm , a stress-elongation curve with a rapid increase in the residual stress at the beginning of each second cycle was obtained. A second glutaraldehyde cross-linked fibril (G2, details: appendix C), which was pre-strained over 190% prior to cross-linking of the fibril, showed a similar stress-elongation behaviour. The amount of residual stress in the pre-strained fibril was higher than for fibril G1. This observation was hypothesized to arise from a higher cross-link density of fibril G2. Due to the pre-straining of fibril G2 the diameter of the fibril was reduced, leading to a reduction in the distance between triple helices, and between microfibrils, which facilitates a more efficient cross-linking.

EDC/NHS cross-linking of collagen fibrils led to stress-elongation behaviour where rapid stress relaxation was apparent. Stress relaxation may proceed via irreversible displacement of microfibrils. For EDC/NHS cross-linked fibrils stress relaxation occurred at a higher rate compared to non-treated fibrils. Surface decoration of microfibrils by N-hydroxysuccinimide esters of aspartate and glutamate residues was hypothesized to facilitate microfibril slipping.

When the stress-elongation curves of glutaraldehyde- and EDC/NHS cross-linked and non-treated fibrils are compared, a general trend in residual stress was observed.

In all cases the amount of residual stress increased towards higher relative elongation values. This phenomenon was explained from the reduction in the fibril diameter during elongation, which leads to a reduced distance between microfibrils. The resulting increase in the amount and strength of non-covalent interactions between the microfibrils, causes a hindering of microfibril slipping, the proposed stress relaxation process.

For glutaraldehyde cross-linked fibrils the increase in residual stress was higher compared to that of the non-treated and EDC/NHS cross-linked fibrils. This result can be explained from the presence of covalent bonds between microfibrils, generated by glutaraldehyde. Consequently, more hindering of microfibril slipping is expected to occur.

5.4 Experimental

5.4.1 Materials

In the experiments described several buffers were used. The MES buffer contained 0.05 M 2-[morpholino]ethanesulfonic acid (Sigma-Aldrich, Steinheim, Germany) and was adjusted to pH 5.4 with 1M NaOH or 1M HCl. The phosphate buffer at pH 7.4 contained a 54 mM $\text{Na}_2\text{HPO}_4 \cdot 2\text{H}_2\text{O}$ solution, and a 13 mM $\text{NaH}_2\text{PO}_4 \cdot \text{H}_2\text{O}$ solution (disodiumhydrogenphosphate and sodiumdihydrogenphosphate were obtained from Merck, Darmstadt, Germany) and was adjusted to pH 7.4 with 1M NaOH or 1M HCl.

The EDC/NHS reagent was prepared from 1-ethyl-3-(3-dimethyl aminopropyl) carbodiimide hydrochloride (EDC) and N-hydroxysuccinimide (NHS), which were obtained from Sigma-Aldrich, Steinheim, Germany. Glutaraldehyde 10 v% solution was obtained from Electron Microscopy Sciences, Ft. Washington, PA. The purity of the reagent was checked by UV-Vis spectrometry analysis of the compound dissolved in demineralised water. The peak at 235 nm corresponds to the Aldol-condensate of the compound, while the peak at 280 nm corresponds to monomeric glutaraldehyde. In the applied glutaraldehyde solution only a single peak was observed, suggesting a purity higher than ~95%.

5.4.2 Cross-linking methodology

Glutaraldehyde cross-linking

A 10 v% solution of glutaraldehyde in demineralised water was diluted in phosphate buffer at pH 7.4 to a concentration of 0.25 v%. The collagen fibril was submersed in this solution for 2 h prior to the tensile testing experiments. This solution was freshly prepared and used within 1 h. To ensure stability of the fibril, the fibril remained in the cross-linking medium during the tensile tests.

EDC/NHS cross-linking

A solution of 1.308 g (6.82 mmol) EDC in 10 ml 0.05 M MES buffer at pH 5.4 was added to a solution of 0.226 g (1.97 mmol) NHS in 10 ml of the same buffer. The collagen fibril was immersed in about 1 ml of the mixture for 4 h prior to the tensile testing experiments. To ensure stability of the fibril, the fibril remained in the cross-linking medium during the tensile tests.

5.5 References

- 1 S. G. V. Ricard-Blum, *Int. J. Biochem.*, 1989, **21**, 1185.
- 2 M. E. Nimni, 'Biochemistry', ed. M. E. Nimni, CRC Press, Boca Raton, FL, 1988.
- 3 D. F. Betsch and E. Baer, *Biorheol.*, 1980, **17**, 83.
- 4 J. Diamant, A. Keller, E. Baer, M. Litt, and R. G. C. Arridge, *Proc. R. Soc. Lond. B*, 1972, **180**, 293.
- 5 A. I. Gasan, Y. E. Perskii, V. Y. Maleyev, and L. A. Utevskaia, *Biophysics*, 1988, **33**, 830.
- 6 C. H. Lee, A. Singla, and Y. Lee, *Int. J. Pharm.*, 2001, **221**, 1.
- 7 C. Meena, S. A. Mengi, and S. G. Deshpande, *Proc. Indian Acad. Sci.*, 1999, **111**, 319.
- 8 A. Cooke, R. F. Oliver, and M. Edward, *Br. J. exp. Pathol.*, 1983, **64**, 172.
- 9 A. Vincentelli, C. Latrémouille, R. Zegdi, M. Shen, P. S. Lajos, J. C. Chachques, and J.-N. Fabiani, *Ann. Thorac. Surg.*, 1998, **66**, S255.
- 10 R. J. Levy, F. J. Schoen, F. S. Sherman, J. Nichols, M. A. Hawley, and S. A. Lund, *Am. J. Pathol.*, 1986, **122**, 71.
- 11 R. J. Levy, *J. Heart Valve Dis.*, 1994, **3**, 101.
- 12 M. N. Girardot, M. Torrianni, D. Dillehay, and J. M. Girardot, *J. Biomed. Mat. Res.*, 1995, **29**, 793.
- 13 G. Golomb, F. J. Schoen, M. S. Smith, J. Linden, M. Dixon, and R. J. Levy, *Am. J. Pathol.*, 1987, **127**, 122.
- 14 K. M. Kim, G. A. Herrera, and H. D. Battarbee, *Am. J. Pathology*, 1999, **154**, 843.
- 15 F. J. Schoen, H. Harasaki, K. M. Kim, and H. C. Anderson, *J. Biomed. Mater. Res.*, 1988, **22 A1**, 11.
- 16 E. Jorge-Herrero, P. Fernandez, N. d. l. Torre, C. Escudero, J. M. García-Páez, J. Buján, and J. L. Castillo-Olivarez, *Biomaterials*, 1994, **15**, 815.
- 17 H. A. Baba, M. Deiwick, D. Breukelmann, B. Glasmacher, H. H. Scheld, and W. Bocker, *Pathologie*, 1998, **19**, 420.
- 18 T. P. Johnston, E. L. Bove, S. F. Bolling, J. A. Boyd, B. I. Ciesliga, G. I. Amidon, F. J. Schoen, and R. J. Levy, *Int. J. of Pharmaceutics*, 1989, **52**, 139.
- 19 J. Chanda, S. B. Rao, M. Mohanty, A. V. Lal, C. V. Muraleedharan, G. S. Bhuvaneshwar, and M. S. Valiathan, *Artif. Org.*, 1994, **18**, 752.
- 20 Y.-S. Lee, *J. Electron Microsc.*, 1994, **43**, 131.

- 21 E. Jorge-Herrero, P. Fernandez, C. Escudero, N. d. l. Torre, M. Zurita, J. M. García-Páez, and J. L. Castillo-Olivarez, *J. Biomed. Mat. Res.*, 1996, **30**, 411.
- 22 G. M. Bernacca, A. C. Fisher, R. Wilkinson, T. G. Mackay, and D. J. Wheatley, *J. Biomed. Mat. Res.*, 1992, **26**, 959.
- 23 J. D. Deck, M. J. Thubrikar, S. P. Nolan, and J. Aouad, in 'Role of Mechanical Stress in Calcification of Bioprostheses.', ed. L. H. Cohn and V. Gallucci, Yorke Med. Books Techn. Publish., 1982.
- 24 M. Thubrikar, J. D. Deck, J. Aouad, and S. P. Nolan, *J. Thorac. Cardiovasc. Surg.*, 1983, **86**, 115.
- 25 M. Deirwick, B. Glasmacher, H. A. Baba, N. Roeder, H. Reul, G. v. Bally, and H. H. Scheld, *Ann. Thorac. Surg.*, 1998, **66**, S206.
- 26 E. Pasquino, S. Pascale, M. Andreon, S. Rinaldi, F. Laborde, and M. Galloni, *J. Mater. Sci. Mater. Med.*, 1994, **5**, 850.
- 27 X. Tingfei, M. Jiazhen, T. Wenhua, L. Xuehui, L. Shuhui, and X. Baosha, *J. Biomed. Mat. Res.*, 1992, **26**, 1241.
- 28 S. C. Vasudev and T. Chandy, *J. Biomed. Mat. Res.*, 1997, **35**, 357.
- 29 R. Zeeman, 'Cross-linking of Collagen-Based Materials', University of Twente, Enschede, 1998.
- 30 R. Zeeman, P. J. Dijkstra, P. B. v. Wachem, M. J. A. v. Luyn, M. Hendriks, P. T. Cahalan, and J. Feijen, *Biomaterials*, 1999, **20**, 921.
- 31 L. H. H. OldeDamink, P. J. Dijkstra, M. J. A. v. Luyn, P. B. v. Wachem, P. Nieuwenhuis, and J. Feijen, *Biomaterials*, 1996, **17**, 765.
- 32 L. H. H. OldeDamink, 'Structure and properties of crosslinked dermal sheep collagen', University of Twente, Enschede, 1993.
- 33 G. N. Ramachandran, in 'Structure of collagen at a molecular level', ed. G. N. Ramachandran, Academic Press, London, 1967.
- 34 Y. P. Kato and F. H. Silver, *Biomaterials*, 1990, **11**, 169.
- 35 J. Kastelic and E. Baer, Symposium of Society for Experimental Biology - Mechanical Properties of Biological Materials, Cambridge University Press, Cambridge, 1980.
- 36 Y. P. Kato, D. L. Christiansen, R. A. Hahn, S.-J. Shieh, J. D. Goldstein, and F. H. Silver, *Biomaterials*, 1989, **10**, 38.
- 37 G. Antoni, R. Presentini, and P. Neri, *Anal. Biochem.*, 1983, **129**, 60.

CHAPTER 6

The structural organisation of collagen fibrils in relation to their mechanical properties

"Si licet magnis componere parva..."

(Abstract)

Two types of deformation can occur during tensile testing of a collagen fibril: elastic elongation of triple helices and/or microfibrils and irreversible deformation by slipping of triple helices and/or microfibrils. Up to stress values of 20 MPa, reversible stress-strain behaviour was observed for collagen fibrils immersed in aqueous media. Because the Young's modulus of the fibril is much lower than that of the triple helix, it is likely that deformation of the triple helices contributes minimally to the stress-strain curve of a fibril immersed in aqueous media. Therefore, the stress-strain behaviour is thought to be dominated by reversible displacement of triple helices and/or microfibrils with respect to each other. The non-linearity of the stress-strain curves of fibrils immersed in aqueous media might be explained by the release of water from the fibril structure during deformation.

At stress values above 20 MPa, permanent lengthening of the fibrils was observed. This might be explained by irreversible displacement of microfibrils and/or triple helices with respect to each other. Several observations such as retainment of the D-period suggest that the latter process did not occur.

The stress-strain behaviour of collagen fibrils at ambient conditions was linear and the Young's modulus of fibrils was determined at 5 ± 3 GPa, which is similar to estimations on the Young's modulus of a collagen triple helix as reported in literature. This suggests that reversible deformation of collagen fibrils at ambient conditions is dominated by reversible deformation of triple helices.

Stepwise elongation up to ~30% relative elongation of glutaraldehyde cross-linked and non-treated fibrils immersed in aqueous media showed a build-up of residual stress only for the first fibril type, which can be explained by the presence of glutaraldehyde-mediated cross-links between collagen microfibrils, which hinders microfibril slipping. When stretching EDC/NHS cross-linked collagen fibrils, slipping of microfibrils occurred at a higher rate than for non-treated fibrils. A possible explanation for this observation is surface decoration of microfibrils with NHS-ester groups.

6.1 Introduction

It has been suggested that collagen fibrils are constructed from aggregated microfibrils, which in turn consist of five triple helices (details: chapter 2). The collagen fibril structure is schematically depicted in Fig. 6.1.

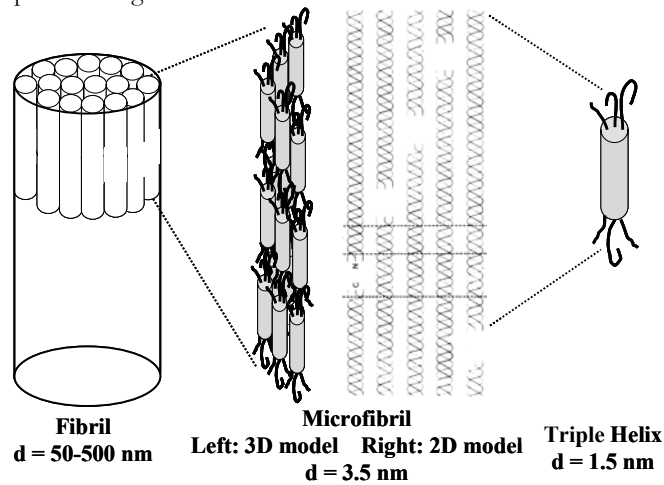


Figure 6.1 Structure of a collagen fibril consisting of hundreds of microfibrils, which in turn are constructed from five triple helices. Microfibril D-period reprinted and adapted from *Cell Biology of Extracellular Matrix*, ed. E.D. Hay, author: T.F. Linsenmayer, Chapter 1 - collagen, 2nd ed., 1991, with permission from Plenum Press, NY.¹

Tensile testing experiments have been carried out to assess the mechanical and elastic properties of individual collagen fibrils. Important factors for the mechanical behaviour of collagen fibrils are the mechanical and elastic properties of the individual microfibrils and triple helices, and furthermore the interactions between microfibrils and between triple helices.

The elastic and irreversible deformation of a fibril can be described by the following deformation mechanisms involving microfibrils and triple helices:

- Elastic deformation of microfibrils and elastic deformation by displacement of microfibrils with respect to each other.
- Elastic deformation of microfibrils may originate from elastic deformation of triple helices, or reversible displacement of assemblies of triple helices or triple helices with respect to each other.
- For irreversible deformation similar mechanisms will occur, but now leading to irreversible deformation or displacement of substructures.

Tensile testing of collagen fibrils has been performed at ambient conditions and with fibrils immersed in aqueous media. The mechanisms described above represents an overview of all possible deformation mechanisms for collagen fibrils. In literature, the presented mechanisms

have not all been described. The obtained experimental results of the mechanical behaviour of collagen fibrils as reported in chapter 4 will be discussed by the mechanisms described above and compared to the mechanisms reported in literature. The influence of cross-linking using glutaraldehyde and a carbodiimide-based reagent on the mechanical properties of fibrils will also be discussed by the described mechanisms, the experimental results of chapter 5, and compared to mechanisms described in literature.

6.2 Reversible deformation of fibrils in aqueous media

6.2.1 Mechanical models

The first mechanism of fibril deformation is the reversible stretching of the triple helix. The three α -amino acid polypeptide chains constituting the triple helix consist of rigid (Gly-X-Y, with X,Y generally Pro or Hyp) sequences with a low conformational freedom as well as more flexible sequences, located in the triple helix segment and in the telopeptides.^{2, 3} The helix is considered to consist of an array of these conformationally rigid and flexible polypeptide segments of 6-12 amino acids in length. The flexible segments contain charged residues which can undergo interactions with neighbouring triple helices. The flexible segments are stretched during mechanical deformation, leading to storage of elastic energy. The rigid sequences prevent stress-induced irreversible unfolding (denaturation) of the triple helix.² The flexible domains of the triple helix are located within the triple helix as well as at the ends (telopeptides) and are thought to account for elastic deformation of the triple helix (Fig. 6.2).

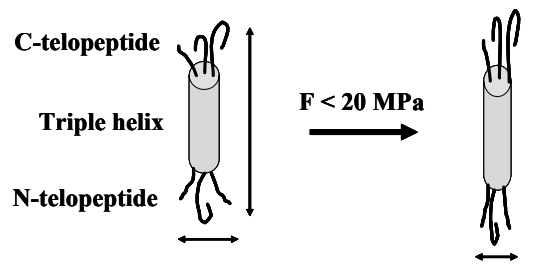


Figure 6.2 Elastic deformation of a triple helix in aqueous media at stress values below 20 MPa. Not only the telopeptides, but also sequences within the triple helix domain can be considered as more flexible domains.^{2, 3}

The Young's modulus of collagen triple helices in aqueous media has been determined with various techniques. Results obtained by directly measuring the mechanical properties of a procollagen triple helix still (details: chapter 2) by an optical trap gave values for the Young's modulus between 350 MPa and 12.2 GPa.⁴ This enormous variation in the Young's modulus is caused by using different radii of the helix in the applied worm-like chain model.⁵

The radius has been calculated at 0.28 nm, based on the backbone of the triple helix, while a radius of 0.68 nm was calculated when the side-chains of the residues are included.⁴

Alternatively, the mechanical properties of a tendon or collagen fibre have been extrapolated towards the mechanical properties of a triple helix by using a structural model for the organisation of triple helices, microfibrils and fibrils in a tendon or fibre.^{3, 6} Other approaches monitored the stress-induced deformation of the triple helix via X-ray diffraction⁷ or Brillouin light scattering.^{8, 9} Via these techniques, a Young's modulus between 2.9 and 9.0 GPa was determined for a triple helix immersed in aqueous media. The wide variation for the latter results in the obtained Young's modulus of the triple helix is caused by two factors.

- No conclusive structural model has been established for the lateral organisation of collagen triple helices, microfibrils and fibrils in a tendon or collagen fibre.
- The radius of the triple helix used in calculations, is determined in two ways, leading to different values. The radius can be calculated from the hydrodynamic volume, which includes the contribution of the charged side-chains of the three polypeptide chains that constitute the triple helix. Alternatively, the radius is calculated from the distance between the polypeptide backbones of the three polypeptide chains, constituting the triple helix.

The Young's modulus of a collagen triple helix as obtained via the first technique (optical trapping) was determined on procollagen, which not only includes the triple helix, but also C- and N-terminal propeptide sequences. Because these propeptides have a different, less rigid conformation than the triple helical segment, these are the first domains to unfold under an applied load. The resulting force-distance curve will therefore consist of a combination of deformation of the propeptide sequences and the triple helix sequences. It can be envisaged that the obtained Young's modulus most likely mainly represents the deformation of the propeptide sequences.

6.2.2 Comparison of experimental results with literature

This study showed that collagen fibrils loaded to a maximal stress of 20 MPa have a Young's modulus of ~300 MPa. The Young's modulus of a triple helix as reported in literature, was ~6 GPa.^{3, 6-9} Although the values for the Young's modulus of a triple helix vary widely, we assumed a value higher than 3 GPa, based on the various models used. The difference in modulus between the fibril and the triple helix suggests that elastic deformation of the triple helix is not the dominating process during tensile testing of collagen fibrils immersed in aqueous media. Possibly, the telopeptides constituting the C- and N-terminal residues of the triple helices might contribute to the deformation of the triple helix. Telopeptides might be elongated, or telopeptides from adjacent triple helices that interact might be pulled from each other. The dominant factors in deformation of collagen fibrils most likely consist of reversible displacement of triple helices and/or microfibrils with respect to each other.

6.2.2.1 Triple helix displacement

The reversible displacement of triple helices can occur via two mechanisms (Fig. 6.3).¹⁰

- a) Increase in the gap region between blocks of triple helices due to a blockwise displacement along the fibril axis.
- b) Relative displacement of laterally adjoining triple helices along the fibril axis.

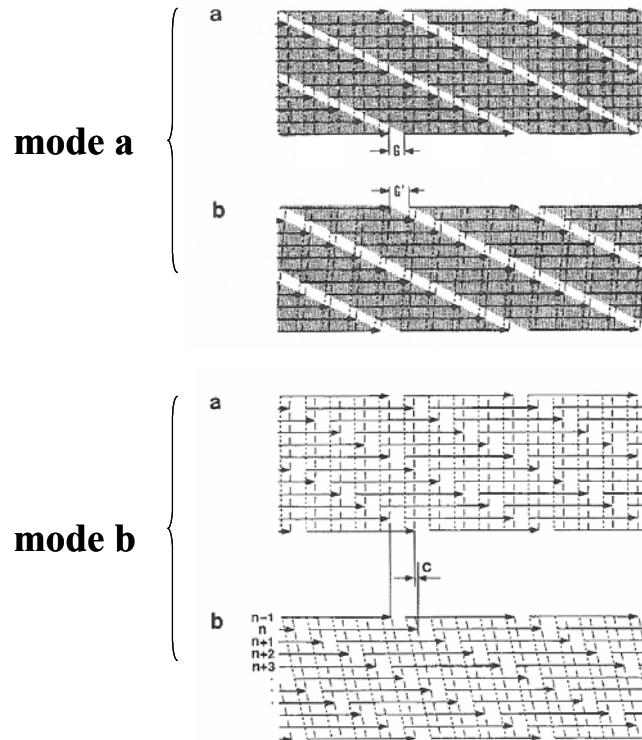


Figure 6.3 Rearrangement of triple helices in a fibril. **(a)** Increase in the gap region, where the interactions between laterally adjoining triple helices are retained. Blocks of triple helices are displaced with respect to the other block, leading to a change in the O/D ratio and the D-period. **(b)** Relative displacement of laterally adjoining triple helices, without a change in the width of the gap region, but with a changing O/D ratio and the D-period. Reprinted and adapted from J. Biomech., N. Sasaki and S. Odajima, "Elongation Mechanism of Collagen Fibrils and Force-Strain Relations of Tendon at Each Level of Structural Hierarchy", vol. 29(9), p. 1131-1136, ©1996, with permission from Elsevier.¹⁰

In mode **a** the displacement process is concentrated in the gap region of the D-period, where the C- and N-telopeptide sequences of axially interacting triple helices come together. This displacement of blocks of triple helices leads to a change in the O/D ratio (ratio of the length of the overlap region to that of the D-period) and an increase in the D-period (Fig 6.3a).

Due to the displacement in mode **a** the bands forming the D-period are no longer orthogonal to the fibril axis, but become tilted. Mode **b** leads to an increase in the D-period as well as a change in the O/D ratio (Fig. 6.3b). Furthermore, mode **b** leads to tilting of the D-period banding pattern. This tilt has not been observed in X-ray studies of tendon collagen under load. It was suggested that mode **a** and **b** operate simultaneously, which prevents tilting of the D-period structure.¹⁰

Collagen triple helices are organised in a staggered way in the microfibril. Due to this organisation the collagen fibrils reveal a periodic banding pattern (D-period), as shown in Fig. 6.4, which increases due to elongation mechanisms **a** and **b**.

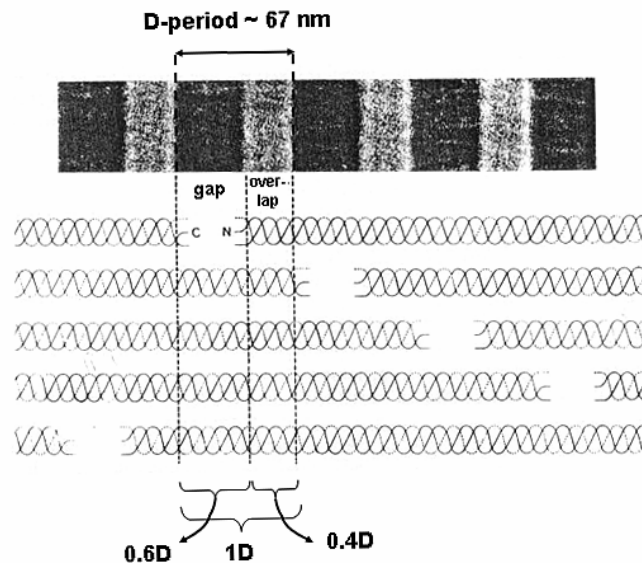


Figure 6.4 Aggregation of collagen triple helices in a microfibril leading to the banding pattern (D-period) as observed on collagen fibrils as shown in the EM image. Reprinted and adapted from *Cell Biology of Extracellular Matrix*, ed. E.D. Hay, author: T.F. Linsenmayer, Chapter 1 - collagen, 2nd ed., 1991, with permission from Plenum Press, NY.¹

Since the internal deformation and D-period during tensile testing of single collagen fibrils were not monitored, for example using X-ray diffraction, the occurrence of displacement of triple helices via mode **a** and **b** during reversible elongation of collagen fibrils at aqueous conditions can neither be confirmed or ruled out.

6.2.2.2 Reversible displacement of microfibrils

Besides reversible displacement of triple helices during tensile testing of collagen fibrils, reversible displacement of microfibrils is also possible. Collagen microfibrils are built from five aggregated triple helices in each cross-section. The outer surface of microfibrils therefore will consist of an array of helices, which have different mutual distances. On the outer surface of triple helices various domains capable of forming non-covalent interactions are present. These domains therefore form a repetitive pattern on the microfibril surface. Slipping of microfibrils might be enabled by the presence of these patterned domains on the outer surface of the microfibrils. Furthermore, the interactions between microfibrils possibly also involve the telopeptides of the triple helices that constitute the microfibril. It has been stated that telopeptides are oriented towards the outside of the microfibril, which enables interactions between the telopeptides of a microfibril and the surface of a neighbouring microfibril.¹¹

The existence of microfibrils as an intermediate substructure between triple helices and fibrils is not generally accepted. A recent structural model of the aggregation of triple helices in a fibril, consists of triple helices in a pseudo-hexagonal packing, in which the microfibril represents a unit cell for the organisation of the triple helices. In this fibril model, which had the best agreement with X-ray diffraction data, the microfibrils located on the outside are more organised than on the inside of the fibril.¹²

In literature, reversible displacement of microfibrils has not been considered as a possible deformation mechanism. The results obtained by tensile testing of collagen fibrils cannot underline neither reject this proposed deformation mechanism.

6.2.2.3 Mechanical model for non-linear stress-strain curves

The stress-strain behaviour of collagen fibrils immersed in aqueous media is non-linear. A possible explanation for the non-linearity in the stress-strain curve might be a stress-induced excretion of water molecules from the fibril. This will result in a reduced diameter of the fibril during deformation. The lateral distance between microfibrils and triple helices will be reduced, which will increase the non-covalent interactions between the triple helices, and between the microfibrils. This results in a gradual increase in the stiffness of the fibril during deformation.

6.3 Irreversible deformation of fibrils in aqueous media

6.3.1 Mechanical models

During irreversible deformation of collagen fibrils in an aqueous environment the same deformation mechanisms as proposed in the previous section for reversible deformation has been suggested. The irreversible deformation mechanisms include:

- Irreversible deformation of microfibrils and irreversible displacement of microfibrils with respect to each other.
- Irreversible deformation of microfibrils may originate from irreversible deformation of triple helices, or irreversible displacement of assemblies of triple helices or triple helices with respect to each other.

6.3.2 Comparison of experimental results with literature

Irreversible deformation of triple helices is not likely to occur during permanent deformation of collagen fibrils, because the Young's modulus of the triple helix (>3 GPa as reported in the previous section) is ten times larger than that of a collagen fibril (~300 MPa, details: chapter 4). At stress values above 20 MPa for collagen fibrils immersed in aqueous media, permanent deformation was observed. The permanent lengthening of collagen fibrils at these stress levels can be explained by irreversible displacement of microfibrils and/or displacement of the triple helices in aggregates (mode **a**, Fig. 6.3a) or individually with respect to each other (mode **b**, Fig. 6.3b).

Three observations contradict with the proposed mechanism of slipping of triple helices during the stress-induced permanent lengthening of the fibrils.

1. The specific ordering of triple helices in the fibril (D-period, equal to a 67 nm repeat banding pattern) was unchanged after elongation of collagen fibrils, even when stretched up to three times their original length. This suggests that no permanent deformation of the triple helices has occurred. The D-period might have changed during loading of the fibril, without leading to permanent displacement of the triple helices.

The change in the D-period during tensile testing of collagenous structures has been described in literature. Whether the change in the D-period is reversible is still under debate. When an Achilles tendon was mechanically tested in a creep experiment, while investigating the microscopic deformation by X-ray diffraction, the D-period was found to increase because of an elongation of the triple helices. At a stress of 10 MPa, rearrangement of the triple helices via slipping was observed.^{13, 14}

Contradictory to this finding, the D-period of collagen tendons was found to change under load, but this change was found to be reversible within 12h.¹⁵ The change in D-period was explained by displacement of the triple helices, leading to a new set of interactions between neighbouring triple helices. The number of interactions at this new position of the triple helices is reduced compared to the original position of the triple helices, leading to reorientation of the triple helices to their original locations after the load is removed.¹⁵

2. For undefined aggregates of collagen triple helices a large influence of calcium ions on the mechanical behaviour of the aggregates was observed.¹⁶ This suggests that inter-helical ionic interactions are influenced by calcium ions. In our experiments, variation of the pH and ion composition of the aqueous medium (including supplying the medium with calcium ions) did not affect the stress-strain behaviour of single collagen fibrils. Apparently, inter-helical interactions are not playing a role in the mechanical behaviour of a collagen fibril. A possible explanation is that the organisation of triple helices in a fibril is too dense for the calcium ions to fit in between the triple helices. The distance between triple helices in a fibril has been reported at 0.15-0.18 nm.¹⁷ In the non-specified aggregates of collagen triple helices, where calcium ions were found to have an influence on the mechanical behaviour, the distances between the triple helices possibly are larger.
Slipping of triple helices with respect to neighbouring helices as described in the elongation mode **a** and **b** are thought to be influenced by inter-helical interactions. These inter-helical interactions include ionic interactions, which are possibly influenced by the ions in the applied medium. The mechanical behaviour of a collagen fibril was found to be unchanged by variation of pH and presence of specific ions in the applied medium. This finding suggests that slipping of triple helices in a collagen fibril during mechanical loading is unlikely to occur.
3. Tensile testing of single collagen fibrils showed that the mechanical behaviour is similar before and after permanent deformation of the fibrils up to ~30% relative elongation of the fibrils. This observation suggests that comparable non-covalent interactions are acting between the slipping subunits constituting the fibril along their length. It is unlikely that during slipping of triple helices over large elongations (up to ~30% of their length) the non-covalent interactions between the triple helices are unchanged.

These three observations suggest that slipping of triple helices does not represent the dominant mechanism during permanent deformation of collagen fibrils. Therefore, only one proposed mechanism remains that might account for permanent deformation of collagen fibrils: slipping of microfibrils with respect to each other.

Slipping of microfibrils has been stated in literature as a possible stress-induced deformation mechanism for collagen fibrils, which causes no change in the collagen D-period.¹⁸ Slipping of microfibrils is only possible when microfibrils are shorter than the entire fibril. When the microfibrils and fibrils would be equally long, the microfibril ends would be fixed together with the fibril ends at the fixation points.¹⁸ This fixation would prevent slipping of microfibrils and when a load is placed on the fibril, this would be directly taken up by the microfibrils.

The weakest points in the aggregate of microfibrils that constitute the collagen fibril most likely are the triple helices on the outside of the microfibrils. These triple helices, at a certain minimal distance from each other have non-covalent interactions, which hold the microfibril aggregate in a fibril together. When a stress above 20 MPa is loaded on the fibril, these non-covalent interactions cannot withstand the load and the microfibrils slip with respect to each other. The outer surface of the microfibrils consists of triple helices which in their turn have a repetitive pattern of segments capable of providing non-covalent interactions at their outer surface. When the microfibrils slip, at a certain distance from their original position, exactly the same pattern of non-covalent interactions can be found. Similarly, the telopeptides of the triple helices located on the outer surface of the microfibrils possibly also contribute to the interaction between microfibrils. It is stated that telopeptides are oriented towards the outside of the microfibril, which enables interactions between the telopeptides of a microfibril and the surface of a neighbouring microfibril.¹¹

6.3.3 Permanent deformation of fibrils above ~30% relative elongation

Via stepwise elongation, the stress-strain curve up to rupture of the fibril was obtained. For non-treated fibrils up to ~30% relative elongation, stress relaxation occurred during the individual stress-elongation curves, resulting in no residual stress at the start of a new stress-elongation cycle. From ~30% relative elongation on, the residual stress in the individual stress-elongation curves increased, which suggests that the relative rate of stress relaxation was reduced. The exact mechanism behind this gradual increase in residual stress at increased relative elongation is unknown. A possible explanation might be an increase in the amount and/or strength of non-covalent interactions between microfibrils during the relative elongation of the fibril. When a collagen fibril has been elongated over ~30% a significant reduction of the diameter of the fibril is expected, based on a Poisson ratio of 0.5. This diameter reduction was also found in tensile tested fibrils (details: appendix A). The reduced diameter possibly also leads to a reduction in the distance between the microfibrils. This will increase the non-covalent interactions between the microfibrils.

At even higher relative elongation values, the diameter of the fibril might be reduced even further by a second mechanism. During slipping of microfibrils with respect to each other at a certain relative elongation of the fibril, a microfibril might reach the end of its neighbouring microfibril. Continued slipping of the microfibrils can cause the first microfibril to add-in at the gap left by the second microfibril. Via this add-in mechanism, the reduction in diameter can continue, without leaving open space between the microfibrils at the original locations of the microfibrils prior to the slipping process.

6.4 Fibril mechanical properties - ambient

6.4.1 Mechanical models

In principle, the same mechanisms of deformation of the fibril at ambient conditions can occur as described for a fibril immersed in aqueous media. These mechanisms were summarized in section 6.1.

The substructures in a collagen fibril at ambient conditions will be organised at closer proximity than those in a fibril immersed in aqueous media. Upon immersion in water of collagen fibrils originally at ambient conditions, the fibril diameter increases by 73% (details: chapter 3), because of the incorporation of water molecules. The reduced diameter of the fibril at ambient conditions (compared to aqueous conditions) implies a smaller distance between the microfibrils and between triple helices within the fibril. This will improve the non-covalent interactions between the microfibrils and between the triple helices. During tensile testing of a collagen fibril, the weakest link in the structure is expected to dominate the mechanical behaviour of the fibril. The weakest link is the substructure within the fibril that undergoes the largest amount of deformation under stress.

6.4.2 Comparison of experimental results with literature

Tensile testing of collagen fibrils was also performed at ambient conditions. A linear, reversible stress-strain behaviour was found, when the maximally applied stress remained below ~90 MPa (Fig. 6.5).

During tensile testing, in principle, all deformation mechanisms can occur. Most likely, due to the increased strength of the interactions between microfibrils and between the triple helices, for a fibril at ambient conditions, the slipping of these substructures during tensile testing is hindered. Therefore, the reversible elongation of triple helices is the most likely deformation mechanism of collagen fibrils at ambient conditions.

This hypothesis is underlined by the Young's modulus of 5 ± 3 GPa (details: chapter 4), which was obtained for collagen fibrils at ambient conditions. This value is similar to the estimations of the Young's modulus of collagen triple helices at ambient conditions between 11.9 and 21.5 GPa, as obtained by Brillouin light scattering experiments.^{8, 9}

Furthermore, for self-assembled fibres and rat tail tendon (RTT) fibres tensile tested at ambient conditions, a Young's modulus of 4.8 and 5.8 GPa, respectively was reported.^{3, 6} For self-assembled collagen fibres these values were claimed to correspond to the Young's modulus of a collagen triple helix.³

When the fibril was loaded to stress values above 90 MPa, permanent deformation was observed. For the same arguments as used in section 6.3 microfibril slipping is thought to be the most likely mechanism that occurs during permanent deformation of the fibril.

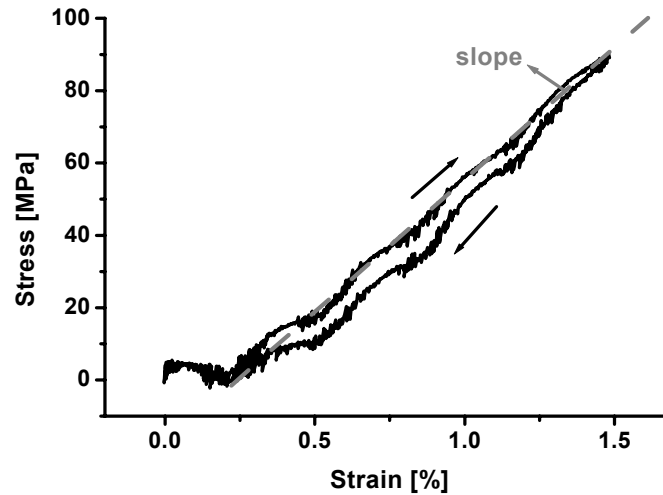


Figure 6.5 Typical stress-strain behaviour of collagen fibril N1 (details: chapter 4) at ambient conditions. To indicate the Hookean stress-strain behaviour at ambient conditions the slope of the curve is shown.

6.5 Fibril mechanical properties - influence of cross-linking

6.5.1 Mechanical models

The elastic and irreversible deformation of a fibril can be described by four deformation mechanisms as shown in section 6.1.

Cross-linking of a collagen fibril will lead to the formation of covalent bonds on an intra-microfibrillar, inter-triple helical and intra-triple helical level. Therefore, cross-linking of collagen fibrils is expected to influence its mechanical behaviour. It was described in section 6.2 that during reversible tensile testing of collagen fibrils immersed in aqueous media at stress values below 20 MPa, three deformation mechanisms can occur. These mechanisms include reversible displacement of microfibrils and/or triple helices in aggregates or individually with respect to each other.

6.5.2 Experimental evidence and literature - glutaraldehyde cross-linking

Glutaraldehyde cross-linking of collagen fibrils results in intra- and inter-triple helical cross-links, as well as inter-microfibrillar cross-links. Furthermore, decoration of the outer surface of triple helices and microfibrils can occur. At stress values up to 20 MPa, the stress-strain behaviour of glutaraldehyde cross-linked fibrils was equal to that of non-treated fibrils.

Apparently, the reversible displacement over small distances of microfibrils and/or triple helices was found not to be influenced by glutaraldehyde cross-linking. It is expected that for larger displacements glutaraldehyde-mediated cross-links will play an important role in hindering the irreversible displacement of microfibrils. This suggests that at small elongations of the fibril the distances over which reversible displacement of microfibrils and/or triple helices occurs are quite small, because over larger displacements the glutaraldehyde-mediated cross-links will hinder a larger deformation.

The absence of an influence of glutaraldehyde cross-linking at low elongation of the fibrils has also been described in literature. The modulus of non-treated self-assembled collagen fibres has been reported at ~13 MPa with a stress at break of 2.4 MPa.¹⁹ For glutaraldehyde cross-linked self-assembled collagen fibres the modulus was reported at 430 MPa with a stress at break of 58 MPa.²⁰ From the presented stress-strain curve of the glutaraldehyde cross-linked fibre in the article by A.K. Garg *et al.*²⁰, the Young's modulus can be estimated by calculating the slope of the stress-strain curve up to a stress of around 3 MPa. A modulus of ~20 MPa was obtained, which is of the same order as the modulus reported for non-treated fibres. This observation suggests that only at high stress values, the modulus of collagenous materials is affected by glutaraldehyde cross-linking. This hypothesis was underlined by studies on the stress-strain behaviour of a rat tail tendon (RTT). The influence of natural cross-linking on the stress-strain behaviour of a RTT immersed in saline was only observed in the yield region, where permanent deformation occurs. The slope of the regime in the stress-strain curve where reversible elongation of the tendon occurs, was independent of the rat's age. In the yield region the slope of the stress-strain curve was influenced by the age of the animal. The slope of the yield region of the stress-strain curve of RTTs from older animals was higher than that of the RTTs of younger rats.²¹ Permanent deformation of the RTT in the yield region was attributed to microfibril and fibril slipping. Possibly, natural cross-links between microfibrils and fibrils in the tendon reduce the rate of stress relaxation via slipping of microfibrils and fibrils.

When loading the glutaraldehyde cross-linked fibrils via stepwise elongation to stress values above 20 MPa, permanent deformation was observed. At these stress values a significant difference in the stress-strain behaviour was observed between non-treated and glutaraldehyde cross-linked fibrils.

For the same arguments as used in section 6.3, microfibril slipping is thought to be the most likely mechanism that occurs during permanent deformation of the fibril, although it might be hindered by glutaraldehyde-mediated cross-links between the microfibrils. Intra-triple helical cross-links mediated by glutaraldehyde might also prevent slipping of triple helices.

During the stepwise elongation of glutaraldehyde cross-linked fibrils, a build-up of residual stress was observed, starting at low relative elongation values. For non-treated fibrils rapid stress relaxation was observed at corresponding relative elongation. Only when the relative elongation of the fibrils exceeded a value of $\sim 30\%$, a residual stress was also observed for non-treated fibrils.

The difference in residual stress between glutaraldehyde cross-linked and non-treated fibrils can be explained from a lower rate of stress relaxation for glutaraldehyde cross-linked fibrils, compared to non-treated fibrils. It was already stated that permanent deformation of collagen fibrils is caused by slipping of microfibrils. Glutaraldehyde cross-linking can generate inter-microfibrillar cross-links. Furthermore, during the cross-linking reaction not only cross-links are being formed, but also surface modification of the outer surface of triple helices and microfibrils is established via the dangling ends of glutaraldehyde molecules that reacted only at one side with lysine and hydroxylysine residues. Possibly, cross-linking as well as surface decoration can lead to a change in the rate of slipping of the microfibrils. Hindering of the slipping of microfibrils will increase the stress needed for collagen fibrils to undergo permanent deformation via microfibril slipping.

6.5.3 Experimental evidence and literature - EDC/NHS cross-linking

Cross-linking with EDC/NHS can generate inter- and intra-triple helical covalent interactions. Tensile testing of EDC/NHS cross-linked fibrils was not investigated, instead the fibrils were loaded to stress values above 20 MPa using stepwise elongation. Again, because of the arguments given in section 6.3 and the presence of EDC/NHS mediated cross-links between the triple helices, microfibril slipping is anticipated to be the only deformation mechanism during elongation of EDC/NHS cross-linked fibrils.

Stepwise elongation of EDC/NHS cross-linked fibrils resulted in stress-elongation behaviour with a low residual stress, similar to the stress-strain behaviour of non-treated fibrils. Up to 30% relative elongation of the fibrils no residual stress was observed, but at higher relative elongation values a gradual increase in the amount of residual stress was observed. The reduced distance between the microfibrils during elongation of the fibrils, resulting in stronger interactions between the microfibrils, might explain this phenomenon.

When the individual stress-strain curves of EDC/NHS cross-linked fibrils were compared to those of non-treated fibrils, a difference was observed. The shape of the stress-strain curve of EDC/NHS cross-linked fibrils suggests that stress relaxation had occurred at an even higher rate than observed for non-treated fibrils. Stress relaxation of collagen fibrils was postulated to

be caused by microfibril slipping. EDC/NHS cross-linking is not expected to lead to cross-links between microfibrils. The observation of higher stress relaxation rates for EDC/NHS cross-linked fibrils compared to non-treated fibrils might be explained by decoration of the outer surface of triple helices and microfibrils. During cross-linking not only cross-links are being formed, but also surface modification via the dangling ends of N-hydroxysuccinimide ester-activated aspartate and glutamate residues, which are not involved in a condensation reaction with lysine and hydroxylysine residues. The conversion of aspartate or glutamate residues into N-hydroxysuccinimide esters reduces the number of negatively charged free carboxylic acids at the microfibril surface.

6.6 Conclusions

In this chapter, an attempt was made to obtain a complete description of all possible deformation mechanisms that may occur during tensile testing of a single collagen fibril. The deformation mechanisms were compared to the experimental findings of chapters 4 and 5 to obtain a new viewpoint on the structure and mechanical properties of a fibril. A comparison between these deformation mechanisms and the experimental observations suggests that the microfibril indeed is an intermediate structure between triple helices and fibrils.

The elastic and irreversible deformation of a fibril can be described by the following deformation mechanisms involving microfibrils and triple helices:

- Elastic deformation of microfibrils and elastic deformation by displacement of microfibrils with respect to each other.
- Elastic deformation of microfibrils may originate from elastic deformation of triple helices, or reversible displacement of assemblies of triple helices or triple helices with respect to each other.
- For irreversible deformation similar mechanisms will occur, but now leading to irreversible deformation or displacement of substructures.

One of the possible deformation mechanisms that can occur during reversible tensile testing of collagen fibrils in aqueous media is elastic deformation of triple helices. This mechanism takes place via deformation of flexible segments (including the telopeptides) in the triple helix. Because of the difference in Young's modulus of triple helices (2.9-9.0 GPa) and that of a collagen fibril (300 MPa, details: chapter 4), elongation of triple helices most likely is not the dominant mechanism during elongation of a collagen fibril.

For collagen fibrils immersed in aqueous media and loaded to stress values below 20 MPa, reversible displacement of microfibrils or triple helices (in aggregates or individually) are possible mechanisms to account for the stress-strain behaviour of the fibril, because no further evidence was found to rule out one of them.

The non-linear stress-strain behaviour of collagen fibrils immersed in aqueous media may be caused by the exclusion of water during elongation of the fibril, which will result in a decrease of the fibril diameter.

When collagen fibrils immersed in aqueous media were loaded to stress values above 20 MPa, permanent deformation was observed. The possible irreversible deformation mechanisms that can account for this stress-strain behaviour are similar to those reported for elastic deformation of fibrils.

In principle, irreversible displacement of triple helices and/or microfibrils can account for the observed permanent deformation. Three experimental observations contradict with the triple helix irreversible displacement mechanism, leaving slipping of microfibrils as the most likely candidate.

- The retention of the collagen D-period after tensile testing.
- No influence of the presence of specific ions in the applied aqueous medium on the stress-strain behaviour.
- Permanent deformation did not change the stress-strain behaviour of the fibril.

The stress-strain curve up to rupture of collagen fibrils immersed in aqueous media was enabled via stepwise elongation. The residual stress in the obtained individual stress-elongation curves increased at relative elongations larger than $\sim 30\%$, which suggests that the relative rate of stress relaxation was reduced. During the relative elongation of the fibril, the diameter of the fibril is expected to decrease, which possibly leads to an increase in the amount and/or strength of non-covalent interactions between microfibrils.

For collagen fibrils at ambient conditions a linear stress-strain behaviour with a Young's modulus of the same order as a triple helix was observed. This suggests that almost exclusively the triple helices are elongated during tensile testing of a collagen fibril at ambient conditions. When the collagen fibril at ambient conditions was loaded to stress values above 90 MPa, permanent deformation was observed. Similarly to the results obtained for fibrils immersed in aqueous media, microfibril slipping was hypothesized to account for the permanent deformation of the fibril.

Glutaraldehyde cross-linking of collagen fibrils leads to cross-links up to inter-microfibril level as well as surface modification. It was found that the mechanical properties of collagen fibrils at stress values below 20 MPa were not influenced by glutaraldehyde cross-linking.

During stepwise elongation of the glutaraldehyde cross-linked fibrils an immediate increase of residual stress was observed, while for non-treated fibrils this effect started at $\sim 30\%$ relative elongation. Most likely, the rate of microfibril slipping is reduced in glutaraldehyde cross-linked fibrils, compared to non-treated fibrils.

EDC/NHS cross-linked fibrils showed similar stress-strain behaviour as non-treated fibrils during stepwise elongation, with an increase in residual stress starting also at ~30% relative elongation. The individual stress-strain curves of EDC/NHS cross-linked fibrils suggested a higher rate of microfibril slipping compared to non-treated fibrils. This finding may be explained by surface modification of microfibrils with NHS-ester groups.

6.7 References

- 1 T. F. Linsenmayer, in 'Chapter 1 - Collagen', ed. E. D. Hay, Plenum Press, New York, 1991.
- 2 F. H. Silver, I. Horvath, and D. J. Foran, *J. Theor. Biol.*, 2002, **216**, 243.
- 3 F. H. Silver, J. W. Freeman, I. Horvath, and W. J. Landis, *Biomacromol.*, 2001, **2**, 750.
- 4 Y. L. Sun, Z. P. Luo, A. Fertala, and K. N. An, *Biochem. Biophys. Res. Comm.*, 2002, **295**, 382.
- 5 C. Bustamante, J. F. Marko, E. D. Siggia, and S. Smith, *Science*, 1994, **265**, 1599.
- 6 F. H. Silver, J. W. Freeman, and G. P. Seehra, *J. Biomech.*, 2003, **36**, 1529.
- 7 N. Sasaki and S. Odajima, *J. Biomech.*, 1996, **29**, 655.
- 8 H. Hofmann, T. Voss, and K. Kühn, *J. Mol. Biol.*, 1984, **172**, 325.
- 9 R. Harley, D. James, A. Miller, and J. W. White, *Nature*, 1977, **267**, 285.
- 10 N. Sasaki and S. Odajima, *J. Biomech.*, 1996, **29**, 1131.
- 11 J. P. R. O. Orgel, A. Miller, T. C. Irving, R. F. Fischetti, A. P. Hammersley, and T. J. Wess, *Structure*, 2001, **9**, 1061.
- 12 D. J. S. Hulmes, T. J. Wess, D. J. Prockop, and P. Fratzel, *Biophys. J.*, 1995, **68**, 1661.
- 13 N. Sasaki, N. Shukunami, N. Matsushima, and Y. Izumi, *J. Biomech.*, 1999, **32**, 285.
- 14 J. Kastelic and E. Baer, Symposium of Society for Experimental Biology - Mechanical Properties of Biological Materials, Cambridge University Press, Cambridge, 1980.
- 15 W. Folkhard, E. Mosler, W. Geercken, E. Knörzner, H. Nemetschek-Gansler, and T. Nemetschek, *Int. J. Biol. Macromol.*, 1987, **9**, 169.
- 16 J. B. Thompson, J. H. Kindt, B. Drake, H. G. Hansma, D. E. Morse, and P. K. Hansma, *Nature*, 2001, **414**, 773.
- 17 G. N. Ramachandran, in 'Structure of collagen at a molecular level', ed. G. N. Ramachandran, Academic Press, London, 1967.
- 18 T. Nemetschek, R. Bowitz, and H. Nemetschek-Gansler, *Verh. Deutsche Ges. Path.*, 1975, **59**, 34.
- 19 Y. P. Kato and F. H. Silver, *Biomaterials*, 1990, **11**, 169.
- 20 A. K. Garg, R. A. Berg, F. H. Silver, and H. G. Garg, *Biomaterials*, 1989, **10**, 413.
- 21 D. F. Betsch and E. Baer, *Biorheol.*, 1980, **17**, 83.

CHAPTER 7

Conclusions and outlook

"De taak der wetenschap is het gebied van onze ervaring uit te breiden en het te ordenen." - N. Bohr

7.1 Structure and mechanical properties of collagen substructures

In chapter 2 an overview of the structure and mechanical properties of collagen type I from the triple helix up to the collagen fibre level is given. Because the detailed structure has not yet been unraveled at the atomic level, the postulated interactions and mechanisms stabilizing the triple helix structure, and causing self-assembly of the triple helices into microfibrils and fibrils are not generally accepted. The stabilization of triple helices via inter- and intra-helical water-mediated hydrogen bonds is under dispute.

Depending on the fibril model, microfibrils have been proposed as structural entities. In literature, extensive evidence for the existence of these microfibrils has been reported based on electron microscopy (EM) and atomic force microscopy (AFM) investigations.

The collagen fibril has an important function as it is part of the extracellular matrix. The internal structure of the collagen fibril remains under debate. The first model¹ describes the fibril as an aggregate of triple helices in microfibrils, which aggregate in subfibrils, and subsequently organise into a fibril. In a second model² the fibril consists of aggregated triple helices only, without intermediate substructures. This alternative model originates from observations of liquid-like behaviour of collagen triple helices within the fibril.

The mechanical properties of triple helices have been reported based on a variety of experimental methods. It was found that the triple helix contains flexible and rigid regions, of which the first are thought to be involved in elastic elongation of triple helices under load.

The mechanical properties of single collagen fibrils are unknown, but extrapolations have been made based on the mechanical properties of macroscopic collagen materials, obtained in combination with X-ray diffraction studies. During mechanically testing of macroscopic collagen materials the collagen D-period of the constituting fibrils was found to change.

It is unclear whether this change is permanent, but the origin can be found in slipping of triple helices within the fibrils.

Further information on the mechanical properties of collagen fibrils was not available before the work described in this thesis was carried out.

7.2 Methodology for tensile testing of fibrils

An AFM was positioned on top of an inverted microscope and a calibrated setscrew was used to tilt the head and therewith increase the distance of the base of the cantilever to the surface. Tensile testing of a single collagen fibril was enabled by fixing a fibril between a substrate surface and an AFM tip using epoxy glue droplets. The fibril was selectively glued to the AFM tip from a Teflon coated glass substrate. The contribution of deformation of the epoxy glue droplets used to fix the fibril to the tip on the overall stress-strain curve of the collagen fibril was found to be negligible.

7.3 Mechanical properties of collagen fibrils

The linear stress-strain curves of non-treated collagen fibrils at ambient conditions yielded a Young's modulus of 5 ± 3 GPa. When exceeding a maximal stress of around 90 MPa, permanent lengthening of the fibrils was observed.

Reversible mechanical loading of collagen fibrils in aqueous media was possible up to stress values of around 20 MPa. A Young's modulus of 280 ± 50 MPa and a modulus of 420 ± 50 MPa at higher stress values above 3 MPa were determined from the stress-strain curves. It was observed that the applied medium (demineralised water, PBS, Na^+ and Ca^{2+} -containing HEPES buffer) in which the fibrils were placed, had no significant effect on their mechanical properties. The applied loading rate between 0.02 and $20 \mu\text{m}\cdot\text{s}^{-1}$, did not result in a significant difference in the stress-strain behaviour of the fibrils. Permanent deformation of the fibril was observed upon exceeding a stress value of around 20 MPa.

Two collagen fibrils were stepwise elongated in an aqueous environment to enable relative elongations larger than $\sim 10\%$. The resulting stress-elongation behaviour of these two fibrils was found to be highly comparable. The residual stress at the start of each cycle increased when going to higher relative elongation values. This presence of residual stress suggests that in these experiments stress relaxation of the fibrils occurs at a lower rate than the extension rate of the cycles. Permanent deformation of fibrils even up to 200% relative elongation did not have a significant effect on their subsequent stress-elongation behaviour.

During tensile testing of the fibril, the fibril is oriented such that two bends close to the fixation points are present. An attempt was made to evaluate the influence of this configuration on the stress-strain behaviour of the fibril by using a finite element model for isotropic materials with an elastic behaviour. A uniform plate with the same length to diameter ratio as the fibril was tensile tested in a bent configuration (similar to that of the fibril) and in

an uniaxial configuration. It was observed that the stress-strain behaviour of the modelled fibril in uniaxial configuration was highly similar to the stress-strain curves experimentally obtained for a collagen fibril. This result, although obtained via calculations on an idealized fully elastic isotropic plate model, suggests that the effect of the bent configuration on the stress-strain behaviour of single collagen fibrils is minimal.

7.4 Influence of cross-linking

Stress relaxation due to stepwise elongation was reduced in glutaraldehyde cross-linked fibrils, as compared to non-treated fibrils in an aqueous environment, most likely due to hindering of microfibril slipping via inter-microfibrillar cross-links. This resulted in significantly higher residual stresses during individual elongation cycles as compared to non-treated fibrils.

The stepwise stress-elongation curves of EDC/NHS (details: chapter 5) cross-linked fibrils showed a higher stress relaxation rate than those of non-treated fibrils. It is hypothesized that this is caused by chemical modification of the surfaces of triple helices constituting the microfibrils, leading to weaker interactions between microfibrils.

7.5 Relating the mechanical behaviour to the structure of fibrils

The triple helices and microfibrils that constitute the fibril provide the mechanical properties. Four different mechanisms of reversible and irreversible deformation of a collagen fibril can be distinguished. The first two consist of deformation and displacement of microfibrils. The deformation of microfibrils may originate from deformation of triple helices, or displacement of assemblies of triple helices or triple helices with respect to each other, which provide the third and fourth mechanism.

During reversible loading of collagen fibrils immersed in aqueous media, reversible displacement of microfibrils and reversible displacement of individual of aggregated triple helices are possible deformation mechanisms. The deformation of triple helices most likely has a minimal contribution to the stress-strain behaviour, because the Young's modulus of a triple helix is much higher than that of the fibril. For fibrils immersed in aqueous media, a non-linear stress-strain curve was observed. It is hypothesized that during elongation stiffening of the fibril occurs because microfibrils and triple helices are brought in closer proximity to each other, which leads to enhanced non-covalent interactions between these substructures.

Permanent deformation observed during tensile testing of a collagen fibril immersed in aqueous media was attributed to irreversible displacement of microfibrils. Several experimental observations ruled out irreversible displacement of triple helix as a possible mechanism.

For a fibril at ambient conditions, reversible tensile testing most likely is dominated by the deformation of triple helices. Similar to fibrils immersed in aqueous media, permanent deformation was attributed to irreversible displacement of microfibrils.

Glutaraldehyde cross-linked collagen fibrils, when subjected to stepwise elongation up to ~30% relative elongation in an aqueous environment, showed a build-up of residual stress. For non-treated fibrils no residual stress was observed. This difference was explained by the presence of glutaraldehyde-mediated cross-links between collagen microfibrils, which hinder microfibril slipping.

When stretching EDC/NHS cross-linked collagen fibrils, slipping of microfibrils occurred at a higher rate than for non-treated fibrils. A possible explanation for this observation is surface decoration of microfibrils with NHS-ester groups.

7.6 Outlook

The tensile testing experiment on collagen fibrils was successful, but a number of corrections and approximations were needed to account for the artefacts of the set-up. In future experiments the set-up should be improved to eliminate or minimize the following factors.

- The hysteresis and non-linear travel of the AFM tube.
- The range in extension of the AFM tube should be increased to a minimum of 100 μm .
- The noise level arising from an interference pattern of the AFM laser should be reduced.
- The orientation of the fibril during tensile testing should be uniaxial. This might be performed using micropipettes as a force transducing element, which could be glued to the fibril via the same fixation methodology as used for the AFM. The fixed fibril can be tensile tested in a direction parallel to the surface, thus eliminating the bending. Alternatively, in this approach the fixed fibril can be moved into a bent position, similar to the tensile testing experiments of the fibrils with the AFM, the amount of bending of the fibril in this position can be verified using the inverted microscope.

Besides improvement of the set-up, several hypothetical experiments might be performed using the developed methodology.

- The developed set-up can be used for tensile testing of other biologically relevant fibrous materials, such as spider silk. Furthermore, the mechanical properties of microscopic man-made fibrous materials might be determined using this methodology. The only limitation for the materials to be tested is the stiffness of the glue that was applied for the fixation of the fibril ($14 \text{ N}\cdot\text{m}^{-1}$ as determined from a force-distance curve, details: chapter 3).

- More detailed information on the collagen structure can be obtained via tensile testing of morphologically different fibrils. For example, genetically modified collagen triple helices could be self-assembled into fibrils, whose mechanical properties can be determined. Changes in the polypeptide α -amino acid sequence can then directly be correlated to the mechanical properties of the fibrils.
- Collagen fibrils are formed and excreted by fibroblasts. A collagen fibril that is fixed at only one end can be brought into contact with a fibroblast cell that is manipulated by a micropipette, for example. By pulling the fibril the micro-mechanical interactions between a fibril and a fibroblast might be determined.
- Collagen fibrils provide a structural framework, which is an important building block of the extracellular matrix. This matrix constitutes an external forces-mediating network that surrounds cells. A fibril can be fixed at one end and brought in contact with a microneedle on which for example glycosaminoglycans (GAGs) are covalently bound. The interaction between the fibril and the GAGs can be determined by pulling the fibril.

7.7 References

- 1 V. Ottani, D. Martini, M. Franchi, A. Ruggeri, and M. Raspanti, *Micron*, 2002, **33**, 587.
- 2 D. J. S. Hulmes, *J. Struct. Biol.*, 2002, **137**, 2.

APPENDIX A

Diameter change of tensile tested collagen fibrils - theory and experiment

A.1 Theoretical calculations

Upon extending a collagen fibril over large distances, the diameter of the fibril will decrease. The change of the diameter must be known to enable the calculation of its cross-sectional area, and thereby to convert the force applied to the stress value upon tensile testing of the fibril. A decrease in diameter leads to a decrease in cross-sectional area, and thus an increase in the calculated stress. Assuming that the total volume of the fibril is not changing during the experiment, the following relation holds (formula A.1):

$$V = L_1 \cdot A_1 = L_2 \cdot A_2 \quad (\text{A.1})$$

$$\text{with } A = \frac{1}{4}\pi \cdot D^2 \quad (\text{A.2})$$

in which L_1 and A_1 are the initial length and cross-sectional area and L_2 and A_2 the corresponding values after extension. D is the diameter of the fibril.

Combining formulas A.1 and A.2 gives:

$$D_1^2 \cdot L_1 = D_2^2 \cdot L_2 \quad (\text{A.3})$$

The stress values upon extension are calculated according to formula A.4:

$$\sigma = \frac{F}{A} = \frac{4 \cdot F}{\pi \cdot D_2^2} \quad (\text{A.4})$$

and the strain is expressed as:

$$\varepsilon = \frac{(L_2 - L_1)}{L_1} \quad (\text{A.5})$$

Combination of formulas A.3, A.4 and A.5 gives:

$$\sigma = \frac{4 \cdot F \cdot (\varepsilon + 1)}{\pi \cdot D_1^2} = \frac{F \cdot (\varepsilon + 1)}{A_1} \quad (\text{A.6})$$

The actual stress value can thus be calculated from the measured value by multiplying the stress by $(\varepsilon + 1)$. In this study, different collagen fibrils were extended over three times their original length (chapters 4 and 5). The fibril diameter was calculated according to formula 6 to obtain the stress values at the applied elongation.

The diameter of the fibrils was measured before and after the experiment. Imaging of fibrils on the surface before the experiment was performed by AFM in tapping mode. The height of the fibril was used as a measure of the diameter. After extension and rupture of the fibril, AFM and SEM images of the fibril ends, were used to measure the diameter. Both parts of the fibril were imaged. It is important to mention here that from the images it can be concluded that necking had not occurred.

In table A.1 the measured and calculated diameters of different fibrils before and after extension (rupture) are presented.

A.2 Experimental findings

In this study, different collagen fibrils were extended over three times their original length (details: chapter 4 and 5). A correction of the diameter of the fibril was performed in order to obtain the corrected stress values. When a Poisson constant of 0.5 is applied, the theoretical reduced diameter can be calculated from formula A.7.

$$D_2 = \sqrt{\frac{D_1^2 \cdot L_1}{L_2}} \quad (\text{A.7})$$

The diameter of the tensile tested fibrils (details appendix C) was measured before and after the tensile testing experiment. Before the experiment the fibril is imaged with AFM and after the experiment the broken ends at the cantilever and on the surface were imaged by AFM and SEM. An important finding from the images of the ruptured ends of the broken fibrils was that necking had not occurred. In Table A.1 the diameters before and after tensile testing are summarized.

Table A.1. Diameters before and after tensile testing, as obtained by AFM and SEM.

Fibril [§]	D ₁ [#] [nm]	D ₂ ^{cant} [nm]	D ₂ ^{surf.} [nm]	D ₂ ^{calc. #} [nm]	ε [%]
G1	214 ± 12	236 ± 16 (SEM)*	212 ± 49 (AFM) 280 ± 81 (SEM)*	183 ± 10	40
G2	116 ± 4	85 ± 10 (SEM)	n.d.	62 ± 4	244
N4	105 ± 5	n.d.	96 ± 5 (AFM)	94 ± 5	30
EN1	109 ± 14	91 ± 21 (SEM)	n.d.	89 ± 11	62
EN2	140 ± 30	84 ± 23 (SEM)	94 ± 11 (AFM)	101 ± 22	104

All diameters shown in the table represent the average value of the fibril diameter at five random locations. The diameter values obtained by AFM imaging were obtained by measuring in tapping mode and correspond to the height of the fibrils (details: chapter 3). Table details: §: details fibrils can be found in appendix C. The diameter values obtained by SEM imaging represent the width of the fibrils. #: corresponds to diameter of the fibrils at ambient conditions, *: excluding 2 × 8 nm width from Au/Pd coating (8 nm grain size).

The calculated diameter of fibrils N4 and EN1 correlated to the experimentally determined diameter. However, due to the experimental error these values are not statistically significant. For fibril G1 no significant increase in the diameter was observed. The decrease in diameter of fibrils G2 and EN2 from 116 to 85 nm ($\varepsilon = 244\%$) and 140 to 90 nm ($\varepsilon = 104\%$), respectively, corresponds well to the the values obtained by calculation of the diameter, according to theory.

APPENDIX B

Calculations on the influence of the relative error in the dimensions of the cantilevers on their stiffness and resonance frequency

B.1 Method

The spring constant of a cantilever can be determined from the spectral analysis of its Brownian motion. Due to the small amplitude of the cantilever used in our set-up, the spring constant could not be determined with the optical deflection method. Therefore, the spring constant was calculated from its resonance frequency, according to the method shown in chapter 3. The specifications of the applied rectangular cantilevers were: $k = 36\text{-}62 \text{ N}\cdot\text{m}^{-1}$, $f_{\text{res}} = 322\text{-}384 \text{ kHz}$, $t = 3.74\text{-}4.41 \text{ }\mu\text{m}$, $w = 29\text{-}31 \text{ }\mu\text{m}$, $L = 122 \text{ }\mu\text{m}$. The AFM tip of the applied cantilevers was removed using focused ion beam milling. Because the tip does not contribute significantly to the stiffness of the girder forming the cantilever, the influence of the removal of the tip on the spring constant of the cantilever was neglected. The spring constant (k) and the resonance frequency of the cantilever (f) are functions of the dimensions elasticity and mass as described in formula (B.1) and (B.2).¹

$$k = \frac{E \cdot w \cdot t^3}{4 \cdot L^3} \quad (\text{B.1})$$

with $E = E\text{-modulus of Si}$

$$f = \frac{\sqrt{k}}{2 \cdot \pi} \quad (\text{B.2})$$

Using formula (B.2) the expression for the resonance frequency can be rewritten:

$$m = V \cdot \rho \quad (\text{B.3})$$

with $V = L \cdot w \cdot t$

$$f = \frac{t \cdot \sqrt{E}}{4 \cdot \pi \cdot L^2} \quad (\text{B.4})$$

The error in the values of the resonance frequency and the spring constant are determined by the error in the dimensions of the cantilever, according to formula B.1 and B.4, respectively.

B.2 Results

When the specifications of the supplier are used, the thickness t of the cantilevers contains an error of $\pm 0.34 \mu\text{m}$, which is equal to 8.2%. The error in the cantilever length L is not specified by the supplier, but can be assumed to be equal to that of the width ($1.0 \mu\text{m}$, supplier data). This results in an error of 0.8% in L . For the width the error is $\pm 1 \mu\text{m}$, equal to 3.3%.

According to formula (4), the error in the frequency is originating from t and L . When using the error percentages calculated for t and L , an error of 9.8% is expected for f . The error in f from the resonance frequency specifications is 8.8%. Since the contribution of the thickness t to the error in f is larger than the contribution of L (8.2% and 1.6%, respectively), the difference in resonance frequency between two cantilevers is dominated by the difference in thickness.

The error in the spring constant is originating from w , t and L , according to formula B.1.

When using the error percentages calculated for w , t and L , an error of 30.3% is expected for k . The error in k from the resonance frequency specifications is 26.5%. Since the contribution of the thickness t to the error in k is far larger than the contribution of w and L (24.6% versus 3.3 and 2.4%, respectively), the difference in spring constant between two cantilevers is dominated by the difference in thickness.

The error in the spring constant is determined by the error in three variables (t , w and L). The variation in t is dominating the error in the spring constant as shown above. The assumption that the spring constant is mainly dominated by the change in thickness of the cantilever seems justified from this finding.

B.3 References

- ¹ D. Sarid, in 'Chapter 1 - Mechanical properties of levers', ed. D. Sarid, New York, 1991.

APPENDIX C

Overview of mechanically tested collagen fibrils

Fibril cond	L [μm]	Exp.	Max. ext.	Ext. rate	Perm. def.	Max. stress	Details in chapter
	d# [nm]		[μm]	[$\mu\text{m}\cdot\text{s}^{-1}$]	[μm]	[MPa]	
N1 ambient	119.0 \pm 0.5 214 \pm 12	TT	2.3	0.3	0	95	C4
N1, ambient	119.0 \pm 0.5 214 \pm 12	TTi	4.0	0.8	1.0	145 (3 times)	
N1, ambient	120.0 \pm 0.5 214 \pm 12	TT	4.0	0.8	5.7	154 (2 times)	
N1, phosphate	125.7 \pm 0.5 370 \pm 20	TT	3.1	0.6	0	9	C4
N1, phosphate	125.7 \pm 0.5 370 \pm 20	TT	4.0	0.8	0	15	C5
N1 = G1 phosphate	125.7 \pm 0.5 370 \pm 20	TT	4.0	0.8	0	15	C5
N1 = G1 phosphate	125.7 \pm 0.5 370 \pm 20	TTi	4.0	0.8	3.3	31 (8 times)	
N1 = G1 phosphate	129.0 \pm 0.5 370 \pm 20	TTB	182	0.7*	n.d.	129	rupture C5
N2, ambient	55.3 \pm 0.5 181 \pm 5	TT	1.0	2.0	0	40	
N2, ambient	55.3 \pm 0.5 181 \pm 5	SR	n.d.	n.d.	1.7	123 (3 times)	
N2, ambient	57.0 \pm 0.5 181 \pm 5	TT	1.9	0.4	0	85	C4
N2, ambient	57.0 \pm 0.5 181 \pm 5	TTi	2.7-4.0	0.7-1.1	1.1	110	C4
N2, ambient	58.1 \pm 0.5 181 \pm 5	LRV	1.0	0.02-20	n.d.	40	C4

Abbreviations used in the table: cond. - conditions, dim. - dimensions, exp. - experiment(al), max. - maximal, ext. - extension, perm. - permanent, def. - deformation, TT(i) - tensile test (irreversible), SR - stress relaxation, CR - creep relaxation, LRV - loading rate variation, TTB - tensile test to break. #: diameter in wet state, fully swollen; *: extension of one cycle.

Fibril, cond.	L [μm]	Exp.	Max. ext.	Ext. rate [$\mu\text{m}\cdot\text{s}^{-1}$]	Perm. def.	Max. stress [MPa]	Details in chapter
	d# [nm]		[μm]		[μm]		
N2, ambient	58.1 \pm 0.5 181 \pm 5	SR	n.d.	n.d.	0.9	110 (2 times)	
N2, ambient	59.0 \pm 0.5 181 \pm 5	CR	Const F	3000 \pm 600	3.3	120 (4 times)	
N2, water	62.3 \pm 0.5 181 \pm 5	TTi	4.0	8.0	1.8	25	
N2, water	64.1 \pm 0.5 181 \pm 5	LRV	2.2	0.02-20	0	10	C4
N2, water	64.1 \pm 0.5 181 \pm 5	CR	Const F	3000 \pm 600	3.5	27 (3 times)	
N2, PBS	67.6 \pm 0.5 181 \pm 5	TTi	4.0	8.0	2.4	21	
N2, PBS	70.0 \pm 0.5 181 \pm 5	LRV	2.2	0.02-20	0	10	C4
N2, PBS	70.0 \pm 0.5 181 \pm 5	CR	Const F	3000 \pm 600	0.7	28	
N2 HEPES	70.7 \pm 0.5 181 \pm 5	TTi	4.0	8.0	1.2	21	
N2 HEPES	71.9 \pm 0.5 181 \pm 5	LRV	2.2	0.02-20	0	10	C4
N2 HEPES	71.9 \pm 0.5 181 \pm 5	CR	Const F	3000 \pm 600	1.4	30	
N2 Ca ²⁺ -HEPES	73.3 \pm 0.5 181 \pm 5	TTi	4.0	8.0	1.0	36	
N2 Ca ²⁺ -HEPES	74.3 \pm 0.5 181 \pm 5	LRV	2.2	0.02-20	0	10	C4
N2 Ca ²⁺ -HEPES	74.3 \pm 0.5 181 \pm 5	CR	Const F	3000 \pm 600	2.0	23	
N3, MES	44.0 \pm 0.5 188 \pm 23	TT	1.0	0.2	0	7	C4
N3 = EN1 MES	44.0 \pm 0.5 188 \pm 23	TTB	19	0.7*	n.d.	87	rupture, C5

Abbreviations used in the table: cond. - conditions, dim. - dimensions, exp. - experiment(al), max. - maximal, ext. - extension, perm. - permanent, def. - deformation, TT(i) - tensile test (irreversible), SR - stress relaxation, CR - creep relaxation, LRV - loading rate variation, TTB - tensile test to break. #: diameter in wet state, fully swollen; *: extension of one cycle.

Fibril, cond.	L [μm]	Exp.	Max. ext.	Ext. rate	Perm. def.	Max. stress	Details in chapter
	d# [nm]		[μm]	[$\mu\text{m}\cdot\text{s}^{-1}$]	[μm]	[MPa]	
N4, MES	72.0 \pm 0.5 182 \pm 9	TTi	2.3-4.0	0.5-0.9	0.3	35	C4
N4, MES	72.0 \pm 0.5 182 \pm 9	TTB	22	0.7*	n.d.	69	rupture, C5
N5, phosphate	101.0 \pm 0.5 201 \pm 9	TT	4.0	0.8	0	19	
N5 phosphate	101.0 \pm 0.5 201 \pm 9	TTB	97	0.7*	91	123	195% elong., C4
N5 = G2 phosphate	290.0 \pm 0.5 119	TTB	246	0.7*	n.d.	714	rupture, C5
N6 = EN2 MES	31.0 \pm 0.5 243 \pm 52	TTB	18	0.7*	n.d.	143	rupture, C5

Abbreviations used in the table: cond. - conditions, dim. - dimensions, exp. - experiment(al), max. - maximal, ext. - extension, perm. - permanent, def. - deformation, TT(i) - tensile test (irreversible), TTB - tensile test to break. #: diameter in wet state, fully swollen; *: extension of one cycle.

APPENDIX D

Change in D-period of collagen fibrils upon tensile testing

D.1 Results

The D-period was determined using AFM imaging in tapping mode, before and after tensile testing. The results are presented in Table D.1.

Table D.1 Collagen D-period as determined before and after tensile testing.

Fibril	D-period before [nm]	D-period after [nm]	Max. Rel. Elong. [%]
G1	60 ± 1 (AFM)	65 ± 1 (SEM)	40
G2	65 ± 1 (AFM)	65 ± 2 (SEM)	244
N4	54 ± 5 (AFM)	57 ± 2 (AFM)	30
EN1	70 ± 6 (AFM)	63 ± 1 (AFM)	62
EN2	n.d.	65 ± 1 (AFM)	104

In these studies, collagen fibrils obtained from bovine Achilles tendon origin were used. The characteristic D-period of the collagen fibrils is easily visualized by AFM or SEM. Previous studies revealed a change in D-period, as measured with X-ray diffraction, upon extending collagen tendons and fibres. Whether the change in the D-period is reversible is still under debate. Mechanical loading of an Achilles tendon at stress values above 10 MPa, while investigating the microscopic deformation by X-ray diffraction, showed an increase in the D-period.^{1, 2} In a different study, the D-period of collagen tendons was also found to change under load, but this change was found to be reversible within 12h.³

In the study reported here, different collagen fibrils were imaged either by AFM or SEM to determine the D-period before and after tensile testing. The non-treated fibril (N4), glutaraldehyde (G1 and G2) and EDC/NHS cross-linked fibrils (EN1 and EN2) possessed a D-periodicity ranging from 54 to 70 nm. These values correspond to average values reported in literature⁴ and the variation is caused by the (partial) dehydration in sample preparation. No significant change in D-periodicity was observed after extending the fibrils. This may be due to the reversibility of the changes induced, although it has been shown that especially in cross-linked collagen the change in the D-period is permanent.³

D.2 References

- 1 N. Sasaki, N. Shukunami, N. Matsushima, and Y. Izumi, *J. Biomech.*, 1999, **32**, 285.
- 2 J. Kastelic and E. Baer, Symposium of Society for Experimental Biology - Mechanical Properties of Biological Materials, Cambridge University Press, Cambridge, 1980.
- 3 W. Folkhard, E. Mosler, W. Geercken, E. Knörzer, H. Nemetschek-Gansler, and T. Nemetschek, *Int. J. Biol. Macromol.*, 1987, **9**, 169.
- 4 J. A. Chapman, M. Tzaphlidou, K. M. Meek, and K. E. Kadler, *Electron Micr. Rev.*, 1990, **3**, 143.

SUMMARY

As the most abundant protein present in mammals, collagen has an essential function in the shape and mechanical properties of tissue. The correlation between the mechanical properties of collagenous tissue and its internal structure is poorly understood. One of the substructures forming the internal structure of collagenous tissue is the collagen fibril, which is secreted by fibroblasts and has a direct mechanical interaction with cells. These fibrils have a typical diameter of 200 nm and a length of tens of micrometers. We succeeded in fixing a single collagen fibril with one end to a substrate and with the other end to the cantilever of an atomic force microscope.

Via this set-up it was possible to measure the mechanical properties of collagen fibrils similar to macroscopic tensile testing of various materials. The results showed that collagen fibrils have a linear stress-strain behaviour at ambient conditions, while fibrils immersed in aqueous media display a non-linear stress-strain behaviour. At a certain stress, which was different for the two conditions, permanent deformation of the fibril was observed. It was hypothesized that permanent deformation of the fibril takes place via microfibril slipping.

Collagen-based biomaterials usually are cross-linked prior to use. This process prevents rapid enzymatic degradation and foreign body rejection, but also alters the mechanical properties of collagen. Two well-described cross-linking reagents (glutaraldehyde and a carbodiimide-based reagent (EDC/NHS)) were used to cross-link the collagen fibrils. It was found that glutaraldehyde cross-linking of the fibrils leads to a lower permanent deformation of the fibrils at high stress values than observed for non-treated fibrils. For the EDC/NHS cross-linked fibrils a similar mechanical behaviour as for the non-treated fibrils was observed.

In chapter 2 of this thesis the structure and mechanical properties of collagen have been reviewed. Around 25 types of collagen are known, of which type I is the most abundant. The triple helix is a characteristic substructure of collagen. It consists of three polypeptide chains in which the triplet Gly-X-Y repeats, where X and Y are generally proline or hydroxyproline residues. Collagen fibrils, which are important components of the extracellular matrix, are formed *in vivo* as well as *in vitro* by the assembly of collagen triple helices. Collagen fibrils are the main constituents of ligaments.

The stability of the triple helix has been related to hydrogen bonding involving the hydroxyproline residues in the helix and water-mediated hydrogen bonding. Although other explanations (steric hindrance and/or the electron inductive effect of the hydroxyl group in Hyp residues) have been postulated, the foregoing mechanism in combination with the asymmetry of the helix seem to provide the best explanation for the stability of the triple helix.

As discussed before, aggregation of triple helices via self-assembly leads to the formation of fibrils, a process which is called fibrillogenesis. The existence of microfibrils as an intermediate structure between triple helices and fibrils is based on X-ray diffraction data.

Analysis of collagenous structures by other techniques (such as NMR and polarized light) suggest a less organised aggregation of triple helices in a fibril, which resembles that of molecules in liquid crystals.

The aggregation of triple helices is regulated by hydration forces, although other non-covalent interactions such as hydrophobic and electrostatic interactions between triple helices have also been suggested. The presence of non-helical telopeptides at the ends of the triple helices increases the rate of triple helix aggregation and regulates the fibril diameter.

Various techniques have been applied to determine the mechanical properties of single triple helices or to extrapolate the mechanical behaviour of macroscopic collagenous structures to that of triple helices. A Young's modulus between 3 and 6 GPa was estimated for a triple helix present in macroscopic collagenous substructures immersed in an aqueous medium. Elongation of triple helices may occur via various mechanisms, including:

- elastic stretching of sequences in the triple helix containing ionic residues, but low in (hydroxy)proline residues,
- stretching of microkinks in the helix,
- disruption of sacrificial bonds in the helix consisting of ionic interactions, which are most likely inter-helical.

Besides elongation of triple helices, sliding has also been described, leading to a change in the collagen D-period.

The mechanical properties of collagen fibrils are virtually unknown. A X-ray diffraction study of an Achilles tendon under stress resulted in a stress-strain curve with a corresponding Young's modulus for a collagen fibril of ~ 450 MPa.

The development of the applied set-up which enables tensile testing of single collagen fibrils was discussed in Chapter 3. An AFM was combined with an inverted microscope. Collagen fibrils, suspended on a partially Teflon-coated glass slide were fixed to the glass substrate at one end with a small epoxy glue droplet. The other end of the fibril, located on the Teflon surface, was glued (epoxy glue) to the AFM cantilever. After curing of the glue the cantilever with the fibril attached to it could be lifted from the Teflon surface and tensile testing of single collagen fibrils was possible using this system. The stiffness of the glue was determined, which showed that the glue did not influence the stress-strain curves of the collagen fibrils.

Using the set-up described in chapter 3, tensile testing of single collagen fibrils resulted in stress-strain curves, which were discussed in chapter 4. Reversible tensile testing of collagen fibrils at ambient conditions was possible up to stress values of 90 MPa. Above this stress level, permanent deformation was observed. For fibrils immersed in aqueous media, including HEPES buffers containing calcium ions, and demineralised water, at a pH range between 5.4 and 7.4 similar stress-strain curves were observed. The applied extension rate was varied between 0.02 and $20 \mu\text{m s}^{-1}$, again showing no difference in stress-strain behaviour.

When a stress value of 20 MPa was exceeded, permanent deformation was observed. Via stepwise elongation of the fibril, the stress at break value of the fibril was determined. One fibril was found to rupture at a stress of 69 MPa, while a second fibril with different dimensions was still intact at a stress of 123 MPa. The stress-elongation curves of both fibrils were similar. At relative elongation values above ~30% elongation, a build-up of residual stress in the individual stress-elongation curves was observed.

Imposed elongation of the fibrils at high stress levels led to permanent lengthening of the fibrils. This did not result in a permanent increase of the D-period of the fibril, which suggests that the organisation of the triple helices in the fibril remained intact. Permanent lengthening of the fibril therefore is thought to occur via slipping of microfibrils with respect to each other. Because of the constraints set by the applied procedure for glueing and tensile testing of the collagen fibril as described in chapter 3, the fibril contains two bending points when lifted and elongated from the glass substrate. In the foregoing results of chapter 4, the tensile test was assumed to be uniaxial. In reality, the bending of the fibril might have a contribution to its stress-strain behaviour.

An attempt was made to evaluate the possible effect of bending of the fibril on the stress-strain curves by a finite element-based modelling experiment using an isotropic plate with the same length to width ratio as found for the collagen fibrils (100 μm to 200 nm), assuming elastic behaviour. The results of this modelling experiment and possible implications for the reported mechanical properties of single collagen fibrils are discussed in the appendix of chapter 4. When the isotropic plate was elongated in an uniaxial configuration, a different stress-strain curve was obtained than for a plate elongated with two bending points (similar to the fibril). The obtained stress-strain curves of the plate were compared to the stress-strain curves for collagen fibrils. It was found that only the modelled stress-strain curve in uniaxial configuration was similar to the experimental results found for the fibrils. Despite the limitations of the applied model, the influence of bending on the stress-strain curves of collagen fibrils is minimal, possibly because bending of the fibril occurs already at very low stress levels.

In chapter 5, the results of the influence of glutaraldehyde and EDC/NHS-mediated cross-linking of collagen fibrils on its mechanical properties were discussed. It was found that a collagen fibril, cross-linked in glutaraldehyde, had the same stress-strain behaviour as a non-treated fibril, when both fibrils were loaded to a stress of 15 MPa. When loaded at higher stress values via stepwise elongation, the glutaraldehyde cross-linked fibril ruptured at a stress of 168 MPa. A collagen fibril cross-linked using EDC/NHS could be loaded to a stress of 87 MPa, when rupture occurred.

Glutaraldehyde cross-linked fibrils were found to display a rapid increase in residual stress in cyclic stress-elongation curves at increasing relative elongation. This suggests that for these experiments the rate of stress relaxation is lower than the applied extension rate.

Glutaraldehyde cross-linked fibrils were found to have a higher residual stress at similar relative elongation values, compared to non-treated and EDC/NHS cross-linked fibrils. This was explained by the presence of covalent bonds between microfibrils in glutaraldehyde cross-linked fibrils.

For non-treated and EDC/NHS cross-linked fibrils a different stress-elongation behaviour was observed. Up to ~30% relative elongation, no residual stress was observed. Possibly, the rate of stress relaxation for these fibrils is higher than that of glutaraldehyde cross-linked fibrils. For EDC/NHS cross-linked fibrils the stress relaxation via microfibril slipping seemed to occur at an even higher rate than observed for non-treated fibrils. This difference in the slipping rate of microfibrils was attributed to surface decoration of microfibrils with NHS-ester groups. Glutaraldehyde cross-linked fibrils showed an increase in residual stress at increasing relative elongation. For non-treated and EDC/NHS cross-linked fibrils an increase in residual stress was observed at relative elongation values above ~30%. The increase in residual stress at increasing relative elongation was hypothesized to be caused by a reduced diameter of the fibrils and a corresponding reduced distance between the microfibrils constituting the fibril. The reduced distance between the microfibrils might improve their mutual non-covalent interactions, which possibly hinders the slipping of microfibrils during permanent deformation of the fibril.

The underlying deformation mechanisms during tensile testing of collagen fibrils was discussed in chapter 6. In principle, the deformation of collagen fibrils consists of reversible/irreversible deformation or displacement of microfibrils, and reversible/irreversible deformation or displacement of triple helices. The deformation of microfibrils can be described by the deformation or displacement of triple helices. For the displacement of triple helices a movement of aggregated triple helices or an individual displacement is possible.

The reversible tensile testing of collagen fibrils immersed in aqueous media was associated with reversible displacement of microfibrils or reversible displacement of aggregated or individual triple helices. Because of the large difference in Young's modulus between a triple helix and a fibril, the contribution of reversible deformation of triple helices was assumed minimal.

The Young's modulus of a collagen fibril tensile tested at ambient conditions was highly similar to the Young's modulus of a triple helix as described in literature. This in combination with an observed linear stress-strain curve suggested that the reversible deformation of a collagen fibril at ambient conditions is dominated by the reversible deformation of triple helices.

During loading of collagen fibrils immersed in aqueous media at stress values above 20 MPa, permanent deformation was observed. This phenomenon most likely is caused by irreversible displacement of microfibrils. The irreversible displacement of aggregated or individual triple helices was discarded as a possible mechanism, because of various experimental observations, including a retained collagen D-period in the tensile tested fibrils. For the same reason,

permanent deformation of collagen fibrils at ambient conditions was also attributed to the irreversible displacement of microfibrils.

Glutaraldehyde cross-linked fibrils showed a significantly different stress-elongation behaviour, compared to non-treated and EDC/NHS cross-linked fibrils, which was mainly attributed to the presence of cross-links between microfibrils. EDC/NHS cross-linked fibrils showed stress relaxation that occurred more rapid than for non-treated fibrils, suggesting an influence of the surface decoration of microfibrils with NHS-esters, which possibly promotes the microfibril slipping process.

Chapter 7 provides an overview of the main conclusions obtained from the results, as reported in this thesis. Furthermore, a number of hypothetical experiments using the setup consisting of an AFM and an inverted microscope are mentioned, which could provide more insight into the relation between the mechanical and structural properties of collagen and other (bio)-polymers. Fibril-cell interactions might be directly measured as a function of external stimuli such as force or specific molecules.

In Appendix A, the permanent change in diameter of the fibril during tensile testing is verified. The diameter of the fibril is thought to decrease upon permanent lengthening. Assuming a Poisson ratio of 0.5 the new diameter can be estimated. These values were compared to the diameters of the broken fibrils, which were determined by microscopic techniques after tensile testing.

The thickness of the AFM cantilever was claimed to regulate its spring constant. This was verified in Appendix B from the geometry and resonance frequencies of the cantilevers, as provided by the supplier.

An overview of the mechanical tests performed on various collagen fibrils and their corresponding geometries is presented in Appendix C.

The possible permanent change in D-period after tensile testing of the fibrils was investigated by microscopic techniques and discussed in Appendix D. The results showed that the D-period does not permanently change due to permanent lengthening of the fibrils.

SAMENVATTING

Collageen is het meest voorkomende eiwit in zoogdieren, daarom heeft het een essentiële functie voor de vorm en mechanische eigenschappen van weefsel. Over de correlatie tussen de mechanische eigenschappen van materiaal op basis van collageen en de interne structuur van collageen is nog maar weinig bekend. Eén van de substructuren van collageen is de collageenfibril, die gevormd en uitgescheiden wordt door fibroblasten en een directe mechanische interactie met cellen heeft. Deze fibrillen hebben een typische diameter van 200 nm en een lengte van enige tientallen micrometers. In dit proefschrift wordt de succesvolle fixatie van één collageen fibril met één uiteinde aan een substraat en met het andere aan de bladveer van een atoomkrachtmicroscop (AFM) beschreven.

Met deze meetopstelling was het mogelijk om de mechanische eigenschappen van collageenfibrillen te bepalen op een vergelijkbare manier als gebruikt tijdens de macroscopische sterktebepaling van allerlei materialen. Uit de resultaten bleek dat een collageenfibril onder atmosferische omstandigheden een lineair spannings-*rek* diagram vertoont, terwijl fibrillen die in een waterig milieu getest waren een niet-lineair gedrag vertonen. Vanaf een specifieke spanning, die verschillend was voor de twee voornoemde omstandigheden, trad permanente deformatie van de fibril op. Van deze permanente deformatie werd aangenomen dat deze optreedt door het verschuiven van zogenaamde microfibrillen.

Biomaterialen op basis van collageen ondergaan normaliter een vernettingsreactie voordat deze gebruikt worden als implantaat. Dit proces voorkomt een snelle enzymatische degradatie en afstoting van lichaamsvreemde stoffen, maar hierdoor worden ook de mechanische eigenschappen van het collageen veranderd. De collageenfibrillen werden vernet met twee algemeen bekende reagentia (glutaaraldehyde en een reagens op basis van carbodiimide (EDC/NHS)). Het is gebleken, dat het vernetten van fibrillen met glutaaraldehyde leidt tot een verminderde permanente deformatie van de fibril bij hoge spanning, dan voor niet-behandelde fibrillen bij dezelfde spanning. Voor de fibril die vernet was met EDC/NHS werden vergelijkbare mechanische eigenschappen als voor niet-behandelde fibrillen gevonden.

In hoofdstuk 2 van deze dissertatie wordt een samenvatting gegeven van de structuur en mechanische eigenschappen van collageen, zoals bekend uit de huidige literatuur. Ongeveer 25 typen collageen zijn bekend, waarvan het type I het meest voorkomt. De triple helix vormt een karakteristieke substructuur van collageen. De triple helix bestaat uit drie polypeptide ketens met het triplet Gly-X-Y als repeterende eenheid, waarbij X en Y meestal uit proline of hydroxyproline aminozuren bestaan. Collageenfibrillen, die een belangrijke component van de extracellulaire matrix vormen, worden zowel *in vivo* als *in vitro* gevormd door de zelf-assemblage van collageen triple helices. Collageenfibrillen vormen het belangrijkste onderdeel van ligamenten.

De stabiliteit van de triple helix wordt veroorzaakt door waterstofbrugvorming, waarbij de hydroxyproline aminozuren in de triple helix en waterstofbruggen via watermoleculen betrokken zijn. Er zijn ook andere verklaringen voor de stabiliteit gepostuleerd (bijvoorbeeld sterische hindering en/of het inductieve effect van de hydroxyl groep in hydroxyproline aminozuren), maar het eerstgenoemde mechanisme, in combinatie met de asymmetrie van de triple helix, lijkt de beste verklaring voor de stabiliteit van de triple helix te bieden.

Zoals al eerder werd besproken, leidt de aggregatie van triple helices via zelf-assemblage tot de vorming van fibrillen, een proces dat fibrillogenese wordt genoemd. Het bestaan van microfibrillen als een intermediaire structuur tussen die van de triple helix en de fibril in is gebaseerd op Röntgendiffractiegegevens. De analyse van materialen op basis van collageen met andere technieken (zoals NMR en gepolariseerd licht) suggereert echter dat de aggregatie van triple helices in een fibril minder georganiseerd is; een aggregatietoestand die vergeleken kan worden met de organisatie van moleculen in vloeibare kristallen.

De aggregatie van triple helices wordt gereguleerd door krachten die optreden door de verandering van hydratiegraad; de aanwezigheid van andere niet-covalente interacties zoals hydrofobe en electrostatische interacties tussen triple helices is echter ook gesuggereerd.

De aanwezigheid van zogenaamde telopeptiden met een conformatie anders dan die van de triple helix aan beide uiteinden van de triple helix, blijkt de snelheid van aggregatie van triple helices te verhogen en de diameter van de gevormde fibrillen te reguleren. Met behulp van verschillende technieken is een poging gedaan om de mechanische eigenschappen van individuele triple helices te bepalen of door extrapolatie van het mechanische gedrag van de macroscopische collageenstructuur naar dat van een triple helix. Aldus werd voor een triple helix in een macroscopische collageen structuur in een waterig milieu de Young's modulus geschat tussen 3 en 6 GPa.

Onder mechanische belasting kan een triple helix oprekken via verschillende mechanismen, waaronder:

- elastisch oprekken van sequenties in de triple helix met daarin veel aminozuren met ionische zijgroepen, maar met weinig (hydroxy)proline aminozuren,
- het oprekken van microscopische knikken in de triple helix,
- het verbreken van zogenaamde "oppofferingsbindingen" in de triple helix, die bestaan uit ionische interacties tussen aminozuren in de triple helix

Behalve verlenging van triple helices is ook de onderlinge verplaatsing van triple helices een mogelijk mechanisme, wat leidt tot een verandering in de D-periode van collageen.

De mechanische eigenschappen van collageenfibrillen zijn vrijwel onbekend. Uit de veranderingen in het Röntgendiffractiepatroon van een Achillespees tijdens het opspannen van de pees werd een spannings-tek diagram verkregen, waaruit een Young's modulus van ongeveer 450 MPa voor de collageenfibril werd bepaald.

In hoofdstuk 3 wordt de ontwikkeling van een meetopstelling besproken, waardoor het spannings-rek diagram van een individuele collageenfibril bepaald kan worden. In de meetopstelling wordt een AFM gecombineerd met een omgekeerde microscoop. Op een glasplaat die gedeeltelijk met een Teflonlaag was bedekt bevonden zich een aantal geïsoleerde collageenfibrillen. Eén enkele fibril werd bevestigd met één uiteinde aan het glasoppervlak door middel van een kleine druppel epoxy-lijm. Het andere uiteinde dat zich op het Teflonoppervlak bevond, werd met epoxy-lijm bevestigd aan de bladveer van de AFM. Na uitharding van de lijm werd de fibril via de bladveer opgetild van het Teflonoppervlak, waarna met dit systeem het spannings-rek diagram van een individuele collageenfibril bepaald kon worden. De stijfheid van de lijm werd gemeten, waardoor aangetoond kon worden dat de lijm geen invloed had op de verkregen spannings-rek diagrammen.

Met behulp van de meetopstelling, zoals beschreven in hoofdstuk 3, werd het spannings-rek diagram van individuele collageenfibrillen bepaald, die bediscussieerd werden in hoofdstuk 4. De reversibele belasting van een collageenfibril onder atmosferische condities was mogelijk bij spanningen beneden 90 MPa. Wanneer deze spanning werd overschreden, trad permanente deformatie van de fibril op. Voor fibrillen in een waterig milieu, waarbij onder andere natrium- en/of calciumhoudende HEPES-bufferoplossingen, gedemineraliseerd water en bufferoplossingen met een pH tussen 5.4 en 7.4 werden gebruikt, werden sterk vergelijkbare spannings-rek diagrammen verkregen. Ook bij variatie van de snelheid van oprekken van de fibril tussen 0.02 and 20 $\mu\text{m s}^{-1}$ werd geen verschil in het spannings-rek gedrag geconstateerd. Als een spanning boven 20 MPa werd opgelegd, trad permanente deformatie op. Door stapsgewijze verlenging van de fibril kon de breukspanning van de fibril worden bepaald. Een fibril vertoonde een breukspanning van 69 MPa, terwijl een tweede fibril met een andere lengte en dikte nog intact was bij een spanning van 123 MPa. De vorm van de spannings-verlenging curves van beide fibrillen waren vergelijkbaar. Bij een relatieve verlenging van de fibril boven ~30% werd een toenemende hoeveelheid restspanning in de individuele spannings-verlenging curves waargenomen.

De opgelegde verlenging van de fibrillen onder hoge spanning leidt tot permanente verlenging van de fibrillen. Hierdoor trad geen permanente toename van de D-periode van de fibril op, wat het behoud van de interne organisatie van triple helices in de fibril suggereert. Vanwege deze observatie wordt aangenomen dat permanente verlenging van de fibril veroorzaakt wordt door het glijden van microfibrillen ten opzichte van elkaar.

Door de beperkingen van de gebruikte lijm methode en methode voor de bepaling van het spannings-rek diagram van een collageenfibril, zoals beschreven in hoofdstuk 3, ontstaan er twee buigpunten in de fibril, wanneer deze wordt opgetild van het glasoppervlak en vervolgens opgerek. In de voorafgaande resultaten uit hoofdstuk 4 werd aangenomen dat het spannings-rek diagram via een uniaxiale configuratie was verkregen. In werkelijkheid zou de buiging van de fibril een bijdrage kunnen leveren aan het geobserveerde spannings-rek gedrag.

De mogelijke invloed van het buigen van de fibril op het spannings-rek gedrag werd geëvalueerd door het gebruik van een modelsysteem, bestaande uit een isotrope plaat met dezelfde lengte-dikte verhouding als van collageenfibrillen (100 μm tot 200 nm), waarbij een volledig elastisch spannings-rek gedrag werd aangenomen. Het resultaat van deze modelstudie en de mogelijke implicaties voor het spannings-rek gedrag van collageenfibrillen is beschreven in de appendix van hoofdstuk 4. Wanneer een isotrope plaat opgerekt wordt in een uniaxiale configuratie, wordt een spannings-rek diagram gevonden dat verschilt van het diagram van een plaat die opgerekt en ondertussen op twee plaatsen gebogen wordt (zoals voor de fibril gebeurt). De verkregen spannings-rek diagrammen van de plaat werden vergeleken met de spannings-rek diagrammen van collageenfibrillen. Het bleek dat alleen het spannings-rek diagram van het modelsysteem, dat via een uniaxiale configuratie verkregen was, vergelijkbaar was met de experimentele resultaten verkregen voor collageenfibrillen. Dit resultaat suggereert dat buiging van de fibril bij zeer lage spanningen optreedt, waardoor het verkregen spannings-rek diagram van een collageenfibril niet beïnvloed wordt.

In hoofdstuk 5 wordt de invloed van vernetting van collageenfibrillen op zijn mechanische eigenschappen beschreven. De fibrillen werden vernet met glutaaraldehyde of EDC/NHS. Het bleek dat het spannings-rek diagram van een niet-behandelde collageenfibril tot een spanning van 15 MPa dezelfde helling had als een fibril die vernet was met glutaaraldehyde. Door stapsgewijze verlenging werd een hogere spanning opgelegd aan de fibril die behandeld was met glutaaraldehyde, waardoor deze brak bij een spanning van 168 MPa. Voor een fibril die vernet was met EDC/NHS werd een breukspanning van 87 MPa bepaald.

Fibrillen die vernet waren met glutaaraldehyde lieten een snelle toename van de hoeveelheid restspanning zien in de cyclische spannings-verlenging curves bij toenemende relatieve verlenging. Dit resultaat suggereert dat tijdens deze experimenten de snelheid van spanningsrelaxatie lager is dan de toegepaste snelheid van oprekken van de fibril.

Voor fibrillen die vernet waren met glutaaraldehyde werd een hogere restspanning waargenomen bij dezelfde snelheid van oprekken, dan voor fibrillen die niet behandeld waren of die vernet waren met EDC/NHS. Dit verschil werd verklaard door de aanwezigheid van covalente bindingen tussen microfibrillen in fibrillen die vernet waren met glutaaraldehyde.

Voor niet-behandelde fibrillen en fibrillen die vernet waren met EDC/NHS werden verschillende spannings-verlenging curves bepaald. Tot een relatieve verlenging van $\sim 30\%$ werd geen restspanning waargenomen. Waarschijnlijk is de snelheid van spanningsrelaxatie voor deze fibrillen hoger dan die van fibrillen die vernet waren met glutaaraldehyde. Voor fibrillen die met EDC/NHS vernet waren, leek de spanningsrelaxatie via het glijden van microfibrillen bij een hogere snelheid op te treden, dan voor niet-behandelde fibrillen. Dit verschil in de snelheid van glijden van microfibrillen werd toegeschreven aan oppervlaktedecoratie van microfibrillen door NHS-ester groepen.

Voor fibrillen die vernet waren met glutaraaldehyde werd een toename in restspanning bij groter wordende relatieve verlenging waargenomen. Voor niet-behandelde fibrillen en fibrillen die vernet waren met EDC/NHS werd een toename in de restspanning waargenomen vanaf een relatieve verlenging van meer dan ~30%. Volgens een aanname wordt de toename in restspanning bij groter wordende relatieve verlenging veroorzaakt door de gereduceerde diameter van de fibril, waardoor ook de onderlinge afstand tussen de microfibrillen vermindert. Door een verminderde afstand tussen de microfibrillen worden mogelijk de niet-covalente interacties tussen de microfibrillen versterkt. Het glijden van microfibrillen dat optreedt tijdens permanente deformatie van de fibril kan hierdoor mogelijk gehinderd worden.

De basale deformatie-mechanismen die optreden gedurende belasting van een collageenfibril werd bediscussieerd in hoofdstuk 6. In principe bestaat het deformatiegedrag van een collageenfibril uit re-(ir)reversibele deformatie of -verplaatsing van microfibrillen en re-(ir)reversibele deformatie of -verplaatsing van triple helices. De deformatie van microfibrillen kan worden beschreven door de deformatie of verplaatsing van triple helices. De verplaatsing van triple helices kan bestaan uit de groepsgewijze - of individuele verschuiving van triple helices.

De reversibele belasting van een collageenfibril in een waterig milieu kon worden geassocieerd met reversibele verplaatsing van microfibrillen of de reversibele verplaatsing van triple helices in groepen of individueel. Vanwege het grote verschil tussen de Young's modulus van een triple helix en een fibril werd de bijdrage van reversibele deformatie van de triple helices verwaarloosd.

De Young's modulus van een collageenfibril onder atmosferische omstandigheden, zoals bepaald uit het spannings-rek diagram, was vergelijkbaar met de Young's modulus van een triple helix zoals gerapporteerd is in de literatuur. Deze constatering, in combinatie met het waargenomen lineaire spannings-rek diagram, suggereert dat de reversibele deformatie van een collageenfibril onder atmosferische omstandigheden gedomineerd wordt door de reversibele deformatie van triple helices.

Wanneer een fibril in een waterig milieu wordt belast tot spanningen boven 20 MPa, treedt permanente deformatie op. Dit fenomeen wordt hoogstwaarschijnlijk veroorzaakt door de irreversibele verplaatsing van microfibrillen. De irreversibele verplaatsing van triple helices (individueel of groepsgewijs) werd uitgesloten als mogelijk mechanisme, vanwege verschillende bevindingen die volgden uit de experimenten. Eén van die bevindingen was de onveranderde D-periode van de collageenfibrillen na het oprekken, waarbij ook permanente deformatie opgetreden was. Om dezelfde reden werd de permanente deformatie van collageenfibrillen die opgerekte werden onder atmosferische omstandigheden ook toegeschreven aan de irreversibele verplaatsing van microfibrillen.

Voor collageenfibrillen die waren vernet met glutaraaldehyde werd een significant verschillend spannings-rek gedrag waargenomen in vergelijking met niet-behandelde fibrillen en fibrillen die vernet waren met EDC/NHS. Dit verschil werd verklaard door de aanwezigheid van covalente bindingen tussen microfibrillen in fibrillen die met glutaraaldehyde waren vernet. De collageenfibrillen die vernet waren met EDC/NHS vertoonden een snellere spanningsrelaxatie dan niet-behandelde fibrillen, wat een invloed van oppervlaktedecoratie van microfibrillen met NHS-esters suggereert. Deze oppervlaktedecoratie kan mogelijk het glijden van microfibrillen vergemakkelijken.

Hoofdstuk 7 biedt een overzicht van de belangrijkste conclusies die volgen uit de resultaten die beschreven worden in deze dissertatie. Verder wordt een aantal hypothetische experimenten beschreven, die mogelijk zijn met de hier beschreven opstelling, bestaande uit een AFM en een omgekeerde microscoop. Deze experimenten kunnen een beter inzicht geven in de relatie tussen de mechanische eigenschappen en de interne structuur van collageen en andere (bio)-polymeren. De interactie tussen fibrillen en cellen kan mogelijk direct worden bepaald als functie van de opgelegde spanning of de aanwezigheid van specifieke moleculen.

In Appendix A wordt de permanente verandering van de diameter van de fibril beschreven, die optreedt gedurende belasting van de fibril. De diameter van de fibril zal waarschijnlijk afnemen gedurende permanente verlenging. Wanneer een Poisson verhouding van 0.5 wordt aangenomen kan de nieuwe diameter worden berekend. Deze waarden werden vergeleken met de diameter van de gebroken fibrillen, zoals bepaald met microscopische technieken na mechanische belasting van de fibrillen.

Van de veerconstante van de AFM bladveren werd aangenomen dat deze voornamelijk afhankelijk zijn van de dikte van de bladveer. Deze aanname werd geverifieerd in Appendix B aan de hand van de geometrie en resonantiefrequenties zoals opgegeven door de fabrikant.

Een overzicht van de mechanische tests die uitgevoerd werden met de verschillende collageenfibrillen en de bijbehorende dikte en lengte van de fibrillen wordt gegeven in Appendix C.

De mogelijke permanente toename van de D-periode, die opgetreden is door mechanische belasting van de fibrillen, werd onderzocht met microscopische technieken en beschreven in Appendix D. De resultaten laten zien dat door permanente verlenging van de fibrillen hun D-periode geen permanente verandering heeft ondergaan.

DANKWOORD

"Patience et longueur de temps font plus que force ni que rage." - La Fontaine

Promoveren doe je niet alleen. Daarom "lest: best!" degenen die gedurende mijn promotie hun bijdrage hebben geleverd aan het proefschrift dat voor u ligt.

Ten eerste professor Feijen: u hebt de bijzondere gave mensen van verschillende disciplines bij elkaar te brengen, waardoor de grenzen van beide disciplines overschreden kunnen worden. De combinatie van de disciplines bestaat immers uit meer dan de som der delen. Dankzij uw methodische manier van schrijven, waar ik veel van geleerd heb, zijn ook ingewikkelde meetgegevens ordentelijk te presenteren. Hartelijk dank voor uw enthousiasme, uitleg en geduld, want een duidelijk proefschrift ligt er niet in één versie.

Ten tweede wil ik graag Piet Dijkstra bedanken voor zijn uitgebreide steun als copromotor/referent. Ondanks dat het onderwerp van mijn onderzoek steeds verder van een voor jou gebruikelijk onderzoeksgebied af kwam te staan, heb je je snel ingelezen en kon je de hoofdstukken op een uitstekende manier corrigeren en stroomlijnen.

Martin Bennink kwam door mijn idee om individuele collageenfibrillen te tensile testen als specialist in beeld door zijn expertise in force spectroscopy van DNA moleculen. Later is je bijdrage zelfs uitgebreid tot die van copromotor. Bedankt voor al je suggesties met betrekking tot mijn onderzoek en je intensieve bijdrage in het snel corrigeren van zelfs de meer chemisch georiënteerde hoofdstukken.

Van essentieel belang voor het ontwerpen, bouwen en meten van/met de beschreven meetopstelling was mijn paranimf Kees van der Werf. Door een combinatie van uitstekende construerende capaciteiten en een interesse en enthousiasme om samen te werken met mensen uit andere vakgebieden, was je voor mij de ideale persoon om dit onderzoek te ondersteunen. Zonder jouw hulp was dit boekje blijven steken bij een eerste aanzet tot hoofdstuk 3, bedankt!!!

Mijn andere paranimf, Matthias Fischer wil ik bedanken voor zijn mentale steun en de afleiding van de promotiesores door fantastische (wijn)dagen in Gimbsheim en omstreken. Aanwezig mogen zijn bij je huwelijk met Anja was erg bijzonder.

Dr. ir. Marc Hendriks wil ik hartelijk danken voor zijn suggesties tijdens de nuttige discussies van dit door het Medtronic Bakken Research Center gefinancierde promotieonderzoek. Initieel had dit project veel meer raakvlakken met het onderzoek bij Medtronic, maar ook de meer fundamentele doelen van dit promotieonderzoek hadden jouw interesse, wat wel bleek uit de goede discussie van de resultaten. Bedankt dat je plaats wilde nemen in de promotiecommissie. Dankzij de faciliteiten en ervaring in de Biofysische Techniek groep kon dit gezamenlijke project succesvol worden afgerond. Professor Greve, bedankt voor uw hulp om dit alles mogelijk te maken en uw aanbod om plaats te nemen in de promotiecommissie. Vakgroepen waar de hoogleraar de tijd neemt om wetenschappelijke- en alledaagse zaken tijdens alle koffiepauzes in een gezellige sfeer door te nemen zijn helaas niet zo alomverteenwoordigd. Professor Baaijens, dr. Bank, prof Vancso en de voorzitter wil ik graag bedanken voor hun plaatsnemen in de promotiecommissie.

Verschillende mensen hebben een bijdrage geleverd waardoor de tijdens het promotieonderzoek uitgevoerde experimenten mogelijk gemaakt werden.

Mark Smithers en Bert Otter van Mesa⁺ wil ik bedanken voor hun SEM analyses. Frans Segerink van de Optical Technology groep ben ik erkentelijk voor zijn bijdrage aan het geschikt maken van de AFM bladveren met FIB. Albert van den Berg van Mesa⁺ wil ik bedanken voor de analyse van de gefluoreerde glas substraten met XPS. Teun Ruardij uit de Biomedical Signals and Systems groep dank ik voor zijn suggesties voor het fluoro-silanderen van de glas substraten. Professor Marani en Remy Wiertz uit dezelfde groep wil ik graag bedanken voor het aanleveren en prepareren van de vezels uit rattenstaarten voor mechanische testen, wat een eerste aanzet gaf tot de resultaten die in dit proefschrift staan vermeld.

Frank Everaerts, Mirian Gillissen en Anita Levels van Medtronic Bakken Research Center wil ik graag bedanken voor de bepaling van de denaturatie temperatuur en het aantal lysine groepen van dermaal schapencollageen, maar ook voor de gezamenlijke tensile tests aan leaflets van varkenshartkleppen. Frank, bedankt voor de gezellige afleiding van de metingen met culinaire hoogstandjes in Maastricht en Enschede. Het getuigt van courage om zelf ook te gaan promoveren tijdens je baan bij Medtronic, veel succes daarbij!

Daarnaast heb ik door discussies en modellering-experimenten een beter inzicht gekregen in de mechanische eigenschappen van collageen.

Professor Huétink and dr. ir. Timo Meinders van de Technische Mechanica groep ben ik zeer erkentelijk voor de modellering experimenten die uitgevoerd zijn om de invloed van buiging van de fibril tijdens het tensile testen te bestuderen en voor de zeer bruikbare discussies van de resultaten.

Paul Weustink van Controllab wil ik graag bedanken voor het uitvoeren van de modellering van de stress-strain curves van collageenfibrillen. De resultaten waren helaas niet in te passen in het proefschrift, maar gaven een goed beeld van de complexiteit van de onderliggende

componenten (veren en dempers) die het mechanische gedrag van collageen kunnen beschrijven.

Dr. ir. C.M.W. Bastiaansen and dr. ir. L.E. Govaert van de TUE wil ik bedanken voor de nuttige discussie van de eerste meetgegevens van het stress-strain gedrag van collageenfibrillen.

Dr. ir. Reinout Gaymans van de STEP groep wil ik graag bedanken voor de discussie en suggesties met betrekking tot permanente deformatie, de Poisson verhouding en vermindering van de diameter van de fibril.

Evert, hartelijk dank voor je hulp bij de layout van dit proefschrift. Veel succes in je verdere loopbaan, met jouw presentatiestijl is de sky the limit...

Ype wil ik graag bedanken voor zijn hulp bij het ontwerpen van de voorkant. Bedankt ook voor jouw inbreng als gezellige kamergenoot en supersportieve/eigenwijze deelnemer aan de zeil- volleybal- en (tafel)tennisactiviteiten.

Aan de UT had ik het geluk vier onderzoeksgroepen tot mijn collega's te mogen rekenen. Naast bijna elke dag taart betekent dat vooral veel sportieve activiteiten {(tafel)tennis, zeilen, (beach)-volleybal en de triathlon}, wetenschappelijke reizen (naar Zwitserland met de PBM groep) en andere gezelligheid. Alle oud-collega's van de PBM, STEP, BFT, MTP en RBT groepen wil ik daarom bij deze bedanken voor de goede werksfeer.

Van de PBM en STEP groep wil ik in het bijzonder bedanken: Zhiyuan (table tennis, and discussions on research and Chinese wisdom), Menno, Bas (kamergenoot en nog iets grotere liefhebber van Italië dan ik), Marcel, Marianne (kamergenoot en party-animator), Francesca Signori (kamergenoot en top-pizzabakker), Karin (wandelende organisator voor PBM en Scandinaviëfan), André, Dirk, Priscilla (volleybal, tennistalent en gezelligheidsmens), Fenghua (levenswijsheid uit China), MOR (volleybal, tafeltennis en recordhouder dineren), Luuk (doe maar gewoon en beun de haas op het plasma apparaat), Laura, Paula, Mark A. (computerhulp), Ingrid (volleybal), Audrey, Boonhua (tafeltennis), Miechel (tafeltennis), Zheng (tafeltennis), Josien (volleybal, zeilfanaat en triathlonorganisator), Martijn, Ana Paula (triathlonorganisator), Judith, Hetty (reisleidster Suisse), Debby (volleybal) en Edwin (volleybal).

Uit de BFT groep wil ik graag bijzonder bedanken: Dessy (wereldreiziger), Svetlana, Anthony, Jurgen, Arjen, Kirsten, Roel, Lisa en Sylvia.

Van de MTP groep bedank ik vooral: Léon (voor de Philips suggestie en alle gezelligheid), Douwe-Wiebe, Béata, Clemens (voor hulp bij verschillende analyses), Holger (voor nuttige discussies) en Barbara.

Van de RBT groep wil ik met name bedanken: Geert, Louis, Annemieke, Andries, Kinsuk (thank you for your corrections, but when will we play cricket?), Pratip, Richard (volleybal), Francesca en Joost (volleybal).

De medewerkers van de bibliotheek van CT wil ik bedanken voor hun hulp bij het bestellen van de onmogelijk te verkrijgen artikelen voor mijn literatuurstudie (hoofdstuk 2).

Uit de membranen groep wil ik Ger, Tao (tafeltennis), Sybrand en Alberto (tafeltennis en vervoer van kasten) bedanken.

De H.S.B.B. met aanhang wil ik culinair verantwoord bedanken voor alle gezelligheid en goede conversaties. Coen, Martijn vV, Martijn vG en Sander: ik verheug me nu al op het eerste lustrum in 2005!

Remco: bedankt voor de gezelligheid en veel succes en geluk samen met Simone in Wales.

Alexander wil ik bedanken voor de filmavonden en fietstochten.

Uit het supergezellige studentenhuus 'Antonio' wil ik al mijn oud-huisgenootjes bedanken. Met name Jaap, Geertruide, Maaïke, Ingmar, Matthijs (tijd voor pakken en whiskey, ibuena suerte en España!), Nienke (avondmens en wereldburger, bonne chance dans la France!), Daniël, Brechtje en Rianne. Bedankt voor de ontzettend leuke tijd samen, de Sinterklaasavonden waren onvergetelijk.

Mijn teamgenoten van Heren 2 van Drienerlo wil ik graag bedanken voor de sportieve en gezellige tijd bij de Boortoren. Het ontbijten in de trein en de sfeer na de wedstrijd zal ik niet gauw vergeten, vooral de rotzooi!

Graag wil ik alle familieleden van van der Rijt, Schuurmans en Ueffing bedanken voor hun interesse in mijn promotieonderzoek. Herman, Ria, Bram en Sanne: bedankt voor al jullie steun, bij jullie voel ik me echt thuis. Ad en Fien: dank je voor alle hulp en steun, want ik voelde dat jullie altijd achter me stonden, ook als de weg naar het promotiedoel erg moeilijk was. Dorien: op jou kon ik altijd rekenen, je bent een erg lieve zus.

De moeilijkste zinnen komen altijd op het laatst. Hoe bedank je iemand van wie je zielsveel houdt en die oneindig geduld had tot dat boekje eindelijk rond was? Meike, dank je wel voor alles wat je voor me gedaan hebt en nog steeds doet. Samen met jou was al bijzonder, maar met David erbij voelt het echt speciaal.



CURRICULUM VITAE

Joost A.J. van der Rijt werd geboren op 23 augustus 1975 in het pittoreske Zeeland (verrassenderwijs gelegen in de provincie Noord-Brabant). Na het behalen van het V.W.O. diploma aan het 'Kruisherer Kollege' te Uden in 1994 werd in datzelfde jaar begonnen met een studie aan de Katholieke Universiteit Nijmegen. Al vanaf de basisschool lag zijn interesse bij scheikunde en geschiedenis. Een bezoek aan een laboratorium gaf de doorslag naar scheikunde. Het propaedeutisch diploma werd in 1996 behaald en begin 1997 werd een hoofdrichting Organische Chemie gevolgd onder begeleiding van prof. dr. R.J.M. Nolte, dr. J.W. Scheeren en dr. R.J. Jansen met als onderwerp: 'Synthese en functionalisering van een nieuwe generatie clipmoleculen'. Vervolgens werd in 1998 in het kader van een uitgebreide nevenrichting Polymeerchemie onderzoek verricht onder begeleiding van prof. dr. E.W. Meijer, dr. R.P. Sijbesma en dr. B.J.B. Folmer aan de Technische Universiteit Eindhoven. Het onderzoek was gericht op de synthese en karakterisering van Supramoleculaire polymeren met een rigide hoofdketen. In 1999 werd het diploma met veel genoegen behaald, waarna begonnen werd met een promotieonderzoek aan de Universiteit Twente in de vakgroep Polymeren en Biomaterialen onder supervisie van prof. dr. J. Feijen, dr. P.J. Dijkstra en dr. ir. M.L. Bennink. De resultaten van dit onderzoek worden beschreven in dit proefschrift. Vanaf februari 2004 is de auteur werkzaam als Plastics Engineer bij Koninklijke Philips N.V. te Drachten.

Joost A.J. van der Rijt was born on the 23rd of August 1975 in the scenic town called Zeeland (amazingly situated in the province of Noord-Brabant). After obtaining his secondary school degree at the 'Kruisherer Kollege' in Uden in 1994, he started a study at the University of Nijmegen that same year. Already since primary school his interest was in chemistry and history. After visiting a laboratory, the decision was made to study chemistry. In 1997 he started his major in Organic Chemistry supervised by Prof. R.J.M. Nolte and Drs. J.W. Scheeren and R.J. Jansen. In 1998 a minor was taken in Polymer Chemistry at Eindhoven University of Technology under supervision of Prof. E.W. Meijer and Drs. R.P. Sijbesma and B.J.B. Folmer. After his graduation in 1999 the author started as a PhD student in the Polymer and Biomaterials group at the University of Twente under supervision of Prof. J. Feijen and Drs. P.J. Dijkstra and M.L. Bennink. The results of this research project are discussed in this thesis. Since February 2004 the author has been working as a plastics engineer at Philips DAP in Drachten.